**António Eduardo Carreiro Furtado**

Mestre em Engenharia Eletrotécnica e de Computadores

# Advanced PHY/MAC Design for Infrastructure-less Wireless Networks

Dissertação para obtenção do Grau de Doutor em

**Engenharia Eletrotécnica e de Computadores**

| | |
|---|---|
| Orientador: | Rodolfo Alexandre Duarte Oliveira,<br>Prof. Auxiliar com Agregação,<br>Universidade Nova de Lisboa |
| Co-orientador: | Rui Miguel Henriques Dias Morgado Dinis,<br>Prof. Associado com Agregação,<br>Universidade Nova de Lisboa |

Júri

| | |
|---|---|
| Presidente: | Prof. Doutor Paulo da Costa Luís da Fonseca Pinto, FCT-UNL |
| Arguentes: | Prof. Doutor João Paulo Vilela, FCT-UC |
| | Prof. Doutor Pedro Joaquim Amaro Sebastião, ISCTE-IUL |
| Vogais: | Prof.ª Doutora Susana Isabel Barreto de Miranda Sargento, UA |
| | Prof. Doutor Marko Beko, ULHT |
| | Prof. Doutor Rodolfo Alexandre Duarte Oliveira, FCT-UNL |

FACULDADE DE CIÊNCIAS E TECNOLOGIA
UNIVERSIDADE NOVA DE LISBOA

**Julho, 2018**

**Advanced PHY/MAC Design for Infrastructure-less Wireless Networks**

*To my Mother and Father*

# ACKNOWLEDGEMENTS

I would like to start by showing my deepest gratitude to my scientific advisor, Professor Rodolfo Oliveira, for his valuable guidance and support throughout this PhD. His deep knowledge and experience certainly contributed to develop my research and to obtain a more consolidated work. Additionally, I would like to address my gratitude to my scientific co-advisor, Professor Rui Dinis, for guiding me through the initial steps of this thesis and for his willingness to help whenever was necessary.

Not least important, I would like to thank Prof. Luis Bernardo and Prof. Paulo Pinto for all their advice and help.

I would like to thank the Departamento de Engenharia Electrotécnica da Faculdade de Ciências e Tecnologia da Universidade Nova de Lisboa (DEE-FCT-UNL), and research centers Instituto de Telecomunicações (IT) and Centre of Technology and Systems (CTS-UNINOVA) for providing me the conditions for developing this research work.

I also acknowledge the indispensable financial support provided by Fundação para a Ciência e Tecnologia (FCT) under the research grant SFRH/BD/88140/2012 and research projects ADIN (PTDC/EEI-TEL/2990/2012), MANY2COMWIN (EXPL/EEI-TEL/0969/2013) and VELOCE-MTC (UID/EEA/5008/2013).

I'm also thankful to my closest friends. They were unconditionally present every time I needed and with them I shared some of the most important moments during my years at this University, which enriched my life.

To Ana Sofia, my girlfriend, for her love and undubitable friendship.

Finally, my utmost gratitude words go to all my family but particularly to my parents and my sisters for their endless support and advice during these years, whose words of encouragement helped me to pursue my dreams.

# ABSTRACT

Wireless networks play a key role in providing information exchange among distributed mobile devices. Nowadays, Infrastructure-Less Wireless Networks (ILWNs), which include ad hoc and sensor networks, are gaining increasing popularity as they do not need a fixed infrastructure. Simultaneously, multiple research initiatives have led to different findings at the physical (PHY) layer of the wireless communication systems, which can effectively be adopted in ILWNs. However, the distributed nature of ILWNs demand for different network control policies that should have into account the most recent findings to increase the network performance.

This thesis investigates the adoption of Multi-Packet Reception (MPR) techniques at the PHY layer of distributed wireless networks, which is itself a challenging task due to the lack of a central coordinator and the spatial distribution of the nodes. The work starts with the derivation of an MPR system performance model that allows to determine optimal points of operation for different radio conditions. The model developed and validated in this thesis is then used to study the performance of ILWNs in high density of transmitters and when the spectrum can be sensed a priori (i.e. before each transmission). Based on the theoretical analysis developed in the thesis, we show that depending on the propagation conditions the spectrum sensing can reduce the network throughput to a level where its use should be avoided. At the final stage, we propose a cross-layered architecture that improves the capacity of an ILWN. Different Medium Access Control (MAC) schemes for ILWNs adopting MPR communications are proposed and their performance is theoretically characterized. We propose a cross-layer optimization methodology that considers the features of the MPR communication scheme together with the MAC performance. The proposed cross-layer optimization methodology improves the throughput of ILWNs, which is validated through theoretical analysis and multiple simulation results.

**Keywords:** Distributed Wireless Networks, Multi-Packet Reception Networks, PHY/MAC Cross-layer design, Performance Evaluation.

# RESUMO

As redes sem fios desempenham um papel fundamental na troca de informações entre dispositivos móveis distribuídos. Atualmente, as Redes Sem Fios sem Infra-estrutura (ILWNs), que incluem redes ad hoc e de sensores, são cada vez mais populares, pois não precisam de uma infraestrutura fixa. Simultaneamente, várias iniciativas de investigação conduziram a diferentes desenvolvimentos na camada física dos sistemas de comunicação sem fios, que podem efetivamente ser adotadas nas ILWNs. No entanto, a natureza distribuída das ILWNs necessita de diferentes políticas de acesso à rede, as quais devem ter em conta as inovadoras técnicas da camada física para aumentar o desempenho da rede.

Esta tese investiga a adoção de técnicas de Recepção de Múltiplos Pacotes (MPR) na camada física das redes sem fios distribuídas, sendo um problema interessante devido à falta de um nó coordenador central e à distribuição espacial dos nós. O trabalho começa com a derivação de um modelo de desempenho de um sistema genérico MPR, o qual permite determinar pontos ótimos de operação para diferentes condições de rádio. O modelo desenvolvido e validado nesta tese é usado para estudar o desempenho de ILWNs em alta densidade de transmissores e quando o estado de ocupação do espectro pode ser detectado a priori (ou seja, antes de cada transmissão). Com base na análise teórica desenvolvida na tese, mostramos que, dependendo das condições de propagação, a detecção do estado de ocupação do espectro pode reduzir o débito da rede a um nível em que seu uso deve ser evitado. Na parte final do trabalho, propomos uma arquitetura múlti-camada que melhora a capacidade da rede. São propostos diferentes esquemas de Controlo de Acesso ao Meio (MAC) para ILWNs adotando comunicações MPR. Por fim, é proposta uma metodologia de otimização múlti-camada que considera as características do esquema de comunicação MPR juntamente com o desempenho do MAC. A metodologia de otimização melhora o débito da rede ILWN, a qual é validada através de análise teórica e por múltiplos resultados de simulação.

**Palavras-chave:** Redes sem fios distribuídas, redes de recepção de vários pacotes, projeto múlti-camada PHY/MAC, avaliação de desempenho.

# CONTENTS

# LIST OF FIGURES

# LIST OF TABLES

# LIST OF SYMBOLS

## General Functions and Symbols

$\mathbb{Q}(x)$ Tail distribution function of the standard normal

$\Gamma(\cdot)$ Gamma function

$\Gamma(p,x)$ Incomplete Gamma function

$\log(\cdot)$ Natural logarithm

$\mathcal{CN}$ Complex Normal distribution

$\overline{F}(x)$ Complementary CDF in $x$

$\mathrm{Ei}(\cdot,\cdot)$ Exponential integral function

$\mathrm{E}_X[\cdot]$ Expectation with respect to the RV $X$

$\mathrm{P}[X]$ Probability of $X$

$\mathrm{Var}_X[\cdot]$ Variance with respect to the RV $X$

$\varphi_X(t)$ Characteristic function of the RV $X$

${}_2\mathrm{F}_1$ Gauss Hypergeometric function

$f_X(\cdot)$ PDF of the RV $X$

$i$ Imaginary unit

$M_X(s)$ Moment-generating function of the RV $X$

## General PHY layer Symbols

$\alpha$ Path loss coefficient

$\gamma_j$ SINR associated to the signal received from node $j$

$\Lambda$ Total power received from multiple transmitters

$\mu_\xi$ Location parameter for the normally distributed logarithm $ln(\xi)$ (Lognormal distribution)

| | |
|---|---|
| $\Psi_k$ | RV representing the composite small-scale and large-scale fading |
| $\rho$ | Width of an annulus |
| $\sigma_\xi$ | Scale parameter for the normally distributed logarithm $ln(\xi)$ (Lognormal distribution) |
| $\sigma_\zeta$ | Scale parameter of the small-scale fading (Rayleigh distribution) |
| $\sigma_{N_0}$ | Standard variation of the noise at the receiver |
| $\tau$ | Spatial density of the transmitters located in area $A$ |
| $\mathrm{P}_{S_1}$ | Probability of successful packet reception of Model I |
| $\mathrm{P}_{S_2}$ | Probability of successful packet reception of Model II |
| $\mathrm{P}_{S_3}$ | Probability of successful packet reception of an ILWN scenario |
| $\theta_\psi$ | Scale parameter of the composite fading (Gamma distribution) |
| $A$ | Area where the transmitters are located |
| $A_l$ | Area of the $l$-th annulus |
| $b$ | MPR receiving threshold |
| $E_{\mathrm{rcv}_1}$ | Average number of successful received packets of Model I |
| $E_{\mathrm{rcv}_2}$ | Average number of successful received packets of Model II |
| $E_{\mathrm{rcv}_3}$ | Average number of successful received packets of an ILWN scenario |
| $I$ | Aggregate power received from multiple transmitters acting as interferers (interference power) |
| $I_l$ | Power received by a node from the transmitters located within the subarea $A_l$ |
| $k_\psi$ | Shape parameter of the composite fading (Gamma distribution) |
| $L$ | Total number of annuls in which area $A$ is subdivided |
| $M_{I_l}^k$ | Moment-generating function of the $k$-th transmitter located at the $l$-th annulus |
| $n$ | Total number of transmitters |
| $n*$ | Optimal number of transmitters |
| $N_0$ | RV representing the noise at the receiver |
| $n_I$ | Total number of interferers |
| $n_{I_l}$ | Number of interferers located within annulus l |

$P_k$ Received power of the $k$-th transmitter

$P_T$ Nodes' transmission power

$R_i^l$ Radius of the inner $l$-th annulus circle

$R_k^l$ RV representing the distance between the transmitter and the receiver

$R_o^l$ Radius of the outer $l$-th annulus circle

## General Cognitive Radio Network Symbols

$\chi$ PUs' level of protection ($P_D$)

$\eta$ Energy detector's decision threshold

$\lambda$ Non-centrality parameter (Chi-square distribution)

$\mathcal{A}_{in}$ Sensing region

$\mu_{in}$ Mean of $s_{in}^{PU}$

$\mu_{out}$ Mean of $s_{out}^{PU}$

$\rho_{ON}$ Probability of finding a PU active

$\sigma_{in}^2$ Variance of $s_{in}^{PU}$

$\sigma_{out}^2$ Variance of $s_{out}^{PU}$

$\tau^{PU}$ PU's spatial density

$\theta_l^{PU}$ Scale parameter of the Gamma distribution of $I_l^{PU}$

$\Theta_{in}$ Mean of $Y_S$ under hypothesis $\mathcal{H}_1$

$\Theta_{out}$ Mean of $Y_S$ under hypothesis $\mathcal{H}_0$

$A^{PU}$ Total area where the PUs are distributed ($A^{PU} = A_{in} + A_{out}$)

$A_{in}$ Sensing area of the sensing region $\mathcal{A}_{in}$

$A_{out}$ Area outside the sensing region where the PUs are located

$I^{PU}$ PUs' Aggregate Interference ($I^{PU} = I_{in}^{PU} + I_{out}^{PU}$)

$I_{out}^{PU}$ Aggregate Interference caused from PUs located outside $\mathcal{A}_{in}$

$k_l^{PU}$ Shape parameter of the Gamma distribution of $I_l^{PU}$

$M_k^{I_l^{PU}}$ MGF of the interference caused by the $k$-th interferer (PU)

$n^{PU}$ Total number of PUs

$n^{SU}$ Total number of SUs

$N_S$ Total number of spectrum sensing samples

$N_S^*$ Optimal (minimum) number of samples to a required $P_D$

$N_T$ Number of a time frame slots

$P_D$ Probability of detection

$P_{FA}$ Probability of false alarm

$P_T^{PU}$ PU's transmission power

$P_T^{SU}$ SU's transmission power

$R_E$ Outer interference region radius

$R_G$ Sensing Radius

$R_{rec}^{'}$ Normalization of the RV $R_{rec}$ ($R_{rec}^{'} = \frac{R_{rec}}{\sigma_{R_{rec}}}$)

$S^{SU}$ Conditional Throughput of the SUs

$s_{in}^{PU}$ Signal amplitude of the Interference caused by the PUs located within $\mathcal{A}_{in}$

$s_l^{PU}$ Signal amplitude of the Interference caused by the PUs located within $A_l$

$s_{out}^{PU}$ Signal amplitude of the Interference caused by the PUs located outside $\mathcal{A}_{in}$

$S_{rec}$ RV of the signal received by the SU

$s_{rec}$ Received signal by the SU (value)

$T_D^{SU}$ SUs' Transmission Period

$T_F^{SU}$ SUs' Frame length

$T_S^{SU}$ SUs' Sensing Period

$W$ Bandwidth of the sensed channel

$w$ Zero-mean additive white Gaussian noise

$X_l^{PU}$ Number of PUs (RV) located within $A_l$

$Y_{\mathrm{OUT}}$ Energy received from outside of the sensing region

$Y_S$ Energy received in $N_S$ samples

**General MAC layer Symbols**

$D_{ACK}$ Duration of the ACK packet

$D_{CTS}$ Duration of the CTS packet

$D_{PKT}$ Duration of the Data packet

$D_{RTS}$ Duration of the RTS packet

$D_{stg_1}$ Duration of the first stage of the MAC scheme

$D_{stg_2}$ Duration of the second stage of the MAC scheme

$E_{data}^{mmpr}$ Average number of Data packet received of the MAC-MMPRR scheme

$E_{data}^{mpr}$ Average number of Data packet received of the MAC-MPRR scheme

$E_{data}^{spr}$ Average number of Data packet received of the MAC-SPRR scheme

$E_{r^*}$ Maximum of the average number of successful received packets

$E_{rts}^{mmpr}$ Average number of RTS packet received of the MAC-MMPRR scheme

$E_{rts}^{mpr}$ Average number of RTS packet received of the MAC-MPRR scheme

$E_{rts}^{spr}$ Average number of RTS packet received of the MAC-SPRR scheme

$E_r$ Average number of successfully received packets when $r$ simultaneous transmissions occur

$h_{MPR}$ Rational function of the average number of successfully received packets

$n$ Total number of nodes competing for the medium to transmit data to the Rx node

$n_t$ Average number of RTS Packets in $t$-th slot

$p$ Probability of access in the $w$ slots of the reservation stage

$p_t$ Probability of access in the $t$-th slot of the reservation stage

$r$ Coordinate of $E_r$

$r^*$ Coordinate of the maximum of $E_r$

$S^{mmpr}$ Throughput of the MAC-MMPRR scheme

$S^{mpr}$ Throughput of the MAC-MPRR scheme

$S^{spr}$ Throughput of the MAC-SPRR scheme

$t$ $t$-th slot of the reservation stage

$T_a$ Duration of the transmission cycle

$T_{PKT}$ Duration of the successful use of the channel

$w$ Number of RTS slots during the reservation stage

$w*$ Optimal number of RTS slots that maximize the throughput

# ACRONYMS

**ACK** ACKnowledgment.

**AKMA** Algebraic KMA.

**AP** Access Point.

**AWGN** Additive White Gaussian Noise.

**BER** Bit-Error Ratio.

**BMDQ** Bit-Map-assisted Dynamic Queue.

**BS** Base Station.

**CBS** Cyclostationarity-based Sensing.

**CDF** Cumulative Distribution Function.

**CDMA** Code Division Multiple Access.

**CF** Characteristic Function.

**CLT** Central Limit Theorem.

**CR** Cognitive Radio.

**CRN** Cognitive Radio Network.

**CSI** Channel State Information.

**CSMA** Carrier Sense Multiple Access.

**CSMA/CA** Carrier Sense Multiple Access with Collision Avoidance.

**CSMA/CD** Carrier Sense Multiple Access with Collision Detection.

**CTS** Clear to Send.

**DCF** Distributed Coordination Function.

**DIFS** Distributed Inter-Frame Space.

**EBS** Energy-Based Sensing.

**FDM** Frequency Division Multiplexing.

**FDMA** Frequency Division Multiple Access.

**FFT** Fast Fourier Transform.

**GCC** Game for Contention Control.

**GDCW** Generic Distributed Contention Window.

**i.i.d.** independent and identically distributed.

**IC** Interference Cancellation.

**ICI** Inter-Carrier Interference.

**ILWN** Infrastructure-Less Wireless Network.

**ISI** Inter-Symbol Interference.

**KMA** Known Modulus Algorithms.

**LOS** Line of Sight.

**LTE** Long Term Evolution.

**MFBS** Matched Filter-based Sensing.

**M-QAM** M-ary quadrature amplitude modulation.

**M-PSK** M-ary phase shift modulation.

**MAC** Medium Access Control.

**MAC-MMPRR** MAC Protocol with Maximization of the MPR Reservation.

**MAC-MPRR** MAC Protocol with MPR Reservation.

**MAC-SPRR** MAC Protocol with SPR Reservation.

**MAI** Multiple Access Interference.

**MF** Matched Filter.

**MGF** Moment Generating Function.

**MIMO** Multiple Input Multiple Output.

**MLSE** Maximum Likelihood Sequence Estimation.

**MMSE** Minimum Mean Square Error.

**MPR** Multi-Packet Reception.

**MPTR** Multi-Packet Transmission and Reception.

**MQSR** Multi-Queue Service Room.

**MRCR** Multi-Round Contention Random-access.

**MUD** Multi-User Detection.

**MU-MIMO** Multi-User Multiple Input Multiple Output.

**OFDM** Orthogonal Frequency Division Multiplexing.

**OFDMA** Orthogonal Frequency Division Multiple Access.

**PDF** Probability Density Function.

**PHY** Physical.

**PIC** Parallel Interference Cancellation.

**PMF** Probability Mass Function.

**PPS** Polynomial Phase Sequences.

**PU** Primary User.

**QoS** Quality of Service.

**RD** Random Direction.

**RSSI** Received Signal Strength Information.

**RTS** Request To Send.

**RV** Random Variable.

**RWP** Random Waypoint.

**S-ALOHA** Slotted ALOHA.

**SDMA** Space Division Multiple Access.

**SFA** Spatial False Alarm.

**SIC** Successive Interference Cancellation.

**SINR** Signal-to-Interference-plus-Noise Ratio.

**SIR** Signal-to-Interference Ratio.

**SPR** Single-Packet Reception.

**SS** Spectrum Sensing.

**SU** Secondary User.

**TDMA** Time Division Multiple Access.

**USRP** Universal Software Radio Peripheral.

**WBS** Waveform-based Sensing.

**WLAN** Wireless Local Area Network.

CHAPTER 1

# INTRODUCTION

## 1.1 Motivation and Scope

Wireless networks are becoming ubiquitous in modern society. The exponential increasing of data demand and number of wireless devices requires not only novel techniques to improve the efficiency of wireless networks but also network-wide analytical tools to generate insights on the design of truly robust and scalable wireless systems. The wireless networks are roughly divided into Infrastructure Wireless Networks and Infrastructure-Less Wireless Networks (ILWNs). The latter does not require an infrastructure. It is assumed that, once deployed, the nodes of the network would self-configure to provide connectivity and to communicate. In the absence of any Base Station (BS) or mobile switching centers the nodes themselves distributively take responsibility for the organization and control of the network. Thus, such a network is robust against the failure of nodes as the network does not rely on a few critical nodes for its operation. Also, new nodes can be added easily to the network, offering the possibility of integrating ILWNs with other networks, like the Internet [URK+08]. There are many emerging applications for ILWNs including law enforcement, military communications, emergency services, video games, direct communication at conferences and business meetings, and extending the range and capacity of infrastructure-based wireless networks.

Recently there has been a huge development of signal processing techniques that provide more flexible and reliable capabilities, by changing the underlying characteristics of the Physical (PHY) layer. These capabilities enable users to successfully decode multiple transmitted data packets simultaneously. The capability of decoding simultaneously multiple packets at the receiver, which were transmitted from different sources, is named Multi-Packet Reception (MPR) and was firstly analyzed in [Ghe+89].

Traditional Single-Packet Reception (SPR) approach implemented today in most of wireless communication systems considers that if one or more transmitted signals interfere with a received

one they are treated as noise. Consequently, the stack protocols proposed for SPR wireless networks have assumed the classical collision channel model and have been designed to avoid interference. In [GK00], Gupta and Kumar demonstrated that ILWNs do not scale well for the case of multi-pair unicast traffic when nodes are able to encode and decode at most one packet at a time. This has motivated the study of different approaches to increase the capacity of ILWNs.

In the last years a considerable amount of results on capacity improvement of MPR schemes have been presented [GLA+07b; Guo+09; Kar+08; Wan+08]. Summarizing the insights collected in the referred works, we highlight that the capacity of ILWNs can be improved by designing wireless networks with MPR capabilities. Consequently, by adopting MPR techniques the performance and scalability of the ILWNs should further be increased.

Despite the increase of the PHY layer capacity, in the literature only a few works were proposed which incorporate MPR capabilities, and most of them were proposed to Infrastructure Wireless Networks [Din+09; Gan+12; Ngo+08; Per+12; ZT04]. This is due to the fact that ILWNs have been designed without using information from the PHY layer, which is adequate for fixed networks with low time-variability of the links, but fails to grasp the dynamics of the wireless networks and it is therefore unsuitable to explore the advantages of innovative PHY layer techniques such as MPR in an ILWN scenario.

Based on the already proposed works for wireless networks with MPR capabilities, it is well-known that MPR techniques increase the throughput capacity of wireless networks [Sad+10]. MPR channels can be found in time-slotted uplink random access of IEEE 802.16e systems [Bibb], 3GPP Long Term Evolution (LTE) [GPP], or even in the Multi-User Multiple Input Multiple Output (MU-MIMO) technology of the IEEE 802.11ac PHY layer [Bibc]. More recently, decentralized PHY/MAC techniques for the uplink of MPR schemes have attracted great interest. These are being motivated by the next generation of the Wifi systems (e.g. IEEE 802.11ax [Bel16]). The adoption of MU-MIMO in the uplink of the next generation Wifi systems will certainly demand for high performance decentralized PHY/MAC schemes. MPR is inherently a many-to-one communication approach, which is particularly useful for the uplink. The adoption of MPR in the PHY layer demands for new scheduling policies able to combine the signals from different sources in an efficient way, rather than avoiding interference. The scheduling should simultaneously allow the exact number of nodes' transmissions that matches the MPR's capability (i.e. maximum number of simultaneously successful decodable packets). This greatly improves the chances that concurrent transmissions may be successfully decoded.

Regarding the scheduling policies in ILWNs, another issue arises from the fact that the wireless channel is controlled in a decentralized way. In a shared channel multiple interferers may decrease the communication performance because they are not controlled by a central entity capable of mitigating the spatial interference. This fact is of particular importance as the density of nodes increase, because the nodes far away from the receiver may also cause non-negligible interference. Therefore, it is necessary to use an accurate interference model for each MPR technique to statistically characterize the performance of the receiver. Thus, an accurate interference model is critical to assess the effective performance of the MPR-based PHY layer. The interference model must be accurate and take into account all effects of radio propagation (e.g. path loss, slow and fast fading)

and topology scenarios (e.g. mobility, spatial interference).

The medium access scheduling based on the interference model aims to maximize spatial reuse and minimize retransmissions due to collisions. When compared to SPR, MPR increases the number of PHY/MAC parameters, highlighting the importance for cross-layer design. Motivated by the importance of the ILWNs, the advantages of the MPR communication schemes and the challenges related to the adoption of MPR in ILWNs, we explore a new PHY/MAC cross-layer design approach to integrate advanced PHY layer techniques in a single architecture.

We start by considering an ILWN scenario where $n$ nodes transmit data simultaneously to a single receiver with MPR capabilities. Each node's architecture is based on a cross-layering design between the PHY and the MAC layer. The performance of the MPR-based PHY layer is characterized in a generic way, therefore to be adopted in the joint PHY/MAC cross-layer optimization. The generic MPR-based PHY layer performance characterization takes into account the impact the propagation effects (i.e., path loss, small-scale fading and shadowing), the decision threshold that characterizes the receiving system, as well as the noise at the receiver side.

Due to the distributed nature of ILWNs, and the fact that nodes simultaneously cooperate and compete for the network resources, we assess the ILWN performance when operating in shared bands. The MPR-based PHY layer performance is also characterized in a generic way.

After having characterized the MPR PHY layer performance, we propose three novel decentralized reservation-based MAC schemes to coordinate the access of multiple transmitters adopting an MPR-based PHY layer. Adopting a generic model for the PHY layer, the throughput achieved by the proposed MAC schemes is characterized when both MAC and PHY layers are considered. The performance of two of the three proposed MAC schemes is evaluated under different scenarios. Then, considering the results of these two MAC schemes and using a similar reservation-based concept, we characterize the throughput achieved by the third decentralized MAC protocol. In the third MAC scheme the access policy during the reservation is redesigned in order to achieve the optimal throughput at the PHY layer. An optimal parameterization of the MAC parameters is proposed, where the number of transmitters is regulated to optimize the cross-layer operation, taking into consideration the features of the MPR PHY layer and the maximum throughput achieved with the proposed MAC design.

## 1.2 Research Question and Hypothesis

This section states the research question and its respective hypothesis, and the candidate's general approach over the same question. The research question is stated as follows:

*Considering an ILWN adopting MPR transmission techniques at the PHY layer, how should the nodes be orchestrated in terms of medium access in order to increase the networks' throughput?*

The research question can be addressed by the following hypothesis:

*A scalable ILWN adopting MPR techniques can be achieved through specific cross-layered PHY/MAC design, which drives to an improvement of throughput capacity.*

## 1.3 Objectives

Regarding the context of this thesis, the following research goals were defined:

1. Specification of the main features of the PHY/MAC architecture;
2. Development of interference models for ILWN communication systems;
3. Exploitation a generic PHY layer performance model;
4. Architect the optimization-based PHY/MAC scheme for decentralized coordination;
5. Optimal parameterization of the MAC layer based on the joint PHY/MAC interaction;
6. Comparison of the analytical values with the simulated values;
7. Dissemination of the results in relevant scientific conferences and journals.

## 1.4 Contributions

The major contribution of this work is the design of novel PHY/MAC cross-layer architectures for ILWNs adopting MPR techniques. Starting by the PHY layer, we studied the performance of a PHY layer with MPR capabilities considering a wireless network where $n$ nodes transmit data simultaneously to a single node (the receiver node). In a first modeling approach, a near-field and a far-field scenarios were considered. In these scenarios, the MPR-based PHY layer performance was characterized by the individual probability of successful packet reception and the number of received packets when $n$ nodes transmit simultaneously to a single receiver [Fur+16c]. In a second modeling approach the aggregate power was approximated by the product of Gamma Characteristic Functions (CFs), which is used to derive the probability of successful packet reception and the average number of received packets [Fur+17b]. As a main contribution of this work, both MPR-based PHY layer performance characterizations take into account the path loss effect, small and large-scale fading propagation effects, the decision threshold that characterizes the receiving system, as well as the influence of noise at the receiver side. The simplicity of the models, as well as their accuracy, makes them a useful tool to assist the design of future MAC mechanisms for MPR wireless systems. Further, the second modeling approach reveals a lower computational complexity when compared to the first one and is better suited to scenarios of high density of transmitters. The impact on the PHY layer performance due to different propagation effects and the noise at the receiver is also studied. The proposed models allow to compute the optimal number of transmitters, $n^*$, for a given receiving threshold, which is an important departing point to design efficient MAC techniques for MPR systems.

With a special focus on the spatial interference problem, the performance of ILWN operating in a shared band was also analyzed for high density of transmitters. We have considered an ILWN network operating in a shared band where each transmitter may adopt an SPR or an MPR-based PHY layer. The performance is assessed in terms of the conditional throughput achieved by the

receiver (i.e. the throughput achieved when the channel is declared idle by the receiver). From the point of view of the transmitters nodes, the spectrum is always sensed before transmitting. In this way the receiver node can postpone the transmission(s) intended to it when high levels of interference are sensed in the channel. In terms of channel sensing, we have analyzed the impact of the path loss on the probabilities of detection and false alarm and on number of samples needed to perform the spectrum sensing with a given probability of detection [Fur+14a]. More importantly, we evaluate the upper bound of the conditional throughput achieved by the ILWN [Fur+16b]. The bound captures the impact of the Spatial False Alarm (SFA) on the spectrum sensing detection probability and on the interference caused to the SPR communication process by the transmitters located outside the sensing region. Additionally to SPR communications assumption, we also consider MPR communications. In this context, the MPR-based PHY layer performance is characterized in a generic way taking into account the path loss effect, the decision threshold that characterizes the MPR receiving system, as well as the influence of the interference caused by the nodes transmitting outside the sensing region.

Having characterized the MPR-based PHY layer in a formal way, we have characterized the design of MAC schemes with MPR capabilities. First we proposed two novel decentralized reservation-based MAC schemes to coordinate the access of multiple transmitters adopting an MPR-based PHY layer for ILWN [Fur+16a; Fur+17a]. The proposed MAC schemes operate over an MPR-based PHY layer and are divided in two stages. In the first stage, which is called Reservation stage, the nodes indicate their willingness to transmit, while in the second one they jointly transmit. The two MAC schemes differ by considering an SPR or an MPR PHY layer in the Reservation stage. Adopting a generic model for the PHY layer, the throughput achieved by the proposed MAC is characterized when both MAC and PHY layers are considered. The performance of the proposed MAC schemes is evaluated under different scenarios. The results obtained through simulation and numerical results indicate the advantages of our solution (in terms of throughput), identifying optimal points of operation.

We have also proposed the design of a third MAC protocol, but this time an optimal parameterization of the MAC parameters is proposed, having into account the joint PHY/MAC interaction [Fur+18a; Fur+18b]. The throughput achieved by the cross-layer scheme is characterized, by modeling the performance of the PHY layer and the random MAC scheme. An optimization algorithm to derive the optimal duration of the Reservation stage of the MAC scheme was proposed. In this way, the number of transmitters is regulated to optimize the cross-layer operation, taking into consideration the features of the MPR PHY layer and the maximum performance achieved with the proposed MAC design.

The following works are considered minor contributions because they are out of scope of this thesis. However all of them contributed somehow to the development, improvement and recognition of the work presented in this document. In [Iri+15] we characterized the wireless interference of an ILWN where the nodes move according to the Random Waypoint (RWP) model. The main contribution was the characterization of the expectation of the aggregate signal received by a fixed node from mobile transmitters located outside the sensing region. The characterization of the interference accounts with the stochastic nature of the path loss due to the mobility of the nodes.

In [Dua+14] we addressed the assessment of energy detection for cognitive radio systems. The performance of an energy detector was characterized through Universal Software Radio Peripheral (USRP) devices. The theoretical performance was successfully validated through practical results. Considering a non-constant licensed users' behavior, we characterize the interference caused by the licensed users [Lui+13]. The results show that when the length of the licensed users' frame is considerably large when compared to the non-licensed users' frame, it is reasonable to assume a constant licensed users' behavior with respect to the non-licensed users' frame. [Fur+13] characterizes the channel availability assessment performed by a non-licensed user adopting an energy detector and assuming a constant and non-constant licensed users' behavior. Finally, departing from a classical random access scheme for Cognitive Radio Networks (CRNs), we derived a solution to estimate the level of activity of the licensed users using the data available at the MAC layer of each non-licensed user [Fur+14b]. Based on the estimation of activity level of the licensed users, it is proposed a solution to regulate the medium access of the non-licensed users in order to maximize the network throughput.

The work in [Oli+13] presents a novel MAC algorithm for single-hop distributed wireless networks designed to increase the reliability regarding the transmission of broadcast messages. The algorithm is mainly motivated by the shared view of the channel where the individual medium access probability and the probability of sensing an idle slot are used to estimate the number of competing nodes.

The list of publications during the PhD period are as follows:

Journal Papers:

- [Fur+16c] A. Furtado, R. Oliveira, R. Dinis, L. Bernardo, "Successful Packet Reception Analysis in Multi-Packet Reception Wireless Systems", IEEE Communications Letters, December, 2016;
- [Fur+16b] A. Furtado, L. Irio, R. Oliveira, L. Bernardo, R. Dinis, "Spectrum Sensing Performance in Cognitive Radio Networks with Multiple Primary Users", IEEE Trans. on Vehicular Tech, March, 2016.
- [Lui+13] M. Luis, A. Furtado, R. Oliveira, R. Dinis and L. Bernardo, "Towards a Realistic Primary Users' Behavior in Single Transceiver Cognitive Networks',' IEEE Communications Letters, February 2013.
- [Oli+13] R. Oliveira, M. Luís, A. Furtado, L. Bernardo, R. Dinis, P. Pinto, "Improving path duration in high mobility vehicular ad hoc networks", Ad Hoc Networks, 2013.

Conference Papers:

- [Fur+18a] A. Furtado, R. Oliveira, L. Bernardo, R. Dinis, "Decentralized PHY/MAC Design for the Uplink of Multi-Packet Reception Wireless Networks", IWCMC, June, 2018;

- [Fur+18b] A. Furtado, R. Oliveira, L. Bernardo, R. Dinis, "Optimal Cross-Layer Design for Decentralized Multi-Packet Reception Wireless Networks", Vehicular Technology Society 2018 IEEE 87th VTC2018-Spring, Porto, Portugal, June, 2018;
- [Fur+17b] A. Furtado, D. Vicente, R. Oliveira, L. Bernardo, R. Dinis,"Performance Analysis of Multi-Packet Reception Wireless Systems in Far-field Region", IWCMC, Valencia, Spain, June, 2017;
- [Fur+17a] A. Furtado, D. Vicente, R. Oliveira, L. Bernardo, R. Dinis, "Performance Analysis of a Distributed MAC Scheme for Multi-Packet Reception Wireless Networks", IWCMC, Valencia, Spain, June, 2017;
- [Fur+16a] A. Furtado, R. Oliveira, R. Dinis, L. Bernardo,"A Distributed MAC Protocol for Multi-Packet Reception Wireless Networks", IEEE PIMRC, Valencia, Spain, September, 2016;
- [Iri+15] L. Irio, A. Furtado, R. Oliveira, L. Bernardo, R. Dinis, "Path Loss Interference in Mobile Random Waypoint Networks", European Wireless 2015, Budapest, Hungary, May, 2015;
- [Fur+14b] A. Furtado, M. Luís, L. Irio, R. Oliveira, L. Bernardo, R. Dinis, "Detection of Licensed Users' Activity in a Random Access Ultra Wideband Cognitive System", IEEE ICUWB, Paris, France, September, 2014;
- [Fur+14a] A. Furtado, L. Irio, R. Oliveira, L. Bernardo, R. Dinis, "Characterization of the Spatial False Alarm effect in Cognitive Radio Networks", IEEE ICCCN, Shanghai, China, August, 2014;
- [Dua+14] M. F. Duarte, A. Furtado, M. Luís, L. Bernardo, R. Dinis, R. Oliveira, "Practical Assessment of Energy-Based Sensing through Software Defined Radio Devices", DOCEIS, Lisboa, Portugal, April, 2014;
- [Fur+13] A. Furtado, M. Luís, R. Oliveira, R. Dinis, L. Bernardo, "Channel Availability Assessment for Cognitive Radios", DOCEIS, Lisboa, Portugal, April, 2013.

## 1.5 Document Structure

This thesis is structured in a total of 6 chapters and 2 appendices, organized as follows:

- Chapter 2 provides an overview of the literature. This chapter is divided into three sections. The first section describes the current works already approaching MPR schemes for the PHY layer. The second section presents recent studies related to the characterization of the aggregate interference. Section 2.3 introduces the MAC protocols already proposed in the literature for networks with MPR capability;
- Chapter 3 proposes two generalized analytical models to characterize the PHY layer performance of MPR schemes. The models rely on the computation of the individual probability of successful packet reception and on the number of received packets when $n$ simultaneous

transmissions. The first modeling approach characterizes the MPR-based PHY layer for near-field and far-field scenarios. In the second approach, a Gamma distribution approximation of the aggregate interference generated by the transmitters is explored.

- Chapter 4 evaluates the performance of an ILWN operating in shared channels, considering that each node uses an energy-based spectrum sensing technique and adopts a PHY layer with SPR or MPR capabilities. A sensing parameterization criterion is proposed and evaluated based on the conditional throughput achieved by the ILWN. This chapter identifies the advantages of adopting a spectrum sensing behavior to avoid undesired levels of interference in shared channels.

- Chapter 5 focuses on the design of decentralized MAC schemes for ILWNs with MPR capabilities. Three MAC schemes are designed in a distributed way and follow a reservation policy based on two stage (Reservation stage and Data Transmission stage). The proposed MPR MAC protocols are: the MAC Protocol with SPR Reservation (MAC-SPRR), the MAC Protocol with MPR Reservation (MAC-MPRR) and the MAC Protocol with Maximization of the MPR Reservation (MAC-MMPRR). The protocols are modeled and evaluated considering the characterization of the PHY/MAC cross-layer. Taking into consideration the joint PHY/MAC interaction, we proposed an optimal parameterization of the MAC parameters, for the MAC-MMPRR scheme.

- Chapter 6 presents the conclusions as well as some guidelines about future work;

- Appendices A and B detail some of the mathematical derivations used to support the PHY layer performance model.

CHAPTER 2

# LITERATURE REVIEW

This chapter presents a comprehensive literature review of current trends and challenges that encompass Multi-Packet Reception (MPR) communication systems. Section 2.1 overviews known Physical (PHY) layers supporting MPR. Recent studies related with the characterization of the aggregate interference are described in Section 2.2. Finally, Section 2.3 introduces different Medium Access Control (MAC) protocols for MPR schemes.

## 2.1 PHY Layer Supporting MPR

Significant improvements to both throughput and capacity of a wireless network can be obtained with MPR. Multiple techniques implement MPR by allowing simultaneous decoding of packets at the receiver. Based on current research achievements related with MPR, this section provides an overview of the PHY layer technologies capable of implementing the MPR concept.

### 2.1.1 PHY Layer Technologies

This subsection introduces several technologies with MPR capabilities adopted at the PHY layer. The description is divided on three different technologies: Code Division Multiple Access (CDMA), Orthogonal Frequency Division Multiplexing (OFDM) and Multiple Input Multiple Output (MIMO).

#### 2.1.1.1 CDMA

In communications the term multiplexing refers to the method of allowing multiple transmitters to send messages simultaneously over a given domain (time, space, frequency, etc.). In Time Division Multiple Access (TDMA), the access to the channel is shared in the time-domain. The nodes transmit in different time slots to have exclusive access to the channel. In Frequency Division Multiple Access (FDMA), the channel access is divided by frequency. The nodes transmit in

different non-overlapping bands. TDMA and FDMA have been adopted in the majority of communication systems. In the last decades we have assisted to the adoption of different multiplexing techniques. CDMA is a channel access method which utilizes spread spectrum technology and orthogonal or pseudo-orthogonal coding schemes to allow multiple users to access a single channel simultaneously. CDMA is currently used by various radio communication technologies [KR02]. At the transmitter side, a locally generated pseudo-random code, called chipping code, runs at a much higher rate than the data to be transmitted [MK03]. The modulation procedure consist on multiplying the data with the chipping code through a Kronecker product [Lau04]. In addition, each user uses a different code to modulate their signal and the code assignment is very important in a CDMA system. At the receiver side, the separation of the signals is made by correlating the signal with its local generated code. If the signal matches with the receiver's code, the signal is destined to the receiver and the transmitted message is decoded. Otherwise, the message is not successfully decoded.

#### 2.1.1.2 OFDMA

OFDMA is a multiuser version of the OFDM digital modulation scheme. Multiple access is achieved in OFDMA by assigning to the transmitters of a single receiver different OFDM sub-channels. This allows simultaneous transmissions from several users to a single receiver.

The principle of a Frequency Division Multiplexing (FDM) system is to split the information to be transmitted into $N$ parallel streams, each of which modulate a carrier using an arbitrary modulation technique. The signal bandwidth over each carrier is $\Delta f$, resulting in a total signal bandwidth of $N \times \Delta f$. In addition, a guard band $G_f$ is introduced to separate the adjacent channels, which means a lower utilization efficiency of the spectrum. OFDM is a special case of FDM in which multiple symbols are transmitted in parallel using different sub-carriers with overlapping frequency bands that are mutually orthogonal. The orthogonality is used to fully utilize the available bandwidth as well as eliminate the interference between the adjacent sub-carriers.

OFDM is a multi-carrier transmission scheme that is well-recognized for its potential for attaining high rate transmission over frequency selective channels. OFDM has several significant advantages: robustness to multipath fading, inter-symbol interference, co-channel interference, and impulsive parasitic noise. Moreover, it presents low implementation complexity when compared to single-carrier solutions and achieves high spectral efficiency in supporting broadband wireless communications.

Because the symbol duration of a narrowband signal will be larger than that of a wideband signal, the amount of time dispersion caused by multipath delay spread can be reduced [Mar+09]. However, OFDM systems are more sensitive to synchronization errors than single carrier systems. Incorrect timing synchronization can introduce Inter-Symbol Interference (ISI) and Inter-Carrier Interference (ICI), which can degrade the system performance severely [Spe+99]. Thus, timing synchronization is a crucial part of OFDM receiver design.

To eliminate ISI caused by delay spread, it is inserted a guard interval (usually two to four times longer than the expected delay spread) so that the multipath components from one symbol

cannot interfere with the next symbol.

Regarding the ICI problem, conventional OFDM receivers require that the channel remains constant within the block duration. If the channel changes within the block duration there can be introduced a frequency offset in the sub-carrier. Therefore, the performance of the communication system would degrade significantly due to the loss of orthogonality among the sub-carriers. A frequency offset can be introduced by relative motion between the transmitter and the receiver (Doppler spread) [Jia+10] and by the inaccuracies in the Local Oscillator [Din+04]. In order to prevent this problem, an OFDM system should have an accurate frame synchronization and frequency offset estimation for maintaining orthogonality among the sub-carriers [SC97].

#### 2.1.1.3 MIMO

A MIMO system uses multiple antennas at both the transmitter and the receiver to improve the performance of communications. MIMO technology is able to offer significant increases in data throughput without additional bandwidth or transmit power. By using antenna array, the MIMO systems are able to achieve Space Division Multiple Access (SDMA) based on the principle of spatial multiplexing. In spatial multiplexing, high data rate signals are divided into multiple low data rate streams and each of these streams is transmitted by different antennas in the same frequency band. The receiver is able to distinguish these streams if they have sufficiently different spatial signatures at the receiver side. In such a way, it can be used for simultaneous transmission to multiple receivers, which is called SDMA [TV05]. In addition, in MIMO systems, the maximum number of spatial streams transmitted in the channel is limited by the number of antennas at the transmitter or receiver. In MIMO systems, a basic problem of the signal separation is to design a channel estimator that allows a receiver to extract its intended packets. The channel estimator design strongly depends on the knowledge of the channel impulse response and the transmission format.

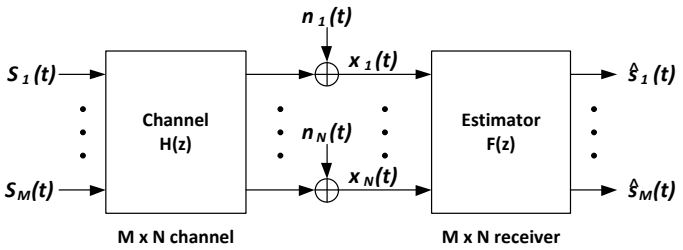


Figure 2.1: A general MIMO model for multiuser communication and MPR receiver.

Figure 2.1 illustrates a general model of the signal separation at the MPR PHY layer [Ton+01]. In the model, $M$ users transmit to a receiver equipped with $N$ antenna array elements. Let $s_i(t)$ denote a transmitted signal from the $i$-th user, $i \in 1,...,M$, and $x_j(t)$ denote a received signal from the $j$-th antenna array element, $j \in 1,...,N$. The received signal relies on the channel noise $n_j(t)$ at the $j$-th antenna. For the signal separation, the receiver needs to detect the multiple transmitted

signals by estimating them based on the multiple observed signals. The estimated signal $\hat{s}_i(t)$ of the $i$-th user can be obtained with an estimator $F(z)$. The design of the estimator relies on the channel impulse response $H(z)$ and also depends on the adopted modulation, the transmission protocol, and the configuration of the transceiver antenna array.

### 2.1.2 PHY Technologies implementing MPR

Traditional MPR techniques were previously summarized in Subsection 2.1.1. Based on the current literature, MPR implementation techniques can be grouped in three different categories: Transmitter Perspective, Transceiver Perspective and Receiver Perspective.

#### 2.1.2.1 Transmitter Perspective

The first category of techniques that enable MPR require a significant effort by the transmitter. Examples such as CDMA and OFDMA fall into this class.

CDMA technique, as described before, allows the receiver to decode multiple data streams with the different codes that are known *a priori*. The ability to decode multiple data packets depends on the selection of the code. For example, the orthogonality is the key that allows the receiver to decode the set of simultaneous signals, and this is performed at the transmitter side.

OFDMA competes with CDMA as a major multi-access technique. As described before, OFDMA is used to increase the wireless channel efficiency based on multi-carrier modulation methods (in IEEE 802.11 a,g,n). With OFDMA, the MPR capability is enabled on a frequency basis, since the sub-channels do not interfere with each other. In [Mor+07], the authors describe a many-to-many communication system in which the transmissions are divided in the frequency domain. Again, OFDMA enables MPR with a great effort for the transmitter in sub-channel selection. Furthermore, it is a pseudo MPR capability, because the bandwidth is also divided at the same time, when the radio channel is divided into sub-channels.

#### 2.1.2.2 Transceiver Perspective

This category includes the PHY technologies that enable MPR capabilities based on the cooperation between the transmitters and the receivers. One of this PHY technology is MIMO [Hua+08], which can achieve MPR by exploiting the spatial diversity of the transmissions. The realization of MPR in a multi-antenna MIMO system requires both transmitters and receivers to implement specific functionalities.

Besides the techniques described in Subsection 2.1.1, there are other MPR techniques that fall into this category, including: Signal Separation [DN00], Polynomial Phase Sequences (PPS) [OL+03] and Resource Allocation [Tsa+00].

The problem of packet separation can be formulated as a signal separation in a MIMO system. In [VT02], the authors present Known Modulus Algorithms (KMA) to allow packet separation in an asynchronous ILWN. In the algorithm, a transmitter needs to send a constant modulus signal multiplied by an amplitude modulating code known at the receiver and an antenna array is used

on the receiver side, which can detect and filter out the desired user among the other interfering signals with the help of the modulation code. The modulation code can be a random binary sequence determined either by the transmitter or the receiver. Also, in [Wu+08] it is proposed a variation of KMA, Algebraic KMA (AKMA), which is based on a matrix perturbation analysis.

In [OL+03], the authors enabled MPR by proposing an algorithm which exploits the fact that the baseband signal exhibits cyclostationarity properties, which are induced at the transmitters after modulation with PPS. Furthermore, the proposed modulation does not expand the bandwidth and can be considered as a color code to distinguish packets from different users.

At last, resource allocation base techniques are mainly based on a network-assisted approach. The network-assisted diversity was firstly introduced in [Tsa+00] as a technique to separate the packets involved in a collision. The collided packets are kept in memory rather than being discarded, and are later combined with future retransmissions to extract the information of the packets involved in the collision. The proposed method is suitable for multiplexing variable-bit-rate sources without affecting the PHY layer bit rate parameter of each source. In [WT03] the authors proposed a Bit-Map-assisted Dynamic Queue (BMDQ) protocol, where the traffic in the channel is viewed as a flow of transmission periods, each of which has a bit-map slot for user detection so that accurate knowledge of active users can be obtained. To summarize, resource allocation reuses signal processing principles at the packet level.

#### 2.1.2.3 Receiver Perspective

The last category includes the techniques that only involve the receiver to decode several packets simultaneously. Among the three categories, this is the one that is closer to the ideal MPR, given that it shifts the responsibility from the transmitters to the receivers.

The Matched Filter (MF) approach is widely used for single user detection. In [Cou+04] MPR capabilities are enabled by using a receiver which can use a bank of MF to decode packets coded with spreading codes that do not even need to be orthogonal. This solution is not optimal when both noise and/or interference are non-gaussian.

Techniques used to separate signals for Multi-User Detection (MUD) are more applicable for MPR because it is a way to alleviate Multiple Access Interference (MAI) during the simultaneous transmissions on the same channel. The MUD detectors can be optimal (e.g. Maximum Likelihood Sequence Estimation (MLSE)) or suboptimal (e.g Minimum Mean Square Error (MMSE)). An optimal detector exhibits high performance in a scenario with central control, which guarantees synchronization among different users [Li+07]. For ILWN application, optimal detectors are too complicated to implement, since it is quite difficult to apply signal processing techniques to separate the asynchronous transmissions.

In suboptimal MUD detectors, two approaches can be identified, linear and nonlinear MUD. In linear MUD, a linear transformation is applied to the soft outputs of the conventional detector in order to produce a new set of decision variables with MAI greatly decoupled. Two of the most cited linear MUDs are the decorrelated detector [LV90] and the MMSE detector [Cou+04]. They are generally complex but the joint detection of all users makes the MUD very robust to near-far

problems. The near-far problem occurs when a stronger received signal imposes a higher noise level in the demodulators for weaker signals, decreasing the probability of successful decoding.

On the other hand, non-linear MUD techniques use interference estimators and remove the interference from the received signal before detection. They are much simpler but have a lower performance when compared to the linear MUD [Mos96]. Multistage Interference Cancellation (IC) is one of the most interesting techniques in this category, where interference cancellation can be carried out either successively (SIC) or in parallel (PIC). For SIC [ZZ12], the multi-user's signals are demodulated and cancelled from the strongest to the weakest according to their received signal power. For PIC [Bue+96], without having the exact knowledge of the interfering bits, their estimates in the previous stage are used instead.

Figure 2.2 presents a tree with the classification of different techniques that may be applied in the ILWN PHY layer responsible for the implementation of the MPR capability.

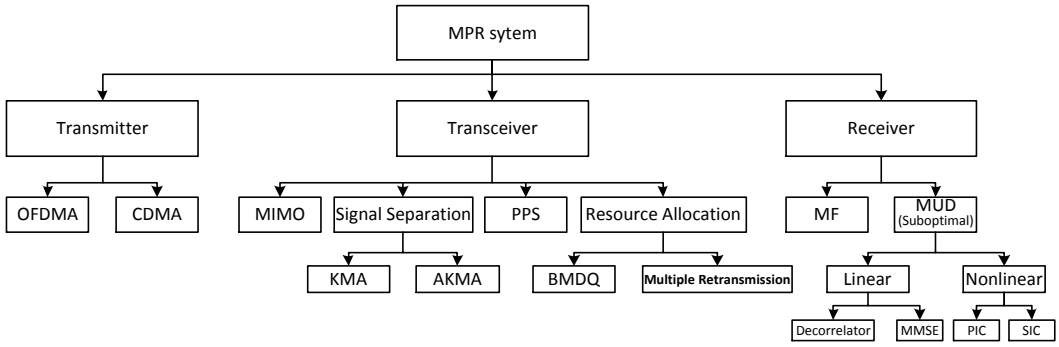


Figure 2.2: Classification of MPR techniques applied in the PHY layer (adapted from [Lu+12]).

### 2.1.3 MPR Models

An MPR model determines the probability of receiving a packet when a certain number of other packets are transmitted simultaneously, which is called capture probability. Introductory non-MPR models for the capture probability in decentralized networks were described in the seminal work of Gupta and Kumar [GK00], which are known as protocol and physical models. More complex models, such as the MPR protocol model in [Ghe+89], combine both protocol and physical models. Next, the protocol and the physical non-MPR models are described and different MPR models are introduced.

#### 2.1.3.1 Protocol Model

The protocol model gives a geometric interpretation of signal propagation, according to which the reception of the signal only depends on the distance between the different transmitters and the common receiver.

Assuming nodes that transmit omni-directionally, let $r_{ij}$ be the distance between nodes $i$ and $j$.

A communication from node $i$ to node $j$ is successful if [GK00],

$$r_{kj} \geq (1 + \Delta) r_{ij}, \tag{2.1}$$

for every other node $k$ simultaneously transmitting over the channel. Once Equation (2.1) is satisfied, it is assumed that the data rate over the link is constant and greater than zero. The quantity $\Delta \geq 0$ is a parameter that depends on the features of the PHY layer. It models cases where a guard zone is specified by the protocol to prevent a neighboring node from transmitting on the same channel at the same time. It also allows for imprecision in the achieved range of transmissions. The protocol model inherently implies that disk areas centered at concurrent receivers are disjoint.

A common assumption is the fact that nodes are homogeneous, i.e., all transmissions employ the same transmission power, which leads to definition of the transmission range. Under the assumption of homogeneous transmission power, the transmission range $R_{\mathrm{Tx}}$ is defined as the maximum distance from which a receiver node can successfully receive a packet.

Based on the definition of transmission range and assuming that all nodes employ the same transmission power, the conditions for successful transmission under the protocol model can be restated as follows. A transmission from node $i$ to node $j$ is successful if, [GK00]

$$r_{ij} \leq R_{\mathrm{Tx}} \Leftrightarrow r_{kj} \geq (1 + \Delta) R_{\mathrm{Tx}}, \tag{2.2}$$

for every other node $k$ simultaneously transmitting over the same channel.

#### 2.1.3.2 Physical Model

The physical model explicitly includes the physical propagation phenomena and the cumulative character of interference in the MPR model, considering the random distribution of the signal powers at the receiver and introducing the Signal-to-Interference-plus-Noise Ratio (SINR) criterion to determine the probability of successful reception of a packet.

Again, it is assumed that nodes transmit omni-directionally. Let $k \in T$ be the subset of nodes simultaneously transmitting over a common Additive White Gaussian Noise (AWGN) channel. Let $P_{ij}$ be the power level of the signal received at node $j$ from node $i$. Then, the transmission from node $i \in T$ is successfully received by node $j$ if [GK00],

$$\frac{P_{ij}}{\eta + \sum_{\forall k \in T; k \neq i} P_{kj}} \geq \delta. \tag{2.3}$$

Once this constraint is satisfied, it is assumed that the data rate over the link is constant and greater than zero. Equation (2.3) models a situation where a minimum SINR of $\delta$ is necessary for successful reception, when a set $T$ of nodes simultaneously transmit. The $\delta$ parameter is often referred in the literature as the capture threshold. $\eta$ represents the zero-mean AWGN.

In radio transmissions, the power of a signal transmitted from node $i$ to node $j$ is attenuated according to the distance between them. Equation (2.4) states that the signal power decays exponentially according to the distance $d_{ij}$ between nodes $i$ and $j$ and depends on the path loss model.

$$P_{ij} = P_{Tx} \psi_{ij} d_{ij}^{-\alpha}. \tag{2.4}$$

$\alpha$ is known as the path loss coefficient, while the $\psi_{ij}$ is the term accounting for other factors such as the gain of transmitter and receiver antennas. $P_{Tx}$ is the transmission power of the node $i$.

Based on the Shannon's capacity for an AWGN channel, the maximum data rate of the physical model can be stated as follows

$$c_{ij} = W \log_2 \left( 1 + \frac{P_{ij}}{\eta + \sum_{\forall k \in T; k \neq i} P_{kj}} \right), \tag{2.5}$$

where $W$ is the bandwidth of the channel in Hertz.

#### 2.1.3.3 Models for PHY Layer with MPR capabilities

The protocol and physical models do not consider wireless networks where the devices adopt MPR technologies. In these networks nodes may be capable of receiving multiple packets simultaneously, and there may be unexpected reception errors due to time varying channels effects. In this section, different models that characterize the PHY layer with MPR capabilities are presented.

In [Ghe+88] and [Ghe+89] the authors proposed a model for a symmetric MPR channel where a matrix of probabilities represent the chance of receiving a packet (in a slotted random access setup) for a given number of concurrent transmitted packets. Let $\epsilon_{n,k}$ denote the probability of successfully receiving $k$ packets out of $n$ packets transmitted simultaneously. The following matrix uniquely defines a generic MPR channel

$$E = \begin{bmatrix} \epsilon_{1,0} & \epsilon_{1,1} & 0 & 0 & \cdots \\ \epsilon_{2,0} & \epsilon_{2,1} & \epsilon_{2,2} & 0 & \cdots \\ \vdots & \vdots & \vdots & \vdots & \cdots \\ \epsilon_{n,0} & \epsilon_{n,1} & \cdots & \epsilon_{n,n} & \cdots \\ \vdots & \vdots & \vdots & \vdots & \ddots \end{bmatrix}. \tag{2.6}$$

This model is generic and includes special cases of interest. For example, the collision channel corresponds to

$$E_{col} = \begin{bmatrix} 0 & 1 & 0 & 0 & \cdots \\ 1 & 0 & 0 & 0 & \cdots \\ 1 & 0 & 0 & 0 & \cdots \\ 1 & 0 & 0 & 0 & \cdots \\ \vdots & \vdots & \vdots & \vdots & \ddots \end{bmatrix}. \tag{2.7}$$

Another example is the capture of a single reception that takes the form of

$$E_{cap} = \begin{bmatrix} 0 & 1 & 0 & 0 & \cdots \\ 1 - x_2 & x_2 & 0 & 0 & \cdots \\ 1 - x_3 & x_3 & 0 & 0 & \cdots \\ 1 - x_4 & x_4 & 0 & 0 & \cdots \\ \vdots & \vdots & \vdots & \vdots & \ddots \end{bmatrix}, \tag{2.8}$$

where $x_n$ denotes the capture probability in the presence of $n$ transmissions. In the model above $E$ represents an MPR channel if at least for $1 < k \leq n$ we have $\epsilon_{n,k} > 0$. Although generic and flexible, this model requires an analytical or experimental method to determine a potentially large number of parameters, namely $\epsilon_{n,k}$ for several values of $n, k$. Also, the model is symmetric as it does not distinguish between different nodes.

If the system is not symmetric and the probability of successful reception of a node's packet is different from other nodes, a more general model is required where $\epsilon_{S,R}$ takes all the possible subsets $S$, $R$ of nodes, instead of only their cardinalities $n = |S|$, $k = |R|$. Such a model was proposed in [Naw+05], which requires an exponentially growing number of parameters and has had limited use in the literature.

In [ZZ12] the authors adopt a physical model and characterize an MPR system by deriving an analytical expression of the capture probability. In MPR systems the capture probability is related with the probability of $r$ signals out of $n$ being successful received. The authors presented an extension of the analysis to SIC systems, by defining an expression for the probability that $r$ signals out of $n$ are decoded by a receiver capable of performing up to $K$ interference cancellation iterations. The approach, adopted in [ZZ12], is similar to other works, such as [Ngu+06], but the solution proposed in [ZZ12] has lower computational complexity.

In [WGLA08] it is adopted a protocol model and it is assumed that the receiver can successful receive multiple signals transmitted within its reception range, provided that all other (interfering) transmitters are further away from the receiver. This approach makes it possible to carry out elegant performance analysis and to derive closed-form bounds for the system capacity in different scenarios, but relies on an idealized and rather unrealistic model.

A different approach is adopted in [Yim+09] to enable MPR capabilities at PHY layer. The authors developed the Dual Power Multiple Access with MPR using Local Channel State Information (CSI) scheme under the context of a structured random access channel. In their work, local CSI and Received Signal Strength Information (RSSI) measurements are used to simplify the receiver's design. Based on CSI, power levels at the receiver are limited to two values to enhance SIC. For example, two colliding packets with different power levels can be successfully decoded if the ratio between the received signal from the transmitter with the highest signal strength and the SINR of the channel plus the received signal from the transmitters with the lowest signal strength is higher than a given decoding threshold. If more users are involved, the receiver is able to decode the packet from an user with the highest signal strength when up to $Q_{max}$ lower signal strength users are involved. The remaining $Q_{max}$ transmitters with the lower signal strength should contend the channel with different power levels according to a pilot sequence from the Base Station (BS).

More recently, Babich et. al. analyzed in [BC13] the problem of modeling the collisions in a distributed and heterogeneous fixed wireless network in which spatial reuse enables coexistence of multiple peer to peer communications (by applying Multi-Packet Transmission and Reception (MPTR)). This work considers the asymmetries of the topology and coexistence of nodes equipped with different antenna systems (e.g. directional antennas). Babich et. al. presents a mathematical framework that provides closed-form expressions for the capture probability, the statistics of the interference power and the Signal-to-Interference Ratio (SIR) experienced by a receiving node. The

work shows that different capture probabilities can be experienced by a given node considering both the same traffic flow from a different position and a different traffic flow from the same position.

As an extension of the work in [BC13] the same authors proposed in [BC14] a similar study for ILWN scenarios. Babich et. al. has investigated the impact of the Nakagami parameter, the radius of the network topology, and the suppression ratio of the antenna system on the capture probability of MPTR networks. The authors conclude that in some cases, severe fading conditions can have a positive influence on the capture probability. Moreover, the results show that a combination of efficient channel coding and interference suppression can provide considerable benefits in the terms of the number of simultaneous peer-to-peer communications that can be sustained by the network.

## 2.2 Aggregate Interference Modeling

In a wireless network composed of many spatially scattered nodes, the communication process is constrained by various impairments such as wireless propagation effects, network interference, and thermal noise. The effects introduced by the propagation in the wireless channel includes the attenuation of transmitted signals with distance (path loss), the blocking of signals caused by large obstacles (shadowing), and the reception of multiple delayed copies of the same transmitted signal (multipath fading). The network interference is due to accumulation of signals radiated by other transmitters, which undesirably affect the network receiving nodes. The thermal noise is associated with the receiver electronics and is usually modeled as Additive White Gaussian Noise (AWGN).

In a Single-Packet Reception (SPR) scheme the MAI caused by more than one transmitter is avoided. On the contrary, in an MPR scenario the MAI is analyzed in order to enable simultaneous transmissions from different sources. Thus, the modeling of network interference is an important problem for the MPR techniques. The interference model can be used to characterize the Bit-Error Ratio (BER) for a given modulation. Thereafter, the interference model can be used to select the appropriate modulation that maximizes the network capacity, guaranteeing an optimized adaptive modulation scheme. By using the interference models through appropriate estimation techniques, it can be known in advance that the probability of successful decoding a given packet is low and the overall system can be optimized accordingly.

In the literature the most common approach to model the interference is by characterizing the interference as a Gaussian random process [Lin+90], [CB02]. When the interference is the summation of a large number of independent signals, the Gaussian random process is an appropriate solution to characterize the interference, since the Central Limit Theorem (CLT) holds [PP02]. The Gaussian process has many well studied properties and often leads to analytically tractable results. However, several studies have mentioned some scenarios where the CLT cannot be applied (e.g., when the number of interferers is low [CH01; EE99; GH08] or when the number of interferers is large but there are dominant interferers [HA07; Win+09] and consequently the power from each node is not independent and identically distributed (i.i.d.)). In particular, it is known that the CLT gives a very poor approximation for modeling the MAI in time-hopping UWB systems [HB04],

[HB03]. In many cases, the Probability Density Function (PDF) of the interference exhibits a heavier tail than what is predicted by the Gaussian model.

In [AY10a] and [AY10b] the authors investigated the conditions for which the Gaussian approximation is valid for the aggregate interference power generated by a Poisson field of interferers. Based on the Berry-Esseen bound [PP02], they summarize in a single mathematical framework some observations reported in the literature about the Gaussian approximation of the distribution of the aggregate interference power. They show that an increase in the size of the guard region (the region near to the receiver node where no active nodes are found) brings the distribution of the aggregate interference power closer to a Gaussian distribution. Increasing the interferers' density has a similar effect. However, the convergence is faster with the increase in the size of the guard region when compared to the increase in the interferers density. In contrast, channel fading causes divergence from Gaussian approximation, diverging more when Shadow fading is considered. This fact has motivated the development of several works that try to characterize the aggregate interference with non-Gaussian models.

### 2.2.1 Interference Characterization

In [HG08], the authors have extensively derived results for the interference characterization in wireless networks that are subject to one or several sources of randomness, including the node distribution and the channel or fading states. The total aggregate interference resultant of MAI can be seen as the summation of the received power of each active transmitter. In [HG08] it is considered the total interference power received by a node in the center of a circular region $l$, as illustrated in Figure 2.3, may be expressed by

$$I = \sum_{i=1}^{N} I_i, \tag{2.9}$$

where $I_i$ is the interference caused by the $i$-th transmitter, and $N$ is the total number of active transmitters. The interference power $I_i$ is given by

$$I_i = P_{Tx} \psi_i d_i^{-\alpha}, \tag{2.10}$$

where $P_{Tx}$ is the transmitted power level of the $i$-th transmitter, $\psi_i$ represents the fading observed in the channel between the receiver and the transmitter $i$, and $d_i$ is the distance between the $i$-th interferer and the receiver. $\alpha$ represents the path-loss coefficient.

Following [Win+09] and, considering the variables $d_i$, $P_{TX}$, $\alpha$ and $\psi_i$ in (2.10), an interference model should consider the essential physical parameters that influence the interference, namely:

1. The spatial distribution of the interferers scattered in the network;
2. The transmission characteristics of the interferers, such as modulation, power, and synchronization;
3. The propagation characteristics of the medium, such as path loss, shadowing, and multipath fading.

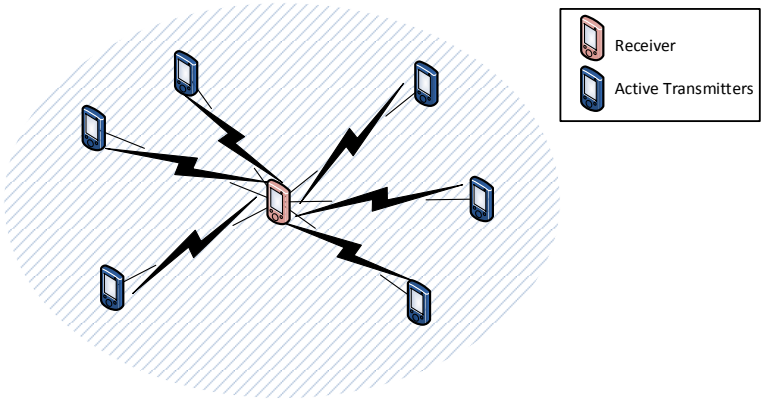


Figure 2.3: Scenario example of MAI sensed by a node in the center of an annulus $l$.

The spatial location of the interferers can be modeled either deterministically (Figure 2.4(a)) or stochastically (Figure 2.4(b)). Deterministic models include square, triangular, and hexagonal lattices in the two-dimensional plane [HG08], which are applicable when the location of the nodes in the network is exactly known or is constrained to a regular structure. In decentralized networks, often only a statistical description of the location of the nodes is available, and thus a stochastic spatial model is more suitable [BB09]. In several works, when the nodes' positions are unknown to the network designer *a priori*, they may be modeled through their spatial distribution (e.g. a homogeneous Poisson point process [Gub06]). The Poisson process has maximum entropy among all homogeneous processes [McF65] and corresponds to a simple and useful model for the location of nodes in a network.

Considering the spatial distribution of the nodes modeled as a homogeneous Poisson process in the two-dimensional infinite plane, the probability of $n$ nodes being within a region $R$ depends only on the total area $A_R$ of the region and is given by [PP02]

$$P[n \text{ in } R] = \frac{(\lambda A_R)^n}{n!} e^{-\lambda A_R}, \tag{2.11}$$

where $\lambda$ is the spatial density of the interferers, in nodes per unit area.

While [Chi97; PW10a; PW10b; Win+09] model the aggregate interference in static networks, the assumption of nodes' mobility introduces a novel degree of uncertainty related with the position of the nodes and their level of mobility.

In [Gul+12] the interference caused by multiple nodes is modeled by an alpha stable distribution. While no mobility is assumed, the authors consider random transmission durations, which can also be interpreted with respect to the varying user mobility. The authors observed that the temporal dependence in interference increases as the user mobility decreases, but this effect is only due to the nodes' velocity, and the work does not address the influence of the spatial distribution of the interferers in the aggregate interference.

Mainly due to the complexity of non-Gaussian modeling approaches, aggregate interference modeling in mobile scenarios have received limited attention. In the current literature, the use of statistical information related with the mobility of the interferers in the interference modeling

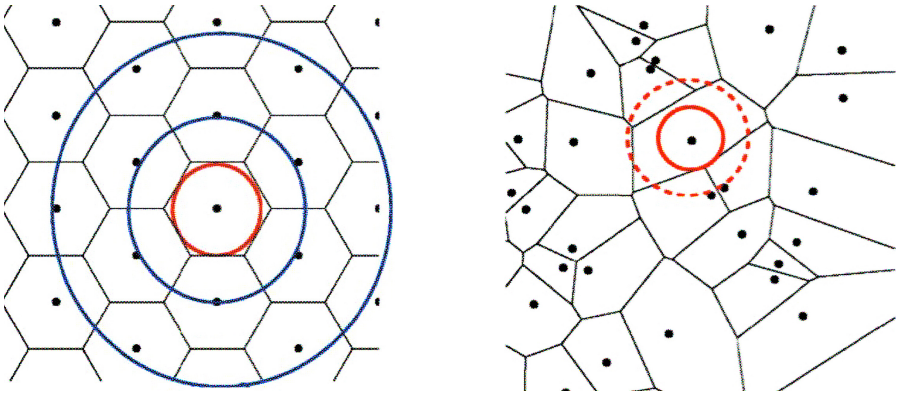

(a) (b)

Figure 2.4: Models for wireless communication (adapted from [Hea+13]):(a) Common fixed geometry model with hexagonal cells and multiple annuli of interference; (b) Stochastic geometric model where all nodes are distributed according to some 2D random process.

was only carried out in a few and very recent works [GH14; Yar+08; Zha+13]. In [Yar+08] the aggregate interference caused by multiple static nodes is characterized for the uplink channel of a single terminal moving according to a random pattern. In this case the interference is caused by static nodes and the terminal mobility only causes a time-varying displacement with respect to the different static nodes.

The work in [Zha+13] considers an ILWN scenario where the nodes move according to the Random Direction (RD) model. The PDF of the distance between any pair of nodes is used to characterize the aggregate interference due to path loss. Because a static receiver is assumed in the RD, the distance variables between interferers and the receiving node are independent, and the CLT applies. In this case, a Gaussian modeling approach is used. [GH14] assumes that the interferers may move according to the Random Waypoint (RWP) mobility model. Differently from the RD uniform model, in the RWP model the vertical and horizontal components of the nodes' position may be slightly correlated [Bet+03], and the assumptions considered in [Zha+13] for the RD model do not hold for the RWP model. [GH14] only considers the contribution from the nearest interferer to the receiver in the distribution of the interference power, neglecting the contribution of the nodes farther away.

Concerning the transmission characteristics of the users in the literature, we find several works that characterize the interference considering that the interfering nodes employ a specific modulation scheme. In [PW10a] the authors characterized the aggregate interference for two different types of modulation such as M-ary phase shift modulation (M-PSK) and M-ary quadrature amplitude modulation (M-QAM). They concluded that the aggregate interference at the output of a linear receiver is related to a skewed stable distribution in a synchronous scenario when the positions of the nodes are fixed. Moreover, the aggregate interference is related to a symmetric stable distribution in the asynchronous scenario, where the nodes randomly change their position.

The last topic to address in the aggregate interference characterization is the propagation

environment. Regarding the path loss, it is usually considered that the average of the signal amplitude decays with the distance $d$, according to $k/d^{\alpha}$, for some given constant $k$. The path loss coefficient $\alpha$ depends on the environment, and can approximately range from 2 in free space to 6 in dense areas [Gol05].

Multipath-fading results in rapid fluctuations of the envelope of the received signal and is caused when plane waves arrive from many different directions with random phases and combine vectorially at the receiver antenna. Depending on the nature of the radio propagation environment, there are different models describing the statistical behavior of the multipath fading envelope, such as Rayleigh, Nakagami-q (Hoyt), Nakagami-n (Rice), Nakagami-m, Weibull, Beckmann and Spherically-Invariant Random Process Model [SA00]. The Rayleigh distribution is frequently used to model multipath fading with no direct Line of Sight (LOS) path. In this case, the channel fading amplitude is characterized by the Rayleigh distribution

$$f_{\zeta}(x) = \frac{x}{\sigma_{\zeta}^2} e^{\frac{-x^2}{2\sigma_{\zeta}^2}}, \tag{2.12}$$

where $\zeta$ is the envelope amplitude of the received signal, and $2\sigma_{\zeta}^2$ is the mean power of the multipath received signal.

In terrestrial and satellite land-mobile systems, the link quality is also affected by a slow variation of the mean signal level due to the shadowing from terrain, buildings and trees. The uncertainty associated with large-scale environmental obstacles leads to the local mean power $\xi$ fluctuating about a constant area mean power $\mu_{\xi}$ [SA00]. Empirical studies have shown that $\xi$ follows a Lognormal distribution

$$f_{\xi}(x) = \frac{1}{\sqrt{2\pi}\sigma_{\xi} x} e^{\frac{-(ln(x)-\mu_{\xi})^2}{2\sigma_{\xi}^2}}, \tag{2.13}$$

where $\mu_{\xi}$ and $\sigma_{\xi}$ are the mean and standard deviation of the variable's ($\xi$) natural logarithm, respectively. The expect value and standard deviation are usually expressed in decibels and are given by $\mu_{\xi dB} = 10/ln(10)\mu_{\xi}$ and $\sigma_{\xi dB} = 10/ln(10)\sigma_{\xi}$, respectively [SA00]. For $\sigma_{\xi} \to 0$, no shadowing results.

Although (2.13) appears to be a simple expression, it is often convenient to be approximated by a more tractable expression when further analyses are required. Therefore, as an approximation of the Lognormal PDF, it is proposed in [AK99] and [Abd+01] the use of a Gamma PDF defined as follows,

$$f_{\xi}(x) = \frac{x^{(v_{\xi}-1)}}{\Gamma\left(v_{\xi}\right)\left(\frac{\omega_{\xi}}{v_{\xi}}\right)^{v_{\xi}}} e^{-\frac{x v_{\xi}}{\omega_{\xi}}}, \tag{2.14}$$

where $v_{\xi}$ and $\omega_{\xi}$ are given by $(e^{\sigma_{\xi}^2} - 1)^{-1}$ and $e^{\mu_{\xi}}\sqrt{(v_{\xi}+1)/v_{\xi}}$, respectively. $\Gamma(\cdot)$ represents the Gamma function [AS65, 255, eq. 6.1.1]. [AAY10] characterizes the composite effects of small-scale fading and shadowing considering Gamma shadowing. Considering Rayleigh fading (2.12) and Gamma shadowing (2.14), the PDF of the composite effects, $\Psi$, may be described as a

Generalized-K distribution [Lew83].

$$f_{\Psi}(x) = \frac{2}{\Gamma(v)}\left(\frac{v}{\omega_s}\right)^{\frac{v+1}{2}} x^{\frac{v-1}{2}} K_{v-1}\left(2\sqrt{\frac{v}{\omega_s}x}\right), \tag{2.15}$$

where $K_{v-1}(\cdot)$ is the modified Bessel function of the second kind and order $v-1$ [AS65, pp. 374, eq. 9.6.1]. Due to the analytical difficulties of the Generalized-K distribution, an approximation of the aggregate interference by a more tractable PDF is presented in [AAY10]. The authors adopt a Gamma distribution approximation of the Generalized-K distribution by using the moment matching method [BS04]. The PDF of the composite effects of small-scale fading and shadowing are approximated by [AAY10]

$$f_{\Psi_k}(x) = \frac{x^{(k_\psi - 1)}}{\Gamma(k_\psi)\theta_\psi^{k_\psi}} e^{-\frac{x}{\theta_\psi}}, \tag{2.16}$$

where $\theta_\psi$ and $k_\psi$ are given by $\left(\frac{2(v+1)}{v} - 1\right)\omega_s$ and $\frac{1}{\frac{2(v+1)}{v}-1}$, respectively.

As wireless communications move away from the traditional coordinated model (e.g. cellular networks) to more heterogeneous and distributed paradigms (e.g. ILWN and Cognitive Radio (CR)) the existing models are not appropriate due to the occurrence of the MAI at the receiver.

For example, in [Szy+11] the authors show that in the case of several interferers, the assumption of independent shadowing paths is very inaccurate and must be replaced by an appropriate correlation model. Considering a large network scenario, the same authors derived in [SY14] a more accurate Lognormal approximation for the distribution of the total interference coming from a large interference field, assuming correlated shadowing.

### 2.2.2 Heterogeneous Networks

In large wireless networks it is not possible to separate a high number of simultaneous transmissions over different bands, due to the scarcity of the wireless spectrum. Some transmissions will necessarily occur at the same time in the same frequency band, separated only in space, and the signals from many undesired or interfering transmitters are added to the desired transmitter's signal at the receiver. The Spatial Interference can be mitigated quite efficiently in systems with centralized control, where a BS or Access Point (AP) can coordinate the channelization and the power levels of the individual terminals, or where sophisticated MUD or IC schemes can be implemented. However, in many emerging classes of wireless systems is not possible to apply any level of centralized control (e.g. sensor networks, mesh networks, distributed Cognitive Radio Network (CRN), and cellular networks with multi-hop coverage extensions), and thereby it is required a more distributed resource allocation. For example, channel access schemes are typically based on carrier sensing, and instead of having a BS that controls the transmission power of the network, the power control is performed on a pairwise transmitter/receiver. In these networks, interference is not tightly controllable and is subject to considerable uncertainty. Consequently, interference is the main factor that limits the performance in the most of emerging wireless networks, and the statistical characterization of the interference power becomes critical.

Spatial Interference was modeled in different scenarios. In [Zha+14] the authors modeled the interference in a heterogeneous cellular network, in which different small cells coexist with a macro cell. Figure 2.5 shows the scenario considered by the authors where a three-tier heterogeneous cellular network composed by picocell and femtocell networks share the same frequency spectrum with the macrocell. [Zha+14] extends the statistical model of the single-region case presented in [Win+09]. The aggregate interference was only characterized for a single receiver, but for an ILWN scenario it is of interest to study the joint distribution of aggregate interference at multiple receivers.

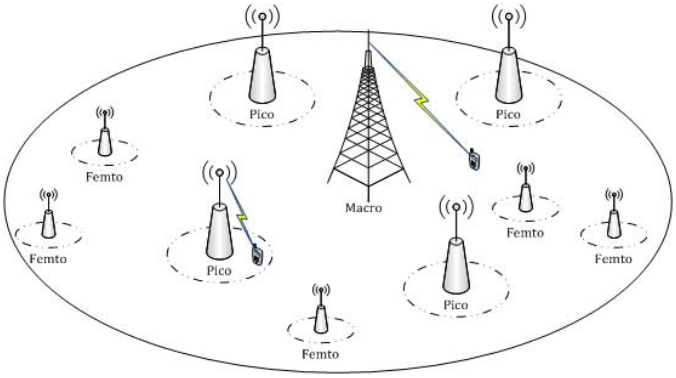


Figure 2.5: Examples of three-tier heterogeneous cellular network with a mix of macro, pico and femtocell BSs (adapted from [Zha+14]).

## 2.3 MAC Design for MPR PHY Systems

The wireless channel is a shared communication medium, so protocols are required to govern how and when terminals may access the channel. The design of MAC protocols for ILWNs has received tremendous attention in the last four decades. A basic underlying assumption in the design and evaluation of legacy MAC protocols (e.g. Aloha) was that any concurrent transmission of two or more packets results in a collision and failure of all packets. Based on this underlying assumption, the traditional approach to MAC protocol design was to avoid concurrent transmission of more than one signal. However, the PHY layer of ILWNs with MPR capability is able to decode multiple overlapping packets transmitted concurrently. This fact changes the underlying assumption about the PHY layer and demands for a new approach in designing MAC protocols, which encourages concurrent transmissions rather than discouraging them to take the full advantage of the MPR capability of the PHY layer. In this section, some of the proposed MAC protocols for ILWNs are presented, which exploit the MPR capability. We highlight that most of the already proposed MAC protocols are based in random access protocols, such as Aloha and random access with Carrier Sense Multiple Access (CSMA).

In the Aloha protocol, each source node in a communication network transmits data every time there is a frame to be transmitted. If the frame successfully reaches the destination, the next frame is transmitted. If the frame is not received at the destination, it will be retransmitted. Slotted

ALOHA (S-ALOHA) is an improvement to the original Aloha protocol, where discrete time slots were introduced to increase the maximum throughput while reducing collisions. This is achieved by allowing source nodes to transmit only at the beginning of a time-slot. CSMA is a MAC protocol, where a node transmits data on a shared transmission channel only after verifying the absence of other transmissions. Carrier Sense Multiple Access with Collision Detection (CSMA/CD) and Carrier Sense Multiple Access with Collision Avoidance (CSMA/CA) are two modifications of the CSMA protocol. CSMA/CD improves performance of CSMA by stopping a transmission as soon as a collision is detected. CSMA/CA improves the performance of CSMA by delaying the transmission by a random duration if the channel is sensed busy. The main difference between Aloha and CSMA is that Aloha protocol does not try to detect whether the channel is free before transmitting. In CSMA protocol, the channel is sensed before transmitting data. Thus CSMA protocol may avoid collisions, while Aloha protocol detects that a channel is busy only after a collisions happens [Tan02].

Zhao et al. [ZT03] proposed a MAC protocol explicitly designed for wireless networks with MPR capability. The protocol Multi-Queue Service Room (MQSR) protocol adaptively grants access to the channel to a number of users such that the expected number of successfully received packets is maximized. MQSR tries to avoid unnecessary empty slots for light traffic and excessive collisions for heavy traffic. The main difficulty of the MQSR protocol lies on its computational complexity, which grows exponentially with the number of users. To overcome this problem, in [ZT04] the same authors proposed a simpler algorithm that achieves a comparable performance to the one in [ZT03].

Ying Zhang [Zha10] proposed the Multi-Round Contention Random-access (MRCR) MAC protocol for wireless networks where $K$ transmitters and one AP can achieve the maximum MPR capacity of $M$ packets simultaneously received. In the MRCR protocol, the nodes contend the wireless medium for multiple rounds until there are enough nodes to transmit data simultaneously. Ying Zhang's work studies the optimal threshold to stop the contention period and start the data transmission phase. The optimal threshold corresponds to a tradeoff between contention overhead and channel utilization. Ying Zhang et al. showed that by using MAC protocol techniques that enable concurrent transmissions from multiple users, these protocols scale super-linearly, i.e. the system throughput increases as the MPR capability increases [Zha+09].

The MQSR and MRCR protocols are not suitable for ILWNs since they have the disadvantage of requiring a central controller that selects an optimal number of users who can access the channel on each slot.

Similarly to [Zha10], in [SU17], the authors present a joint uplink-downlink MU-MIMO based MAC protocol utilizing multi-round contentions in the uplink while considering a physical interference model with attenuation, fading and shadowing. In the multi-round contention based MAC protocols, the AP has to wait some time for extracting the requests from desired number of users which is called waiting time. This leads to increase of packet delay in the system. Thus, multiround contention based MAC protocols suffer from higher packet delay [SU17]. Both the throughput and delay are very important performance metrics for any network. The authors conclude that the performance of the proposed protocol does not change significantly due to the variations of

shadowing parameter and SINR threshold which provides an advantage in network planning and design.

[Cel+10] analyzed the impact of spatial node's distribution on system's performance. This is particularly important because in MPR the nodes closer to the receiving one have more chances to successfully transmit, and can result in channel access unfairness [Cel+08]. In such a way, [Cel+10] proposed a random access scheme, called Generic Distributed Contention Window (GDCW) protocol, where the medium access probability is increased for distant nodes and decreased for the nearest ones. The backoff model, named Alternative Model, decreases the transmission probability after a successful transmission and increases it after a failed transmission. However, the authors do not justify the advantage of such heuristic in terms of fairness, and do not give insights about how to regulate the access probabilities according to the MPR capability of the receiving node.

Sarker et al. proposed a random access protocol for autonomic ILWNs where the nodes self-control their access to the medium (without an AP) in such a way that maximizes the network throughput [SM11]. The ILWN is autonomic (i.e., self-optimizing) in the sense that each mobile node can control the network traffic very precisely to obtain the maximum throughput. In the protocol, each node would be in one of the following three modes: transmitting mode; receiving mode or idle mode. Each node is able to calibrate its ratio of transmission probability and receiving probability to control the network traffic load very precisely. For a fixed MPR capability, each node control their receptions and transmissions in order to obtain the maximum network throughput. Since the increase of MPR capability increases the throughput, but also increases the cost per mobile node, Sarker et al. [SM11] estimated the optimum number of MPR capability that provides a reasonable trade-off between the throughput per node and the cost per mobile node.

In [Ina+12] a random access Game for Contention Control (GCC) protocol was proposed and analyzed using the Nash equilibrium. GCC protocol derives the Nash equilibrium conditions for setting persistence probabilities in an adaptive p-persistent S-ALOHA protocol in which persistence probabilities are adaptively updated according to the derived equilibrium strategies. Tangible applications are demonstrated in which equilibrium conditions are solved for specific channel models to derive contention resolution strategies and to analyze the resulting network performance.

Babich et al. [BC10] developed a mathematical framework that assumes asynchronous MPR transmissions under an IEEE 802.11 distributed network. The framework assumes a slotted CSMA scheme, the knowledge of the backoff decreasing probability and the conditional packet failure probability. The cross-layer implementation can sustain up to a maximum of $M$ transmissions, but still using the collision avoidance mechanism. A transmission slot is considered busy if there are more than $M$ transmissions. Thereby a node is allowed to decrease its backoff counter as long as the channel is empty or the number of ongoing transmissions is lower than $M$. A generic error correction code is assumed to protect data frames. Based on the results obtained from the theoretical model and simulations, the authors claim that the asynchronous MAC scheme can provide considerable performance gains compared to the synchronous one due to higher utilization of the channel.

[JL11] proposed an Opportunistic MAC protocol for coordinating simultaneous transmissions in a MU-MIMO wireless network. The protocol allows more nodes to opportunistically transmit

packets even when they do not exchange any control packets for transmission coordination if the AP can concurrently receive more packets due to the MPR capability. On receiving several Requests To Send (RTSs), the AP sends an adapted Clear to Send (CTS) to notify the group of nodes that won the channel contention, as well as to announce the available channel space. Nodes that did not send RTS will compete for the available channel space if their frame transmission is shorter than the longest frame of the nodes that have won. This information is indicated in the duration field of the CTSs. Simulation results demonstrate that the proposed protocol significantly improves the network throughput of the IEEE 802.11 Distributed Coordination Function (DCF) and outperforms the MRCR protocol [Zha10] previously described.

An asynchronous MAC protocol is proposed in [Jun+12], which allows senders to asynchronously start their transmissions without waiting for the completion of all the ongoing transmissions in a MU-MIMO wireless network. In the protocol, an AP informs the nodes about its MPR vacancy through an additional feedback channel. The proposed MAC procedure is shown in Figure 2.6. On receiving an RTS from Node 1, the AP replies with a CTS that includes the MPR vacancy (the remaining space for parallel transmissions). Nodes who overhear the MPR vacancy will compete for the channel to transmit along with Node 1. Once a node finishes transmitting ahead of the other one, the AP immediately sends an ACKnowledgment (ACK) with the updated MPR vacancy information through the additional channel. This allows other nodes to compete for the newly available MPR space. Based on results obtained from the analytic model and simulations, the authors claim that the proposed scheme coordinated by the AP achieves higher channel efficiency in scenarios where the frame size and transmission rates are dynamically varying. The authors also assume that an orthogonal training sequence is included in the preamble of each frame for estimating the channel.

As stated before, the analysis of an MPR scenario requires the modification of the classical

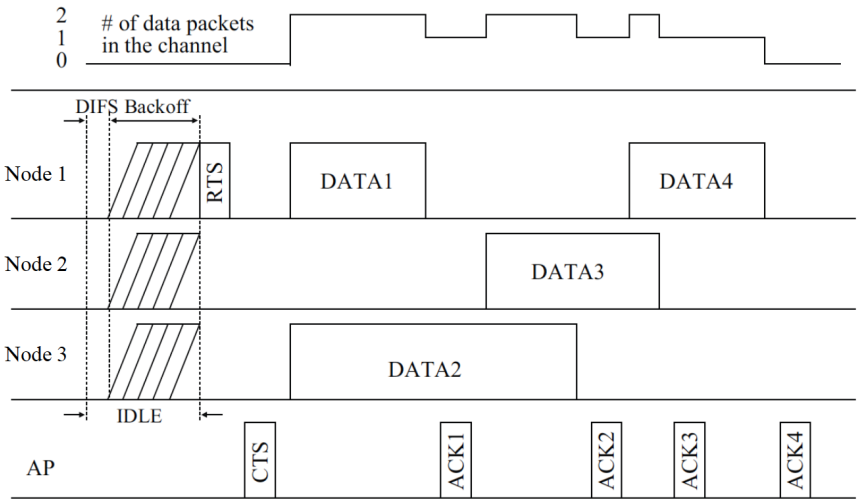


Figure 2.6: Operation of the asynchronous MAC protocol in a scenario with 2-MPR capability (adapted from [Jun+12]).

collision model, which assumes a successful reception only if an unique communication is active. Furthermore, a fundamental element that considerably influences the performance of a CSMA scheme in any MPR network is the carrier sense mechanism, whose functionality requires a reliable collision model and an accurate evaluation of the SINR experienced by each receiving node. Focused on that, Chan et al. [Cha+13] investigated the performance of CSMA communications in SPR and MPR scenarios. The work analyzed the maximum achievable stable throughput with decentralized control and identified the throughput gain over a S-ALOHA MAC protocol. This gain decreases as the PHY layer MPR capabilities increases, thereby decreasing the need for channel sensing. Chan et al. pointed out that CSMA schemes, can been evolved support MPR communications and can enhance the utilization of MPR capacity when compared to S-ALOHA.

Table 2.1 summarizes the general aspects of the MAC protocols that have been discussed. In the table each protocol is analyzed considering different aspects. The first aspect is the PHY layer technology that is used by each protocol in order to enable MPR capabilities. The MAC scheme is considered next, being classified in two random access schemes: ALOHA and CSMA.

In the table, "Impl" stands for Implementation, which can be Distributed ("Distr.") or Centralized ("Centr."). Although some of the proposed MAC protocols considered only one receiver, such as an AP (e.g. [Jun+12]), this does not invalidate the presence of other receivers in the wireless network. Thus, it can be possible to have multiple receivers, where each one is able to receive simultaneous transmissions. In this case the MAC protocol is considered suitable for a distributed implementation. The "MPR adaptation" describes the key characteristic of the MAC protocol to handle the behavior of the MPR communication scheme.

Table 2.1: Taxonomy of MAC protocols for MPR PHY Systems.

| Work | PHY Technology | MAC scheme | Impl. | MPR Adaptation |
|---|---|---|---|---|
| MQSR [ZT03] | CDMA | S-ALOHA | Centr. | Estimation of the state of the users |
| MRCR [Zha10] | (not assessed) | CSMA | Centr. | Multi-round contentions |
| MU-MIMO MAC [SU17] | MIMO | CSMA/CA | Distr. | MAC protocol considers the effect of the physical interference model |
| GDCW [Cel+10] | CDMA | CSMA | Distr. | Switching between two transmission probs |
| Autonomic ILWN [SM11] | (not assessed) | S-ALOHA | Distr. | Receiving and transmitting prob. parametrized based on the optimal througput |
| GCC [Ina+12] | (not assessed) | p-pers. S-ALOHA | Distr. | Persistent probabilities adaptively updated using Nash equilibrium |
| Asynchronous MPR [BC10] | CDMA | CSMA/CA | Distr. | Backoff counter decreases depending on the available MPR capacity |
| Opportunistic MAC [JL11] | MIMO, OFDM | CSMA/CA | Distr. | Access to the data period without contention |
| Asynchronous MAC [Jun+12] | MIMO, OFDM | CSMA/CA | Distr. | Senders start transmissions asynchronously based on available MPR capacity |

CHAPTER 3

# MPR PHY LAYER MODELING

## 3.1 Introduction

In Infrastructure-Less Wireless Networks (ILWNs) with MPR PHY layer capabilities, the MAC protocols must be designed to force the collision of $n > 1$ transmissions according to the optimal number of transmitters that maximize the performance of the PHY layer. Consequently, the number of transmitters ($n^*$) that maximize the performance of the PHY layer is a crucial parameter that must be known in advance. The parameter $n^*$ depends on the MPR technology adopted at the PHY layer, but also on the radio propagation conditions, the transmitted power, and the spatial distribution of the transmitters (due to path loss effect). Therefore, the characterization of PHY layer performance plays an important role regarding the design of the MAC protocol, and the PHY/MAC architecture must be designed and optimized in a cross-layer manner.

As mentioned in the previous chapter, the analysis of the capture phenomenon was extended in [GK00] to include basic physical propagation aspects. Two different approaches for modeling signal capture in radio systems were followed: one based on the protocol model (see Subsection 2.1.3.1); and the other on the physical model (see Subsection 2.1.3.2). The protocol model gives a geometric interpretation of signal propagation, according to which the capture of a signal only depends on the distance between the different transmitters and the common receiver [GLA+07a; WGLA08]. This approach makes it possible to carry out elegant performance analysis and to derive closed-form bounds for the system capacity in different scenarios, but relies on an idealized and rather unrealistic model (i.e., unit disk model). On the other hand, the physical model, adopted in this work, explicitly includes the physical propagation phenomena and the cumulative character of interference, considering the random distribution of the signal power at the receiver and introducing the Signal-to-Interference-plus-Noise Ratio (SINR) criterion to determine the capture probability [ZZ12].

In this chapter, we propose two generalized mathematical models to characterize the PHY layer

performance of MPR schemes. The models rely on the computation of the individual probability of successful packet reception and on the number of received packets when $n$ simultaneous transmissions occur. The proposed models are based on the receiving condition presented in [Ngu+06] and [ZZ12], in which the reception of a packet succeeds if the received power that defines the SINR is higher than a receiving threshold, $b$.

In the first modeling approach, near-field and far-field scenarios are considered. In these scenarios, the Characteristic Function (CF) of the successful packet receiving condition is derived. Then, the CF is used to compute the probability of successful packet reception and the average number of received packets when $n$ simultaneous transmissions occur.

In the second modeling approach, a mathematical methodology is proposed to characterize the aggregate power. The method starts by subdividing the area where the multiples transmitters are located into smaller annuli, to increase the model's accuracy due to the non-linearity of the path loss effect. The aggregate power received from the transmitters located in each annulus is then approximated by a Gamma distribution. Hence, the CF of the aggregate power is approximated by the product of Gamma CFs. Summing up, the characterization of the probability of successful packet reception and the average number of received packets is obtained by using the Gamma distribution in the capture model. When compared to the first modeling approach, this model has lower computational complexity and is better suited to scenarios of high density of transmitters.

As the main contribution of this work, both proposed solutions take into account the presence of the propagation effects, i.e., path loss, small-scale fading and shadowing, as well as the noise at the receiver side. While [Ngu+06] considers only path loss and small-scale fading and [ZZ12] does not consider the propagation effects in a joint manner, our work considers the joint occurrence of the multiple propagation effects. The impact of the noise at the receiver on the PHY layer performance is also studied. The same applies to the different propagation effects.

Finally, the proposed models allow to compute the optimal number of transmitters, $n^*$, for a given receiving threshold, which is an important departing point to design efficient MAC techniques for MPR systems.

### Chapter Contents

- **Section 3.2**: This section starts introducing the network scenario considered in the chapter. Then, the communication assumptions related with the capture of the multiple packets are introduced, including the near-field and far-field conditions. The radio propagation effects considered in the models are also described. Finally, the section ends up with the description of the necessary steps to model the individual power received from a single transmitter in both near-field and far-field scenarios;

- **Section 3.3**: Presents the PHY layer performance Model I, where the first modeling approach is adopted. This model is capable of characterizing both near-field and far-field scenarios;

- **Section 3.4**: Presents the PHY layer performance Model II, where the second modeling approach is adopted. The model uses an approximation of the PHY layer performance model that takes advantage of the aggregate interference power approximated by a Gamma distribution. This model is preferable for high density of transmitters, because of its lower computational complexity;
- **Section 3.5**: This section evaluates the proposed models I and II, through the comparison of numerical and simulated results. Section 3.5 also presents a method to derive the number of transmitters ($n^*$) that maximize the performance of the PHY layer;
- **Section 3.6**: This section summarizes the chapter's conclusions.

## 3.2 System Description

In the analysis presented in this chapter we consider an ILWN network where $n$ nodes transmit data simultaneously to a single node (the receiver node), as represented in Figure 3.1. Each node is equipped with an omni-directional antenna, and the nodes share the same frequency band. Time is divided into equal size slots that are grouped into frames. The transceiver at each node is half-duplex, and hence a transmitting node cannot receive packets from other nodes at the same time. Without loss of generality, we assume that all nodes are synchronized. All transmitters adopt the same transmitting power level, and no power control is adopted.

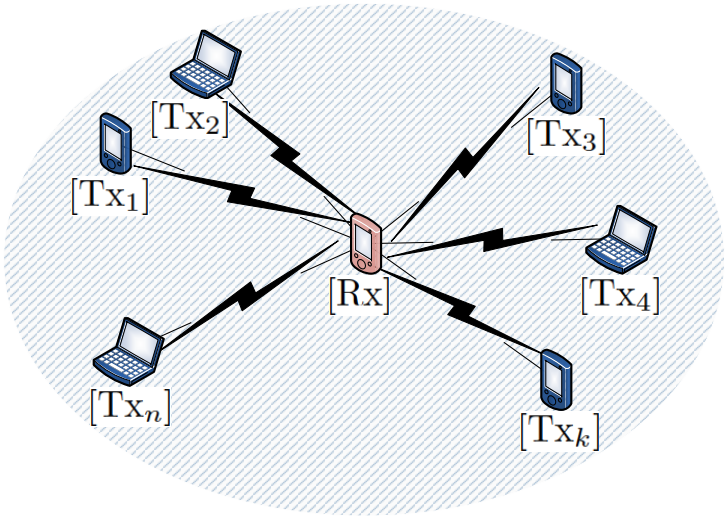


Figure 3.1: $n$ nodes simultaneously transmit data to a single receiver node.

### 3.2.1 Assumptions

It is assumed that the signals received from the transmitters are independent and identically distributed (i.i.d.) Random Variables (RVs), characterized by the PDF $f_{P_k}$. The total power received

by the Rx node from the multiple transmissions is given by

$$\Lambda = \sum_{k=1}^{n} P_k + N_0, \tag{3.1}$$

where $P_k$ is a RV representing the power received from the $k$-th transmitter and $N_0$ is a RV representing the noise power at the receiver.

We assume an MPR receiver where the SINR associated with the signal received from transmitter $j$ is defined by

$$\gamma_j = \frac{P_j}{\Lambda - P_j}. \tag{3.2}$$

Following the capture condition defined in [Ngu+06] the signal received by transmitter $j$ is potentially decodable, despite the interference caused by the other overlapping signals, when the following condition holds

$$\gamma_j > b. \tag{3.3}$$

The receiving threshold $b > 0$ is a parameter determined by several factors such as the type of modulation and sensitivity of the receiver. The capture condition is general enough to represent distinct types of PHY layers. Typically for SPR systems $b$ is between 1 and 10, and for MPR systems $b < 1$ [Haj+97]. Conventional narrowband systems with a single antenna necessarily have a receiving threshold $b \geq 1$ and, as a consequence, at most one signal at a time can be successfully decoded by the receiver [Ngu+06]. Conversely, in CDMA systems, the capture threshold can be significantly less than 1, depending on the length of the spreading codes that are used to distinguish the signal of each user. CDMA systems trade the spectral efficiency of each user with a SINR gain proportional to the length of the spreading code, which may result in a capture threshold $b < 1$. Hence, CDMA systems are capable of decoding up to $1/b$ overlapping signals, thus exhibiting MPR capabilities.

We consider that the signals at the receiver are affected by random attenuation factors and, consequently, the number of signals that can be captured is non-deterministic. As stated in Section 2.2, one of the fundamental aspects of MPR communications that make the problem challenging is the channel attenuation phenomenon. Such fluctuation is due to the dynamic behavior of the small-scale effect of multi-path fading, as well as large-scale effects such as path loss via distance attenuation and shadowing by obstacles such as buildings and hills. With regards to the propagation effects, we consider that the received power from each transmitter is influenced by three propagation effects: path loss, small-scale fading and shadowing.

Regarding the spatial distribution of the nodes, we consider that the transmitting nodes are uniformly distributed within the $l$ annulus with area $A_l = \pi\left(\left(R_o^l\right)^2 - \left(R_i^l\right)^2\right)$ encircling the receiver. Considering the area $A_l$ we can model: (1) a near-field scenario (Figure 3.2(a)) where the transmitters are located within a circle with area $A_l = \pi\left(R_o^l\right)^2$ (with $R_i^l = 0$); (2) a far-field scenario (Figure 3.2(b)) where the transmitters are located within an annulus with area $A_l = \pi\left(\left(R_o^l\right)^2 - \left(R_i^l\right)^2\right)$.

The power received from the $k$-th transmitter, $P_k$, is given by

$$P_k = P_T \Psi_k \left(R_k^l\right)^{-\alpha}, \tag{3.4}$$

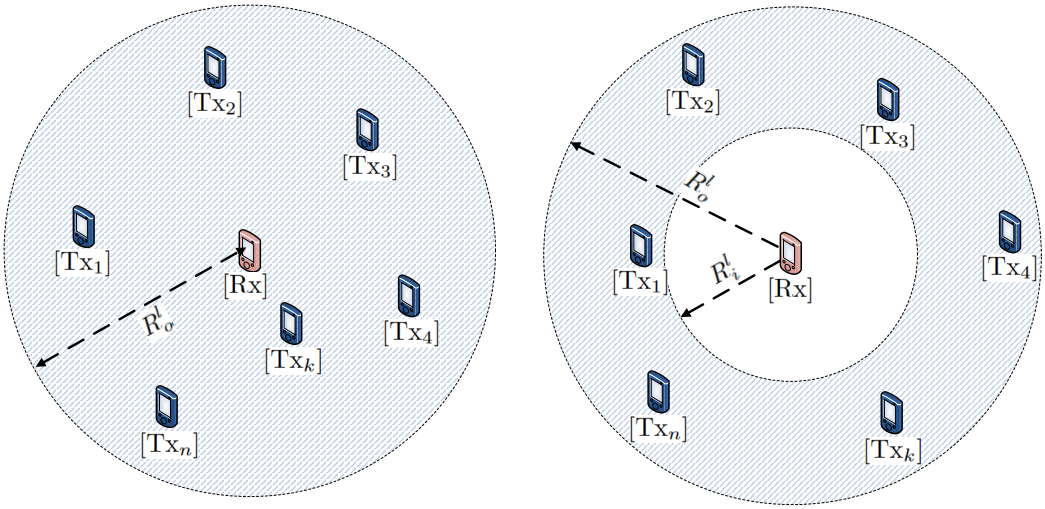


Figure 3.2: Spatial distribution of the nodes: (a) Near-field scenario; (b) Far-field scenario.

where $P_T$ is a constant representing the transmitted power (adopted by all transmitters), $\Psi_k$ is a RV that represents the composite effects of small-scale fading and shadowing observed in the channel between the receiver and the $k$-th transmitter. The RV $R_k^l$ represents the distance between the $k$-th transmitter and the receiver, and $\alpha$ is the path loss coefficient.

In the particular case of the near-field scenario, the adoption of (3.4) to model the received power is not valid, because when $r_k^l < 1$ the received power, $P_k$, is greater than the transmitted power. Therefore, a near-field path loss approximation presented in [Ngu+06] is adopted, where the gain due to path loss is equal to $\left(R_k^l + 1\right)^{-\alpha}$. Hence, the power received from the $k$-th transmitter of the near-field scenario is given by

$$P_k = P_T \Psi_k \left(R_k^l + 1\right)^{-\alpha}. \tag{3.5}$$

### 3.2.2 Characterization of the Received Power

In this subsection we derive the CF of the individual power $P_k$, denoted by $\varphi_{P_k}$, considering the near-field and the far-field scenarios. Assuming that the nodes are uniformly distributed within the annulus $l$ with area $A_l = \pi\left(\left(R_o^l\right)^2 - \left(R_i^l\right)^2\right)$ encircling the receiver, the PDF of the distance between the $k$-th transmitter and the receiver, $R_k^l$, can be written as the ratio between the perimeter of the circle with radius $r$ and the total area $A_l$, as follows

$$f_{R_k^l}(r) = \begin{cases} \dfrac{2\pi r}{A_l} & R_i^l \leq r \leq R_o^l \\ 0, & \text{otherwise} \end{cases}. \tag{3.6}$$

In (3.6) $R_i^l$ and $R_o^l$ represent the inner radius and outer radius of the region $l$ where the transmitters are located (see Figure 3.2), respectively. Note that the radius $R_i^l$ is equal to zero when considering the near-field scenario.

The channel small-scale fading amplitude, $\zeta$, is assumed to be distributed according to a Rayleigh distribution (see Subsection 2.2.1). Therefore, the power of the small-scale fading effect, $\zeta^2$, is distributed according to an Exponential distribution, which is given by

$$f_{\zeta^2}(x) = \frac{x}{2\sigma_\zeta^2} e^{-\frac{x}{2\sigma_\zeta^2}}, \tag{3.7}$$

where $2\sigma_\zeta^2$ is the mean of the Exponential distribution (a normalized power is adopted hereinafter, i.e. $2\sigma_\zeta^2 = 1$).

Regarding the large-scale fading (also known as shadowing), $\xi$, is assumed to be distributed according to a Lognormal distribution parameterized by $\mu_\xi$ and $\sigma_\xi$, as shown in Subsection 2.2.1. In this work we normalize $\xi$ to have a unit mean, resulting in $\mu_\xi = -\sigma_\xi^2/2$. As stated in Subsection 2.2.1, due to the mathematical intractability of conducting further analysis with the Lognormal distribution, we have assumed that the large-scale fading effect follows a Gamma distribution, as proposed in [AK99]. The Gamma distribution is defined as

$$f_\xi(x) = \frac{x^{(v_\xi - 1)}}{\Gamma\left(v_\xi\right)\left(\frac{\omega_\xi}{v_\xi}\right)^{v_\xi}} e^{-\frac{x v_\xi}{\omega_\xi}}, \tag{3.8}$$

where $v_\xi$ and $\omega_\xi$ are given by $(e^{\sigma_\xi^2} - 1)^{-1}$ and $e^{\mu_\xi}\sqrt{(v_\xi + 1)/v_\xi}$, respectively. $\Gamma(\cdot)$ represents the Gamma function [AS65, 255, eq. 6.1.1].

$\Psi_k$ in (3.4) represents the composite effects due to small and large-scale fading. Having considered Rayleigh fading and Gamma shadowing, the PDF of $\Psi_k$ is represented by a Generalized-K distribution [Lew83]. To overcome the analytical difficulties associated with the Generalized-K distribution, [AAY10] proposed a Gamma distribution approximation relying on the moment matching method [BS04], showing that the PDF of the composite effects of small-scale fading and shadowing is approximated by [AAY10]

$$f_{\Psi_k}(x) = \frac{x^{(k_\psi - 1)}}{\Gamma(k_\psi)\theta_\psi^{k_\psi}} e^{-\frac{x}{\theta_\psi}}, \tag{3.9}$$

where $\theta_\psi > 0$ and $k_\psi > 0$ are given by $\left(\frac{2(v_\xi + 1)}{v_\xi} - 1\right)\omega_\xi$ and $\frac{v_\xi}{v_\xi + 2}$, respectively.

#### 3.2.2.1 CF of Noise Power

Regarding the noise at the receiver, $N_0$ in (3.1), Zero-mean Additive White Gaussian Noise (AWGN) is assumed. Since the AWGN follows a complex Normal distribution, $\mathcal{CN}(0, {\sigma_{N_0}}^2)$, its power is exponentially distributed and the CF of its power is given by [PP02]

$$\varphi_{N_0}(t) = \frac{\sigma_{N_0}^2}{\sigma_{N_0}^2 + it}, \tag{3.10}$$

where $\sigma_{N_0}^2$ represents the noise variance.

#### 3.2.2.2 Near-field scenario

Here we consider the near-field scenario, where the receiver is surrounded by $n$ transmitters which are located within a circle with area $A = \pi\left(R_o^l\right)^2$.

The CF of the power received from the $k$-th transmitter is written as

$$\varphi_{P_k}(t) \quad = \mathrm{E}_{P_k}[e^{itP_k}] = \int_{-\infty}^{\infty} \mathrm{e}^{itx} f_{P_k}(x)\,\mathrm{d}x, \tag{3.11}$$

where $i$ is the imaginary unit.

Taking into account (3.5), $\varphi_{P_k}$ is rewritten as

$$\varphi_{P_k}(t) \quad = \mathrm{E}_{\Psi_k}\left[\mathrm{E}_{R_k^l}[e^{itP_k}]\right] = \int_0^{\infty}\int_0^{R_o^l} e^{itP_T x(r+1)^{-\alpha}} f_{R_k^l}(r) f_{\Psi_k}(x)\,\mathrm{d}r\,\mathrm{d}x, \tag{3.12}$$

which using (3.6) and (3.9) can be simplified to

$$\varphi_{P_k}(t) = \frac{1}{\Gamma(k_\psi)\theta_\psi^{k_\psi}} \int_0^{\infty} x^{k_\psi - 1} e^{\frac{-x}{\theta_\psi}} \varphi_{P_k^{PL}}(t)\,\mathrm{d}x, \tag{3.13}$$

where $\varphi_{P_k^{PL}}$ is given by

$$\begin{aligned} \varphi_{P_k^{PL}}(t) = & \quad \frac{2}{\left(R_o^l\right)^2} \int_0^{R_o^l} e^{itP_T x(r+1)^{-\alpha}} r\,\mathrm{d}r \\ = & \quad \frac{2}{\left(R_o^l\right)^2} \left[ \int_0^{R_o^l} e^{itP_T x(r+1)^{-\alpha}} (r+1)\,\mathrm{d}r - \int_0^{R_o^l} e^{itP_T x(r+1)^{-\alpha}}\,\mathrm{d}r \right]. \end{aligned} \tag{3.14}$$

To derive the CF $\varphi_{P_k}$ in a comprehensive manner, we first calculate the two integrals in (3.14). Then the integral in (3.13) is solved. To this end we introduce Lemma 3.1.

**Lemma 3.1.** *If $\alpha \neq 0$ and $-\frac{c+1}{\alpha} \notin \mathbb{Z}$, the following equality holds (A)*

$$\int e^{a(r+1)^{-\alpha}} (r+1)^c dr = \frac{(r+1)^{(c+1)} Ei\left(1+\frac{2}{\alpha}, -a(r+1)^{-\alpha}\right)}{\alpha},$$

*where Ei is the Exponential integral function ($Ei(p,x) = \int_1^{\infty} e^{-xt} t^{-p}\,\mathrm{d}t$ [Zwi03, eq. 6.15.2]).*

Considering Lemma 3.1 (proved in Appendix A) in the first and the second integrals in (3.14), we obtain the following expression,

$$\varphi_{P_k^{PL}}(t) = \quad \frac{2}{\left(R_o^l\right)^2} \left[ \left[ \frac{\mathrm{Ei}\left(1+\frac{2}{\alpha}, -itP_T x(r+1)^{-\alpha}\right)}{\alpha(1+r)^{-2}} \right]_0^{R_o^l} - \left[ \frac{\mathrm{Ei}\left(1+\frac{1}{\alpha}, -itP_T x(r+1)^{-\alpha}\right)}{\alpha(1+r)^{-1}} \right]_0^{R_o^l} \right]. \tag{3.15}$$

Note that the path loss coefficient, $\alpha$, should be such that the conditions $\frac{2}{\alpha} \notin \mathbb{Z}$ and $\frac{1}{\alpha} \notin \mathbb{Z}$ in Lemma 3.1 hold true.

Considering the upper and lower bounds in (3.15), $\varphi_{P_k^{PL}}$ can be rewritten as

$$\begin{aligned}\varphi_{P_k^{PL}}(t) = \frac{2}{\alpha\left(R_o^l\right)^2} \quad & \Big[(1+R_o^l)^2 \mathrm{Ei}\Big(1+\frac{2}{\alpha}, -itP_T x(R_o^l+1)^{-\alpha}\Big) - \mathrm{Ei}\Big(1+\frac{2}{\alpha}, -itP_T x\Big) - \\ & -(1+R_o^l)\mathrm{Ei}\Big(1+\frac{1}{\alpha}, -itP_T x(R_o^l+1)^{-\alpha}\Big) + \mathrm{Ei}\Big(1+\frac{1}{\alpha}, -itP_T x\Big)\Big].\end{aligned} \tag{3.16}$$

Replacing (3.16) in (3.13), the CF $\varphi_{P_k}$ is now written as

$$\begin{aligned}\varphi_{P_k}(t) = \quad & \frac{2}{\alpha\left(R_o^l\right)^2 \Gamma(k_\psi)\theta_\psi^{k_\psi}} \cdot \\ & \cdot\Bigg[\int_0^\infty x^{k_\psi-1} e^{\frac{-x}{\theta_\psi}} \mathrm{Ei}(1+\frac{1}{\alpha}, -itP_T x)\,\mathrm{d}x - \\ & -\int_0^\infty x^{k_\psi-1} e^{\frac{-x}{\theta_\psi}} (1+R_o^l)\mathrm{Ei}(1+\frac{1}{\alpha}, -itP_T x(R_o^l+1)^{-\alpha})\,\mathrm{d}x - \\ & -\int_0^\infty x^{k_\psi-1} e^{\frac{-x}{\theta_\psi}} \mathrm{Ei}(1+\frac{2}{\alpha}, -itP_T x)\,\mathrm{d}x + \\ & +\int_0^\infty x^{k_\psi-1} e^{\frac{-x}{\theta_\psi}} (1+R_o^l)^2 \mathrm{Ei}(1+\frac{2}{\alpha}, -itP_T x(R_o^l+1)^{-\alpha})\,\mathrm{d}x\Bigg].\end{aligned} \tag{3.17}$$

To solve the four integrals in (3.17) we use the following lemma.

**Lemma 3.2.** *If $a > -1$ and $(p+b) > 1$, the following condition holds [Olv+10, eq. 8.19.25]*

$$\int_0^\infty e^{-ax} x^{b-1} Ei(p, cx) dx = \frac{\Gamma(b)(a+cx)^{-b}}{p+b-1} {}_2F_1\Big(1, b, p+b; \frac{a}{a+cx}\Big),$$

*where ${}_2F_1$ represents the Gauss Hypergeometric function [Olv+10, pp. 384, eq. 15.2.1].*

Considering the four integrals in (3.17), Lemma 3.2 can be used if the conditions $\frac{1}{\theta_\psi} > -1$, $\left(1+\frac{1}{\alpha}+k_\psi\right) > 1$ and $\left(1+\frac{2}{\alpha}+k_\psi\right) > 1$ are verified. Since the parameters $\theta_\psi$, $k_\psi$ and $\alpha$ only admit positive and non-zero values, the three previous conditions always hold and therefore Lemma 3.2 can be applied.

Using Lemma 3.2, $\varphi_{P_k}$ in (3.17) is rewritten as follows

$$\begin{aligned}\varphi_{P_k}(t) = \quad & \frac{2}{\alpha\left(R_o^l\right)^2\Gamma(k_\psi)\theta_\psi^{k_\psi}}\cdot \\ & \cdot\Bigg[\frac{\Gamma(k_\psi)}{(\theta_\psi^{-1}-itP_T)^{k_\psi}(\frac{1}{\alpha}+k_\psi)}{}_2\mathrm{F}_1\left(1,k_\psi,1+\frac{1}{\alpha}+k_\psi;\frac{\theta_\psi^{-1}}{\theta_\psi^{-1}-itP_T}\right)- \\ & -\frac{(1+R_o^l)\Gamma(k_\psi)}{(\theta_\psi^{-1}-itP_T(R_o^l+1)^{-\alpha})^{k_\psi}(\frac{1}{\alpha}+k_\psi)}{}_2\mathrm{F}_1\left(1,k_\psi,1+\frac{1}{\alpha}+k_\psi;\frac{\theta_\psi^{-1}}{\theta_\psi^{-1}-itP_T(R_o^l+1)^{-\alpha}}\right)- \\ & -\frac{\Gamma(k_\psi)}{(\theta_\psi^{-1}-itP_T)^{k_\psi}(\frac{2}{\alpha}+k_\psi)}{}_2\mathrm{F}_1\left(1,k_\psi,1+\frac{2}{\alpha}+k_\psi;\frac{\theta_\psi^{-1}}{\theta_\psi^{-1}-itP_T}\right)+ \\ & +\frac{(1+R_o^l)^2\Gamma(k_\psi)}{(\theta_\psi^{-1}-itP_T(R_o^l+1)^{-\alpha})^{k_\psi}(\frac{2}{\alpha}+k_\psi)}{}_2\mathrm{F}_1\left(1,k_\psi,1+\frac{2}{\alpha}+k_\psi;\frac{\theta_\psi^{-1}}{\theta_\psi^{-1}-itP_T(R_o^l+1)^{-\alpha}}\right)\Bigg].\end{aligned} \tag{3.18}$$

(3.18) can be further simplified by using the equality [Zwi03, eq. 6.17.2]

$${}_2\mathrm{F}_1\left(a,b,c;z\right) = (1-z)^{-b}{}_2\mathrm{F}_1\left(b,c-a,c;\frac{z}{z-1}\right), \tag{3.19}$$

leading to

$$\begin{aligned}\varphi_{P_k}(t) = \quad & \frac{2}{\left(R_o^l\right)^2(-itP_T\theta_\psi)^{k_\psi}}\cdot \\ & \cdot\Bigg[\frac{1}{\alpha k_\psi+1}{}_2\mathrm{F}_1\left(k_\psi,k_\psi+\frac{1}{\alpha},1+\frac{1}{\alpha}+k_\psi;-\frac{i}{tP_T\theta_\psi}\right)- \\ & -\frac{(R_o^l+1)^{\alpha k_\psi+1}}{\alpha k_\psi+1}{}_2\mathrm{F}_1\left(k_\psi,k_\psi+\frac{1}{\alpha},1+\frac{1}{\alpha}+k_\psi;-\frac{i(R_o^l+1)^\alpha}{tP_T\theta_\psi}\right)- \\ & -\frac{1}{\alpha k_\psi+2}{}_2\mathrm{F}_1\left(k_\psi,k_\psi+\frac{2}{\alpha},1+\frac{2}{\alpha}+k_\psi;-\frac{i}{tP_T\theta_\psi}\right)+ \\ & +\frac{(R_o^l+1)^{\alpha k_\psi+2}}{\alpha k_\psi+2}{}_2\mathrm{F}_1\left(k_\psi,k_\psi+\frac{2}{\alpha},1+\frac{2}{\alpha}+k_\psi;-\frac{i(R_o^l+1)^\alpha}{tP_T\theta_\psi}\right)\Bigg].\end{aligned} \tag{3.20}$$

Finally, using the notation

$$\mathbb{I}_m(z) = {}_2\,\mathrm{F}_1\left(k_\psi,k_\psi+\frac{m}{\alpha},1+k_\psi+\frac{m}{\alpha},-\frac{iz}{tP_T\theta_\psi}\right), \tag{3.21}$$

the CF of $P_k$ is written as

$$\begin{aligned}\varphi_{P_k}(t) = \quad & \frac{2}{\left(R_o^l\right)^2(-itP_T\theta_\psi)^{k_\psi}}\cdot \\ & \cdot\left[\frac{\mathbb{I}_1(1)-(1+R_o^l)^{1+\alpha k_\psi}\mathbb{I}_1\left((1+R_o^l)^\alpha\right)}{1+\alpha k_\psi}+\frac{(1+R_o^l)^{2+\alpha k_\psi}\mathbb{I}_2\left((1+R_o^l)^\alpha\right)-\mathbb{I}_2(1)}{2+\alpha k_\psi}\right].\end{aligned} \tag{3.22}$$

#### 3.2.2.3 Far-field scenario

Regarding the far-field scenario, the derivation of the CF of $P_k$ is similar to the CF derivation of the near-field scenario. Using (3.4) and (3.11), the CF of the power received from the $k$-th transmitter

is written as

$$\varphi_{P_k}(t) = \mathrm{E}_{P_k}[e^{itP_k}] = \int_0^{\infty} \int_{R_i^l}^{R_o^l} e^{itP_T x r^{-\alpha}} f_{R_k^l}(r) f_{\Psi_k}(x)\,\mathrm{d}r\,\mathrm{d}x. \tag{3.23}$$

Replacing the PDFs of the nodes' spatial distribution, (3.6), and fading, (3.9), $\varphi_{P_k}$ can be simplified to

$$\varphi_{P_k}(t) = \frac{1}{\Gamma(k_\psi)\theta_\psi^{k_\psi}} \int_0^{\infty} x^{k_\psi - 1} e^{\frac{-x}{\theta_\psi}} \varphi_{P_k^{PL}}(t)\,\mathrm{d}x, \tag{3.24}$$

where $\varphi_{P_k^{PL}}$ is given by

$$\varphi_{P_k^{PL}}(t) = \frac{2}{\left(\left(R_o^l\right)^2 - \left(R_i^l\right)^2\right)} \int_{R_i^l}^{R_o^l} e^{itP_T x r^{-\alpha}} r\,\mathrm{d}r. \tag{3.25}$$

We solve the integral in (3.25) by using Lemma 3.1. To adopt Lemma 3.1 we have verified that the condition $\frac{2}{\alpha} \notin \mathbb{Z}$ holds. Thus, by using Lemma 3.1 in (3.25), $\varphi_{P_k^{PL}}$ can be rewritten as

$$\varphi_{P_k^{PL}}(t) = \frac{2}{\alpha\left(\left(R_o^l\right)^2 - \left(R_i^l\right)^2\right)} \left[\left(R_o^l\right)^2 \mathrm{Ei}\left(1 + \frac{2}{\alpha}, -itP_T x\left(R_o^l\right)^{-\alpha}\right) - \left(R_i^l\right)^2 \mathrm{Ei}\left(1 + \frac{2}{\alpha}, -itP_T x\left(R_i^l\right)^{-\alpha}\right)\right]. \tag{3.26}$$

Replacing (3.26) in (3.24), the CF $\varphi_{P_k}$ is now written as

$$\begin{aligned} \varphi_{P_k}(t) = & \frac{2}{\alpha\left(\left(R_o^l\right)^2 - \left(R_i^l\right)^2\right)\Gamma(k_\psi)\theta_\psi^{k_\psi}} \cdot \\ & \cdot \left[\int_0^{\infty} x^{k_\psi - 1} e^{\frac{-x}{\theta_\psi}} \left(R_o^l\right)^2 \mathrm{Ei}\left(1 + \frac{2}{\alpha}, -itP_T x\left(R_o^l\right)^{-\alpha}\right)\mathrm{d}x - \right. \\ & \left. - \int_0^{\infty} x^{k_\psi - 1} e^{\frac{-x}{\theta_\psi}} \left(R_i^l\right)^2 \mathrm{Ei}\left(1 + \frac{2}{\alpha}, -itP_T x\left(R_i^l\right)^{-\alpha}\right)\mathrm{d}x\right]. \end{aligned} \tag{3.27}$$

As in Subsection 3.2.2.1, we use Lemma 3.2 to solve the two integrals in (3.27). Since the parameters $\theta_\psi$, $k_\psi$ and $\alpha$ only admit positive and non-zero values, the two conditions in Lemma 3.2 hold. By using Lemma 3.2 and applying the equality (3.19), (3.27) can be simplified to

$$\begin{aligned} \varphi_{P_k}(t) = & \frac{2}{\left(\left(R_o^l\right)^2 - \left(R_i^l\right)^2\right)(-itP_T\theta_\psi)^{k_\psi}} \cdot \\ & \cdot \left[\frac{\left(R_o^l\right)^{\alpha k_\psi + 2}}{\alpha k_\psi + 2} {}_2\mathrm{F}_1\left(k_\psi, k_\psi + \frac{2}{\alpha}, 1 + \frac{2}{\alpha} + k_\psi; -\frac{i\left(R_o^l\right)^\alpha}{tP_T x\theta_\psi}\right) - \right. \\ & \left. - \frac{\left(R_i^l\right)^{\alpha k_\psi + 2}}{\alpha k_\psi + 2} {}_2\mathrm{F}_1\left(k_\psi, k_\psi + \frac{2}{\alpha}, 1 + \frac{2}{\alpha} + k_\psi; -\frac{i\left(R_i^l\right)^\alpha}{tP_T x\theta_\psi}\right)\right]. \end{aligned} \tag{3.28}$$

Finally, using the notation (3.21), the CF in (3.28) is written as

$$\varphi_{P_k}(t) = \frac{2}{\left(\left(R_o^l\right)^2 - \left(R_i^l\right)^2\right)(2+\alpha k_\psi)(-itP_T\theta_\psi)^{k_\psi}} \cdot \left[\left(R_o^l\right)^{2+\alpha k_\psi} \mathbb{I}_2\left(\left(R_o^l\right)^\alpha\right) - \left(R_i^l\right)^{2+\alpha k_\psi} \mathbb{I}_2\left(\left(R_i^l\right)^\alpha\right)\right]. \tag{3.29}$$

## 3.3 PHY layer Performance Model I

The aim of this section is the characterization of the performance of a generic MPR PHY layer to be adopted in the joint PHY/MAC cross-layer optimization. The performance of a generic MPR PHY layer can be evaluated using the capture condition in (3.3) to define the probability of successful reception. Considering (3.3) and using (3.2), the necessary condition for successful reception of the signal transmitted by node $j$ is given by

$$P_j > \Lambda \frac{b}{b+1}, \tag{3.30}$$

which may be rewritten as

$$P_j > b'\Lambda, \tag{3.31}$$

where

$$b' = b/(b+1). \tag{3.32}$$

From (3.31), the probability of successful reception may be written as follows

$$\mathrm{P}_{S_1} = 1 - \mathrm{P}[P_j - b'\Lambda \leq 0]. \tag{3.33}$$

Considering the auxiliary RV $\beta = P_j - b'\Lambda$ and using (3.1) and (3.32), it follows

$$\beta = \frac{P_j}{b+1} - b' \sum_{k=1,k\neq j}^{n} P_k - b'N_0, \tag{3.34}$$

and the CF of $\beta$ is given by

$$\varphi_\beta(t) = \varphi_{P_j}\left(\frac{t}{b+1}\right) \cdot \prod_{k=1,k\neq j}^{n} \varphi_{P_k}(-b't) \cdot \varphi_{N_0}(-b't), \tag{3.35}$$

where $\varphi_{P_k}$ is the CF of the power received from the $k$-th transmitter, given by

$$\varphi_{P_k}(t) \triangleq \int_{-\infty}^{\infty} \mathrm{e}^{itx} f_{P_k}(x)\,\mathrm{d}x. \tag{3.36}$$

By assuming that each individual power $P_k$ is i.i.d., the PDF of the aggregate power given a total of $n$ active transmitters is the convolution of the PDFs of each $P_k$. Thereby, the CF of the aggregate power is given by

$$\varphi_{agg}(t) = \varphi_{P_1}(t) \cdot \varphi_{P_2}(t) \cdot \ldots \cdot \varphi_{P_k}(t) = \left(\varphi_{P_k}(t)\right)^n. \tag{3.37}$$

Following this rationale, the CF of the aggregate power excluding the power received from the node $j$ is given by

$$\prod_{k=1,k\neq j}^{n} \varphi_{P_k}(-b't) = \left(\varphi_{P_k}(-b't)\right)^{n-1}. \tag{3.38}$$

Using (3.38) in (3.35), the CF of the RV $\beta$ can be written as

$$\varphi_{\beta}(t) = \varphi_{P_j}\left(\frac{t}{b+1}\right) \cdot \left(\varphi_{P_k}(-b't)\right)^{n-1} \cdot \varphi_{N_0}(-b't). \tag{3.39}$$

The CF $\varphi_{P_j}$ is equal to $\varphi_{P_k}$, which was derived in Subsection 3.2.2 ((3.22) and (3.29) for the near-field and far-field scenarios, respectively) taking into account the spatial distribution of the transmitters and the propagation effects of the communication channel.

Finally, the distribution $f_{\beta}(x)$ can be obtained by the inverse CF, as follows

$$f_{\beta}(x) = \frac{1}{2\pi} \int_{-\infty}^{\infty} \mathrm{e}^{-ixt} \varphi_{\beta}(t)\, \mathrm{d}t, \tag{3.40}$$

and using (3.39), we obtain

$$f_{\beta}(x) = \frac{1}{2\pi} \int_{-\infty}^{\infty} \mathrm{e}^{-ixt} \varphi_{P_j}\left(\frac{t}{b+1}\right) \cdot \left(\varphi_{P_k}(-b't)\right)^{n-1} \cdot \varphi_{N_0}(-b't)\, \mathrm{d}t. \tag{3.41}$$

From (3.33), the probability of successful packet reception can be written as

$$\mathrm{P}_{S_1} = 1 - \mathrm{P}[\beta \leq 0], \tag{3.42}$$

and, using (3.41), it can be written as follows

$$\mathrm{P}_{S_1} = 1 - \int_{-\infty}^{0} \frac{1}{2\pi} \int_{-\infty}^{\infty} \mathrm{e}^{-ixt} \varphi_{P_j}\left(\frac{t}{b+1}\right) \cdot \left(\varphi_{P_k}(-b't)\right)^{n-1} \cdot \varphi_{N_0}(-b't)\, \mathrm{d}t\mathrm{d}x. \tag{3.43}$$

The PDF $f_{\beta}(x)$ can be computed through the Fourier transform of the CF $\varphi_{\beta}(t)$ in (3.39). By numerically computing (3.43) we obtain the individual probability of a successful reception, $\mathrm{P}_{S_1}$, given $n$ simultaneous transmissions. Finally, the average number of successful receptions is approximated by

$$E_{\mathrm{rcv}_1} = \sum_{k=1}^{n} \mathrm{P}_{S_1} \approx n\mathrm{P}_{S_1}, \tag{3.44}$$

which takes into account the assumption that the multiple $P_k$ are i.i.d..

## 3.4 PHY layer Performance Model II

The model presented in Section 3.3 allows to compute the individual probability of successful reception and the average number of received packets when $n$ simultaneous transmissions occur. Thus, it is possible to characterize the PHY layer performance and obtain important parameters to be considered in the MAC layer. However, the computational complexity of the model increases with the number of simultaneous transmissions. To overcome this problem, in this section we

propose an approximation of the aggregate interference power distribution, i.e. the distribution of the power received from the transmitters acting as interferers.

As stated in Section 3.2, the power of the signals received from the $n$ transmitters are considered as being i.i.d. RVs. The aggregate power received from the multiple transmissions that act as interferers when a single signal is to be decoded from a transmitter $j$ is given by

$$I = \sum_{k=1,k\neq j}^{n} P_k = \sum_{k=1}^{n-1} P_k, \tag{3.45}$$

where $P_k$ is the RV representing the power received from one of $n-1$ interferers.

Starting from the capture condition of the MPR receiver defined in (3.2), and using (3.45), the SINR associated to the signal received from node $j$ is defined by

$$\gamma_j = \frac{P_j}{I + N_0}, \tag{3.46}$$

where $N_0$ is a RV representing the noise power at the receiver.

Considering capture condition in (3.3), and using (3.46), the necessary condition for successful reception of the signal from node $j$ is given as

$$P_j > b(I + N_0). \tag{3.47}$$

From (3.47), the probability of successful reception may be written as follows

$$\mathrm{P}_{S_2} = 1 - \mathrm{P}[P_j - bI - bN_0 \leq 0]. \tag{3.48}$$

Considering the auxiliary RV $\varepsilon = P_j - bI - bN_0$, the CF of $\varepsilon$ is given by

$$\varphi_\varepsilon(t) = \varphi_{P_j}(t) \cdot \varphi_I(-bt) \cdot \varphi_{N_0}(-bt). \tag{3.49}$$

As can be seen, $\varphi_\varepsilon(t)$ in (3.49) is similar to $\varphi_\beta(t)$ in (3.35), apart from the arguments of $\varphi_{P_j}(t)$, $\varphi_{N_0}(t)$, and the characteristic of the interference $\varphi_I(t)$. Instead of deriving the CF of the $n-1$ interferers ($\prod_{k=1,k\neq j}^{n} \varphi_{P_k}(-b't)$ in (3.35)), as we have proposed in Section 3.3, in this section we approximate the interference $I$ to derive the probability of successful packet reception. The main motivation to derive a model that is based on an approximation of the interference is related with the decrease of the computational complexity required to compute the probability of successful packet reception. *A priori* estimation of the interference, although not explored in this work, may also ease the computation of the model, whenever available.

### 3.4.1 Interference Power

The aim of this subsection is the characterization of the aggregate interference power as defined in (3.45). We consider the scenario illustrated in Figure 3.3, where the central node Rx receives data packets from $n$ transmitters located in the far-field area $A = \pi\left((R_o^L)^2 - (R_i^1)^2\right)$. The number of interferers, $n_I$, is given by $n_I = n-1$, $n \geq 1$, because to decode the signal transmitted by one of the $n$ transmitters the remaining ones $(n-1)$ act as interferers. The area $A$ can be obtained via calculus

by dividing the annulus up into an infinite number of annuli of infinitesimal width $\mathrm{d}\chi$ and area $2\pi\chi\ d\chi$ and then integrating from $\chi = R_i^1$ to $\chi = R_o^L$, i.e. $A = \int_{R_i^1}^{R_o^L} 2\pi\chi\,\mathrm{d}\chi$. Using the Riemann sum, $A$ can be approximated by the sum of the area of a finite number ($L$) of annuli of width $\rho$, $A \approx \sum_{l=1}^{L} A_l$, where $A_l = \pi\left(\left(R_o^l\right)^2 - \left(R_i^l\right)^2\right)$ denotes the area of the annulus $l$. $R_o^l = (R_i^1 + l\rho)$ and $R_i^l = (R_i^1 + (l-1)\rho)$ represent the radius of the outer and inner circles of the annulus $l$, respectively.

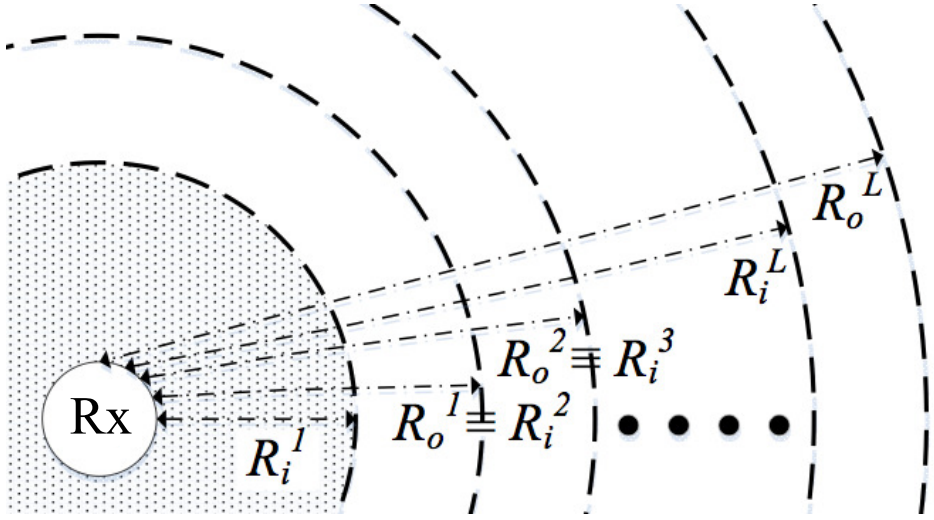


Figure 3.3: The node Rx receives from the $n$ transmitters located in the area $A = \pi\left((R_o^L)^2 - (R_i^1)^2\right)$.

The transmitters are uniformly located in the area $A_l$. The number of interferers located in a specific annulus $l \in \{1,...,L\}$, represented by the RV $X_l$, is distributed according to a Poisson distribution. Its Probability Mass Function (PMF) is truncated to $n_I$, and is represented as follows [PP02]

$$P[X_l = x] = \frac{\frac{(\tau A_l)^x}{x!} e^{-\tau A_l}}{1 - \overline{F}(n_I)}, x = 0, 1, ..., n_I, \tag{3.50}$$

where $\overline{F}(n_I)$ is the complementary Cumulative Distribution Function (CDF) of a Poisson distribution given by

$$\overline{F}(n_I) = \sum_{k=n_I}^{\infty} \frac{(\tau A_l)^k}{k!} e^{-\tau A_l}. \tag{3.51}$$

In (3.50) and (3.51), $\tau$ is the spatial density of the nodes transmitting in the $l$-th annulus. Since the $n_I$ interferers are uniformly distributed within the area $A$, for each annulus $l$ the nodes' density is given by $\tau = \frac{n_I}{\pi\left((R_o^L)^2 - (R_i^1)^2\right)}$.

Considering the scenario illustrated in Fig 3.3, the aggregate interference power $I$ can be rewritten as

$$I = \sum_{l=1}^{L} I_l, \tag{3.52}$$

where $I_l$ is the the amount of power received by the node Rx from the interferers located within the $l$-th annulus. The power $I_l$ is given by

$$I_l = \sum_{k=1}^{n_{I_l}} P_k, \tag{3.53}$$

where $P_k$ is the power received from the $k$-th interferer, and $n_{I_l}$ is the total number of interferers located within the annulus $l$.

Let $M_{I_l}^k(s)$ represent the Moment Generation Function (MGF) of $P_k$ received from the $k$-th interferer ($k = 1, ..., n_{I_l}$) located within the $l$-th annulus. $M_{I_l}^k(s)$ is defined as follows

$$M_{I_l}^k(s) = \mathrm{E}_{P_k}[e^{sP_k}] = \mathrm{E}_{\Psi_k}\Big[\mathrm{E}_{R_k}[e^{sP_k}]\Big]. \tag{3.54}$$

Using (3.4), (3.6) and (3.9), (3.54) is rewritten as follows

$$M_{I_l}^k(s) = \int_0^{+\infty} \int_{R_i^l}^{R_o^l} e^{sP_k} f_{R_l}(r) f_{\Psi_k}(\psi)\, \mathrm{d}r\, \mathrm{d}\psi. \tag{3.55}$$

Using the CF of $P_k$ (in (3.29)) and knowing that for a RV $X$ the MGF can be obtained from its CF, i.e. $M_X(s) = \varphi_X(-is)$, (3.54) can be written as follows

$$M_{I_l}^k(s) = \frac{2\pi}{A_l(2+\alpha k_\psi)(P_T\theta_\psi s)^{k_\psi}} \left( \left(R_o^l\right)^{2+\alpha k_\psi} \mathbb{I}\left(R_o^l\right) - \left(R_i^l\right)^{2+\alpha k_\psi} \mathbb{I}\left(R_i^l\right) \right), \tag{3.56}$$

where $\mathbb{I}(z) = {}_2\mathrm{F}_1\left(k_\psi, k_\psi + \frac{2}{\alpha}, 1 + k_\psi + \frac{2}{\alpha}, -\frac{z^\alpha}{P_T\theta_\psi s}\right)$.

Taking into account the fact that the individual power $P_k$ is i.i.d. with respect to the other transmitters, the PDF of the power $I_l$ given a total of $n_{I_l}$ interferers located within the $l$-th annulus is the convolution of the PDFs of each $P_k$. Following this rationale, the MGF of $I_l$ is given by

$$M_{I_l|n_{I_l}}(s) = \prod_{k=0}^{n_{I_l}} M_{I_l}^k(s) = \left(M_{I_l}^k(s)\right)^{n_{I_l}}. \tag{3.57}$$

Using the law of total probability, the PDF of the power $I_l$ can be written as

$$f_{I_l}(j) \;\; = \sum_{n_{I_l}=0}^{\infty} f_{I_l}(j|X_l = n_{I_l}) \mathrm{P}(X_l = n_{I_l}), \tag{3.58}$$

leading to the MGF of the aggregate interference power, $I_l$, which can be written as

$$\begin{aligned} \mathrm{E}_{I_l}[e^{sI_l}] \;\; &= \sum_{n_{I_l}=0}^{\infty} \left( \int_{-\infty}^{+\infty} e^{sj} f_{I_l}(j|X_l = n_{I_l})\, \mathrm{d}j\, \mathrm{P}[X_l = n_{I_l}] \right) \\ &= \sum_{n_{I_l}=0}^{\infty} M_{I_l|n_{I_l}}(s)\, \mathrm{P}[X_l = n_{I_l}]. \end{aligned} \tag{3.59}$$

Using (3.57), the MGF of $I_l$ is given as follows

$$\mathrm{E}_{I_l}[e^{sI_l}] = \sum_{n_{I_l}=0}^{\infty} \left(M_{I_l}^k(s)\right)^{n_{I_l}} \mathrm{P}[X_l = n_{I_l}]. \tag{3.60}$$

By replacing the PMF of the $X_l$ in (3.60), the MGF of $I_l$ is given as

$$\begin{aligned} \mathrm{E}_{I_l}[e^{sI_l}] &= \sum_{n_{I_l}=0}^{\infty} \left(M_{I_l}^k(s)\right)^{n_{I_l}} \frac{(\tau A_l)^{n_{I_l}}}{n_{I_l}!} e^{-\tau A_l} \frac{1}{1-\overline{F}(n_I)} \\ &= \frac{e^{-\tau A_l}}{1-\overline{F}(n_I)} \sum_{n_{I_l}=0}^{\infty} \frac{\left(\tau A_l M_{I_l}^k(s)\right)^{n_{I_l}}}{n_{I_l}!}. \end{aligned} \tag{3.61}$$

Knowing that $\sum_{k=0}^{\infty} \frac{x^k}{k!} = e^x$ [Jef+07, pp. 26, eq. 1.211.1], the MGF of $I_l$ is finally written as

$$\mathrm{E}_{I_l}[e^{sI_l}] = \frac{e^{\tau A_l\left(M_{I_l}^k(s)-1\right)}}{1-\overline{F}(n_I)}. \tag{3.62}$$

Given the mathematical complexity of the MGF (3.62), we performed multiple simulations and compared the distribution of the aggregate interference power achieved by simulation with different distributions (e.g. Gamma, Normal, Exponential, Lognormal, Poisson, Rayleigh and Weibull). The comparison was made adopting the log-likelihood goodness of fit [PP02]. The log-likelihood test indicated that the Gamma distribution is the one that better approximates the simulation results (as confirmed by the results presented in Figure 3.8 and 3.9). Consequently in what follows we assume that the aggregate interference can be approximated by a Gamma distribution. Therefore, by employing a moment matching method, the parameters of the Gamma distribution can be obtained [AAY10]. For the Gamma approximation, the first and second order matching of moments are sufficient to find its shape and scale parameters that parameterized the Gamma distribution. Using the Law of Total Expectation and Law of Total Variance, the expected value and the variance of the aggregate power can be determined. Since the individual power $P_k$ is i.i.d., it can be shown that

$$\begin{aligned} \mathrm{E}_{I_l}[I_l] &= \mathrm{E}_{X_l}\left[\mathrm{E}_{I_l}[I_l|X_l]\right] \\ &= \mathrm{E}_{X_l}[X_l]\mathrm{E}_{P_k}[P_k], \end{aligned} \tag{3.63}$$

and,

$$\begin{aligned} \mathrm{Var}_{I_l}[I_l] &= \mathrm{E}_{X_l}\left[\mathrm{Var}_{I_l}[I_l|X_l]\right] + \mathrm{Var}_{X_l}\left[\mathrm{E}_{I_l}[I_l|X_l]\right] \\ &= \mathrm{E}_{X_l}[X_l]\mathrm{Var}_{P_k}[P_k] + \mathrm{E}_{P_k}[P_k]^2\,\mathrm{Var}_{X_l}[X_l]. \end{aligned} \tag{3.64}$$

Since $X_l$ follows the truncated Poisson distribution defined in (3.50), the expected value and the variance of $X_l$ are respectively given by (see Appendix B)

$$\mathrm{E}_{X_l}[X_l] = \frac{\tau A_l}{1-\overline{F}(n_I)}, \tag{3.65}$$

and,

$$\mathrm{Var}_{X_l}[X_l] = \frac{\tau A_l}{1-\overline{F}(n_I)}\left((1+\tau A_l) - \frac{\tau A_l}{1-\overline{F}(n_I)}\right). \tag{3.66}$$

Regarding the expected value and variance of the individual power $P_k$, the first moment of $P_k$ is represented by,

$$\begin{aligned} \mathrm{E}_{P_k}[P_k] &= \frac{\partial M_{I_l}^k(0)}{\partial s} \\ &= \frac{2P_T e^{\mu_\xi}\sqrt{e^{\sigma_\xi^2}}}{\left(R_o^l\right)^2 - \left(R_i^l\right)^2}\left(\frac{\left(R_o^l\right)^{2-\alpha} - \left(R_i^l\right)^{2-\alpha}}{2-\alpha}\right), \end{aligned} \tag{3.67}$$

and the second moment of $P_k$ is written as follows

$$\begin{aligned} \mathrm{E}_{P_k}[{P_k}^2] &= \frac{\partial^2 M_{I_l}^k(0)}{\partial s^2} \\ &= \frac{{P_T}^2 k_\psi \theta_\psi^2 (1+k_\psi)}{\left(R_o^l\right)^2 - \left(R_i^l\right)^2}\left(\frac{\left(R_o^l\right)^{2-2\alpha} - \left(R_i^l\right)^{2-2\alpha}}{1-\alpha}\right). \end{aligned} \tag{3.68}$$

Knowing $\mathrm{E}_{P_k}[P_k]$ (3.67), and $\mathrm{E}_{P_k}[{P_k}^2]$ (3.68), and using (3.65) and (3.66), the expected value of the aggregate power is given by

$$\mathrm{E}_{I_l}[I_l] = \frac{\tau A_l}{1-\overline{F}(n_I)}\mathrm{E}_{P_k}[P_k], \tag{3.69}$$

and the variance of the aggregate power is given as follows

$$\mathrm{Var}_{I_l}[I_l] = \frac{\tau A_l}{1-\overline{F}(n_I)}\left(\mathrm{E}_{P_k}[{P_k}^2] + \left(\mathrm{E}_{P_k}[P_k]\right)^2\left(\tau A_l - \frac{\tau A_l}{1-\overline{F}(n_I)}\right)\right). \tag{3.70}$$

Consequently, the shape and the scale parameters of the Gamma distribution that characterizes the aggregate interference caused by the transmitters within the annulus $l$ are respectively given by

$$\begin{aligned} k_l &= \frac{\mathrm{E}_{I_l}[I_l]^2}{\mathrm{Var}_{I_l}[I_l]}, \\ \theta_l &= \frac{\mathrm{Var}_{I_l}[I_l]}{\mathrm{E}_{I_l}[I_l]}. \end{aligned} \tag{3.71}$$

The accuracy of the Gamma approximation will be evaluated in detail in Section 3.5. In this way, we assume that the power $I_l$ received from the transmitters located within the $l$-th annulus is approximated by a Gamma distribution, with CF the $\varphi_I^l(t) = (1 - i\theta_l t)^{-k_l}$.

Since the annulus of width $R_o^L - R_i^1$ is expressed as a summation of $L$ annuli of width $\rho$, the CF of the aggregate power received from the $n_I$ transmitters that may be located within the $L$ annuli is given by

$$\varphi_I(t) \approx \prod_{l=1}^{L}(1 - i\theta_l t)^{-k_l}. \tag{3.72}$$

### 3.4.2 Probability of Successful Packet Reception

The distribution $f_\varepsilon(x)$ in (3.49), can be obtained by the inverse CF, as follows

$$f_\varepsilon(x) = \frac{1}{2\pi}\int_{-\infty}^{\infty} \mathrm{e}^{-ixt}\varphi_\varepsilon(t)\,\mathrm{d}t. \tag{3.73}$$

From (3.48), the probability of successful packet reception can be written as

$$\mathrm{P}_{S_2} = 1 - \mathrm{P}[\varepsilon \leq 0], \tag{3.74}$$

and, using (3.73), we obtain

$$\mathrm{P}_{S_2} = 1 - \int_{-\infty}^{0} f_{\varepsilon}(x)\mathrm{d}x. \tag{3.75}$$

Considering the CF of $\varepsilon$ in (3.49), and the CFs $\varphi_{P_j}(t)$, $\varphi_{N_0}(t)$ and $\varphi_I(t)$, respectively defined in (3.29), (3.10) and (3.72). By using (3.49) and (3.72), the probability of successful packet reception is written as follows

$$\mathrm{P}_{S_2} \approx 1 - \frac{1}{2\pi}\int_{-\infty}^{0}\int_{-\infty}^{\infty} \mathrm{e}^{-ixt}\varphi_{P_j}(t)\cdot\prod_{l=1}^{L}(1+i\theta_l bt)^{-k_l}\cdot\varphi_{N_0}(-bt)\mathrm{d}t\mathrm{d}x, \tag{3.76}$$

where $\varphi_{P_j}(t)$ is given in (3.29) and $\varphi_{N_0}(t)$ is given in (3.10). By numerically computing (3.76) through a Fast Fourier Transform (FFT) algorithm, we obtain the individual probability of a successful reception, $\mathrm{P}_{S_2}$.

Finally, the average number of received packets ($E_{\mathrm{rcv}_2}$) is approximated by

$$E_{\mathrm{rcv}_2} \approx n\mathrm{P}_{S_2}. \tag{3.77}$$

## 3.5 Performance Evaluation

This section presents a set of performance results of the two models proposed in Section 3.3 and Section 3.4. The model presented in Section 3.3 is evaluated in the Subsection 3.5.1. A method to compute the optimal point of operation of the PHY layer performance is proposed in this subsection. The impact of the noise power at the receiver, and the propagation effects in the performance of the MPR PHY layer are also analyzed. Subsection 3.5.2 describes a set of simulations and numerical results to validate the aggregate interference approximation presented in Section 3.4. Finally, Subsection 3.5.3 presents a set of performance results to assess the accuracy of the PHY layer performance model.

### 3.5.1 PHY layer Model I

This subsection describes a set of simulations and numerical results to validate the probability of successful packet reception ($\mathrm{P}_{S_1}$), as well as the average number of received packets ($E_{\mathrm{rcv}_1}$), both related with the model proposed in Subsection 3.3. In each simulation trial $n$ transmitters were randomly spaced from the receiver. The individual distance between each transmitter and the receiver was randomly chosen using a uniform distribution in the interval [1 m, $R_o^l$]. The fading was randomly generated for each transmitter through a random generator implementing the PDF in (3.9). The power received from each transmitter ($P_k$) was then computed according to (3.4). At the final stage, the capture criterion (3.3) was applied to each transmitter to obtain the number of transmissions successfully received in a simulation trial. Finally, the number of successful

transmissions was averaged over the total number of trials to obtain $E_{\mathrm{rcv}_1}$, the expected number of received packets.

The simulations were parametrized according to the data presented in Table 3.1 and were computed using the Matlab software package.

Table 3.1: Parameters adopted in the simulations for the PHY layer Model I validation.

| Number of trials | $1 \times 10^5$ | $P_T$ | 5 dB |
|---|---|---|---|
| $R_i^l$ | 0 m | $R_o^l$ | 10 m |
| $\alpha$ | 2 | $\sigma_{N_0}$ | 1 (0 dB) |
| $\sigma_\xi$ | 0.7 | | |

Figures 3.4 and 3.5 illustrate the individual reception probability and the average number of received packets given $n$ transmitters, for different values of $b$. The curves identified as "Simul." represent the data obtained through simulation and the ones denoted as "Teor." were obtained through the numerical computation of (3.43) and (3.44) (to obtain $\mathrm{P}_{S_1}$ and $E_{\mathrm{rcv}_1}$, respectively). To compute $\mathrm{P}_{S_1}$ in (3.43) we have first computed $f_\beta(x)$ in (3.41) through the FFT algorithm (the domain $x$ was set to $[-10, 10]$ and a step of $3 \times 10^{-4}$ was adopted in the FFT algorithm).

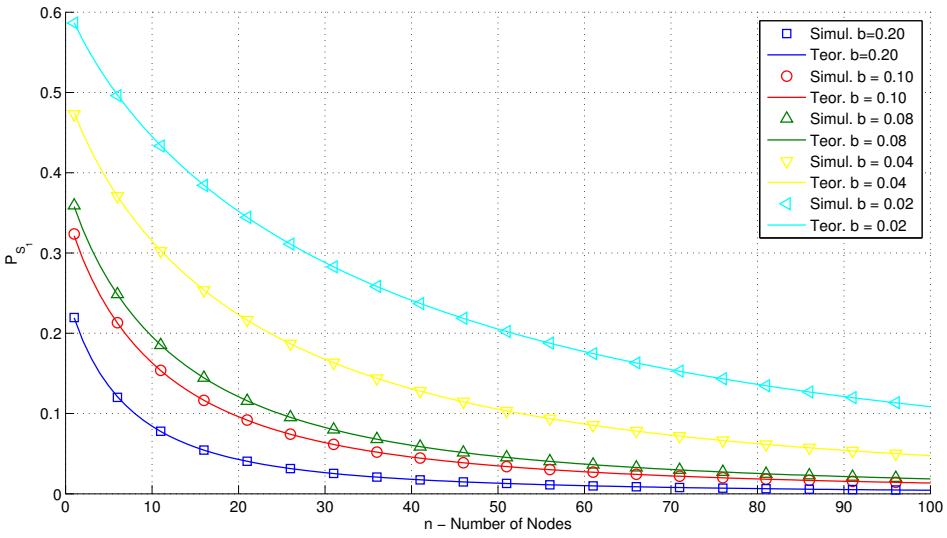


Figure 3.4: Packet reception probability ($\mathrm{P}_{S_1}$) given $n$ transmitters.

In Figure 3.4 we observe that the numerical values of $\mathrm{P}_{S_1}$ closely follow the results obtained by simulation. The figure also shows that the probability of successful packet reception decreases as $n$ increases. This is an expected behavior because the SINR associated to a transmission decreases as the number of nodes increases, and a lower SINR leads to a smaller probability of successful packet reception. Finally, for a given value of $n$, the results confirm that the probability of successful packet reception increases as the receiving threshold $b$ decreases, and the numerical results were also validated for multiple threshold values.

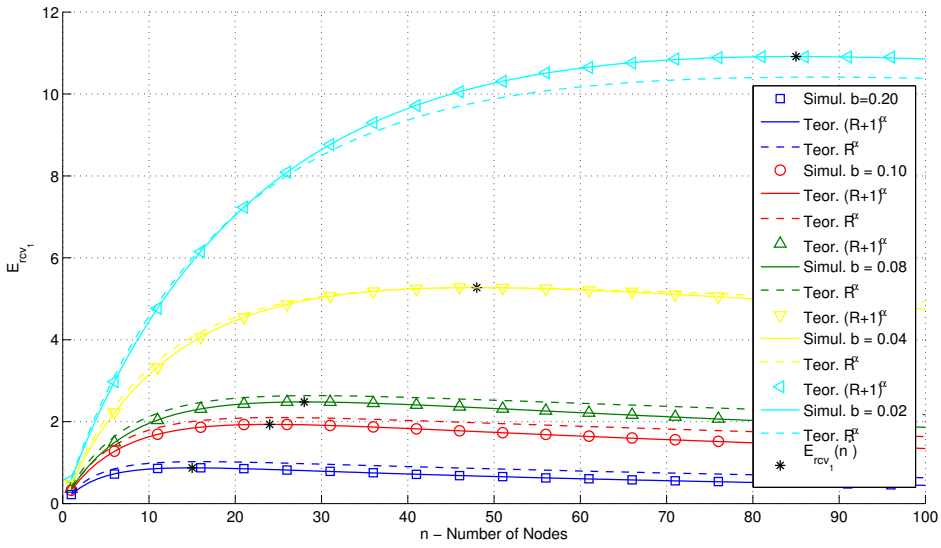


Figure 3.5: Average number of received packets ($E_{\text{rcv}_1}$) given $n$ transmitters.

Figure 3.5 shows the average number of received packets given $n$ transmitters. The curves identified as "Teor. $R^{-\alpha}$" and "Teor. $(R+1)^{-\alpha}$" assume the far-field propagation model (i.e., (3.4)) and the near-field propagation model (i.e., (3.5)), respectively. We observe that the far-field propagation model is not adequated to characterize the average number of received packets when one or more transmitters are close to the receiver. Regarding the adoption of the near-field path loss approximation, the numerical results are still close to the results obtained by simulation. As can be seen, for each threshold value $b$ there is an optimal number of simultaneous transmitters that maximize the number of successful received packets, represented by the maximum value of each curve. Moreover, $E_{\text{rcv}_1}$ asymptotically converges to 0 as $n \to \infty$.

The optimal number of transmitters, $n^*$, that maximize $E_{\text{rcv}_1}$ can be determined by computing the root of the partial derivative $\frac{\partial E_{\text{rcv}_1}}{\partial n}$, given by

$$\begin{aligned}\frac{\partial E_{\text{rcv}_1}}{\partial n} = 1 &- \frac{1}{2\pi}\int_{-\infty}^{0}\int_{-\infty}^{\infty} \mathrm{e}^{-ixt}\varphi_{P_j}\left(\frac{t}{b+1}\right)\cdot\left(\varphi_{P_k}(-b't)\right)^{n-1}\cdot\varphi_{N_0}(-b't)\,\mathrm{d}t\,\mathrm{d}x \\ &- \frac{n}{2\pi}\int_{-\infty}^{0}\int_{-\infty}^{\infty} \mathrm{e}^{-ixt}\varphi_{P_j}\left(\frac{t}{b+1}\right)\cdot\left(\varphi_{P_k}(-b't)\right)^{n-1}\cdot\varphi_{N_0}(-b't)\cdot\log\left(\varphi_{P_k}(-b't)\right)\mathrm{d}t\,\mathrm{d}x.\end{aligned} \tag{3.78}$$

Departing from the partial derivative $\frac{\partial E_{\text{rcv}_1}}{\partial n}$ in (3.78), the solution of $\frac{\partial E_{\text{rcv}_1}}{\partial n} = 0$ for $n$ has no closed-form and, consequently, only a numerical approximation can be computed. Considering that $n \in \{1, 2, ..., \mathrm{N}\}$, the optimal number of transmitters can be approximated by the following optimization problem

$$n^* \triangleq \underset{n\in\{1,2,...,\mathrm{N}\}}{\arg\min}\left|\frac{\partial E_{\text{rcv}_1}}{\partial n}\right|. \tag{3.23}$$

In this way, $n^*$ can be computed through a brute-force search that numerically computes $\left|\frac{\partial E_{\text{rcv}_1}}{\partial n}\right|$ in each of the $N$ iterations. In Figure 3.5 the black asterisks positioned over each curve represent the optimal value of $E_{\text{rcv}_1}$ obtained for $n^*$ computed through (3.23).

In order to compare $E_{\text{rcv}_1}$ with and without considering noise at the receiver ($N_0$), two simulation scenarios with different transmitting power levels ($P_T$) were also characterized: $P_T = 1$ dB and $P_T = 5$ dB. The remaining parameters adopted in the simulations are according to the values presented in Table 3.1. The simulated and numerical results are plotted in Figure 3.6, being close to each other. When noise is absent ($\sigma^2_{N0} = 0$) the average number of received packets increases. When noise is considered ($\sigma^2_{N0} = 1$), we observe that for the same threshold $b$ an increase of the transmission power $P_T$ leads to an increase of the average number of received packets because higher SINR values are achieved at the receiver.

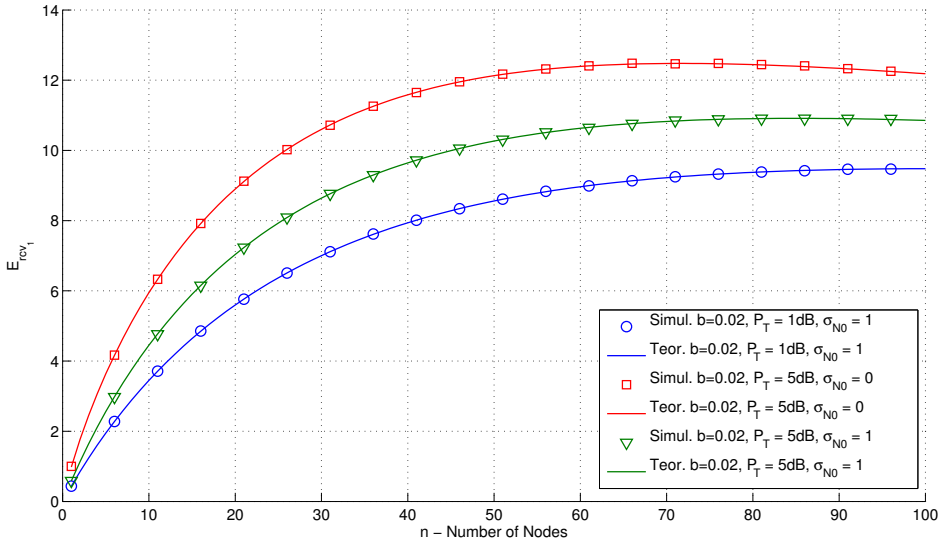


Figure 3.6: Average number of received packets ($E_{\text{rcv}_1}$) given $n$ transmitters ($P_T = \{1, 5\}$ dB, $\sigma^2_{N0} = \{0, 1\}$).

Figures 3.7 (a) and (b) show $E_{\text{rcv}_1}$ for different propagation effects considering near-field and far-field scenarios, respectively. The near-field scenario is represented by the area $A_l = \pi\left(R_o^l\right)^2$ and the far-field scenario is represented by the area $A_l = \pi\left(\left(R_o^l\right)^2 - \left(R_i^l\right)^2\right)$. The curves identified as "Simul." represent the data obtained through simulation, while the ones identified as "Teor." were obtained with (3.44). The CFs (3.22) and (3.29) were adopted in the numerical computation of the near-field and far-field scenarios, respectively. Regarding the figure's legend, "PL" represents the case where only path loss effect is considered, $\sigma_\xi \to 0$ indicates that both path loss and Rayleigh fading is considered, and $\sigma_\xi = 0.7$ indicates that the three effects were considered (path loss, Rayleigh fading and shadowing). Regarding the FFT algorithm, we set the domain of $x$ to $[-200, 200]$ and a step of $61 \times 10^{-4}$. The remaining parameters adopted in the simulations are according to the values presented in Table 3.2.

Table 3.2: Parameters adopted in the simulations of a near-field and a far-field scenarios.

| Number of trials | $1 \times 10^5$ | $P_T$ | 20 dB |
|---|---|---|---|
| $\alpha$ | 2 | $\sigma_{N_0}$ | 1 (0 dB) |
| $\sigma_\xi$ | 0.7 | $b$ | 0.04 |

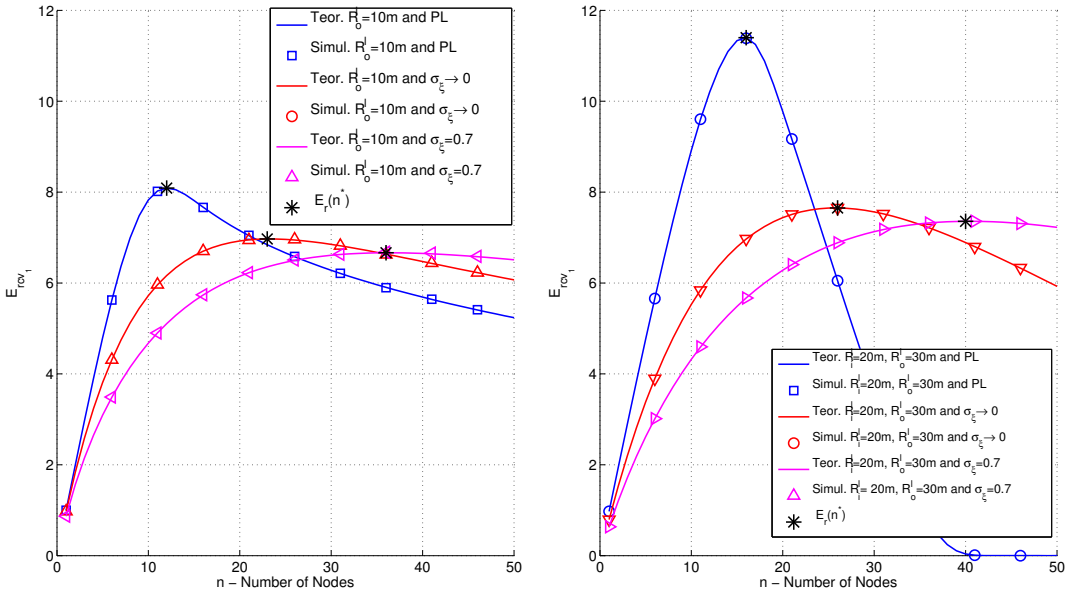


(a) (b)

Figure 3.7: Average number of received packets ($E_{\text{rcv}_1}$) given $n$ transmitters: (a) Near-field scenario; (b) Far-field scenario.

The simulated and numerical results are close to each other. Regarding the three scenarios of propagation effects, the far-field scenario has a maximum average number of received packets always higher than the near-field scenario. This is an expected result because a bigger area is adopted in the far-field scenario, allowing the nodes to be more dispersed, which leads to higher SINR values (considering the average of all received signals). For both near-field and far-field scenarios the maximum average number of received packets is higher when only path loss effect is considered. $E_{\text{rcv}_1}$ decreases as the level of fading increases. As can be observed in the figure, the noise and the propagation effects have a significant impact on the PHY layer performance. Consequently, for an accurate characterization of the PHY layer performance, the noise at the receiver side and the propagation effects (i.e. path loss, small-scale fading and shadowing) should be considered.

Although the trend of the results presented in Figures 3.7 (a) and (b) is as expected, we point out that the proposed methodology to compute the numerical values of $\text{P}_{S_1}$ and $E_{\text{rcv}_1}$ effectively constitutes an advantage in terms of computational time due to the use of the FFT algorithm in (3.43). Moreover, the proposed characterization is particularly useful to derive the optimal number of transmitters, which is an important parameter when cross-layer optimization techniques are

adopted to jointly improve the efficiency of the PHY layer with the upper layers.

### 3.5.2 Validation of the Aggregate Interference Distribution

This subsection evaluates the assumption that the aggregate interference power is distributed according to a Gamma distribution, as described in Subsection 3.4.1. It is considered a scenario formed by multiple nodes transmitting simultaneously to a single receiver. The transmitters are located in annulus $l$ with area $A = \pi\left(\left(R_o^l\right)^2 - \left(R_i^l\right)^2\right)$, and distributed according to a 2D Poisson point process.

Figure 3.8 represents the CDF of the aggregate interference caused by the transmitters located within annulus $l$, for different values of $\tau$. Figure 3.9 shows the CDF of the aggregate interference caused by the transmitters positioned within the annulus $l$, for a density $\tau = 2\times10^{-3}$nodes/m$^2$ and considering different scenarios of propagation effects (different values of $\sigma_\xi$). The curve identified as "Simul." represents the data obtained by simulations. The curves representing the Gamma distribution approximation are parameterized with the shape and scale parameters computed through (3.71). In Figure 3.9 the curve identified as "Gamma Approx. (PL)" represents a scenario where only Path Loss effect is considered.

From the results in Figure 3.8 and 3.9, we observe that the Gamma approximation proposed in Subsection 3.4.1 accurately characterizes the aggregate interference, being valid for different density values and different scenarios of signal propagation (i.e. path loss, small-scale fading and slow fading).

Figure 3.10 illustrates the PDF of the aggregate interference computed for the scenarios considered in Figure 3.9. From the results we observed that the distribution is similar to a Gaussian

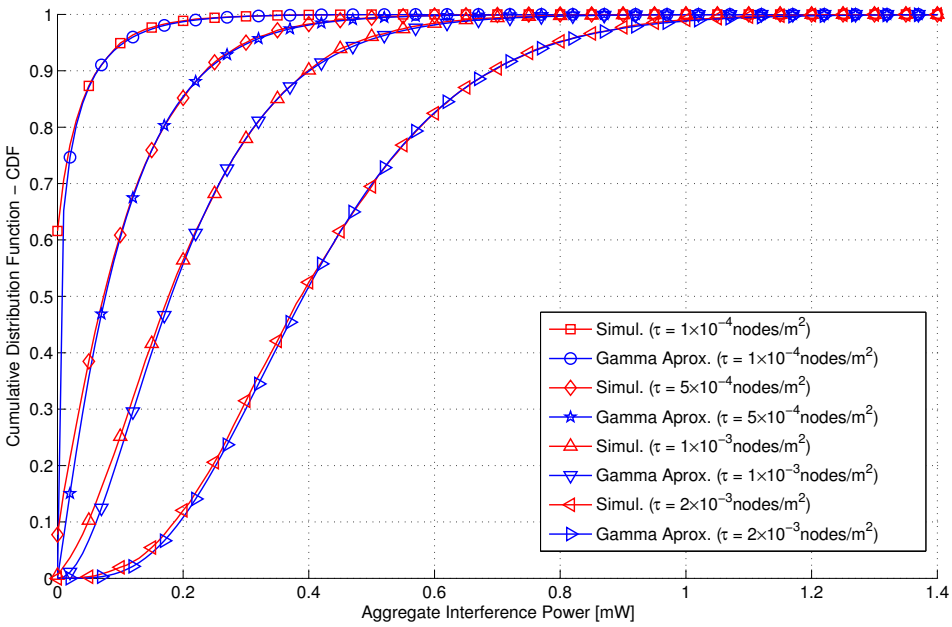


Figure 3.8: CDF of the aggregate interference and the Gamma approximation for different nodes' density $\tau$ ($P_T = 20$ dB, $R_i^l = 50$ m, $R_o^l = 70$ m, $\sigma_\xi = 0.7$ and $\alpha = 2$).

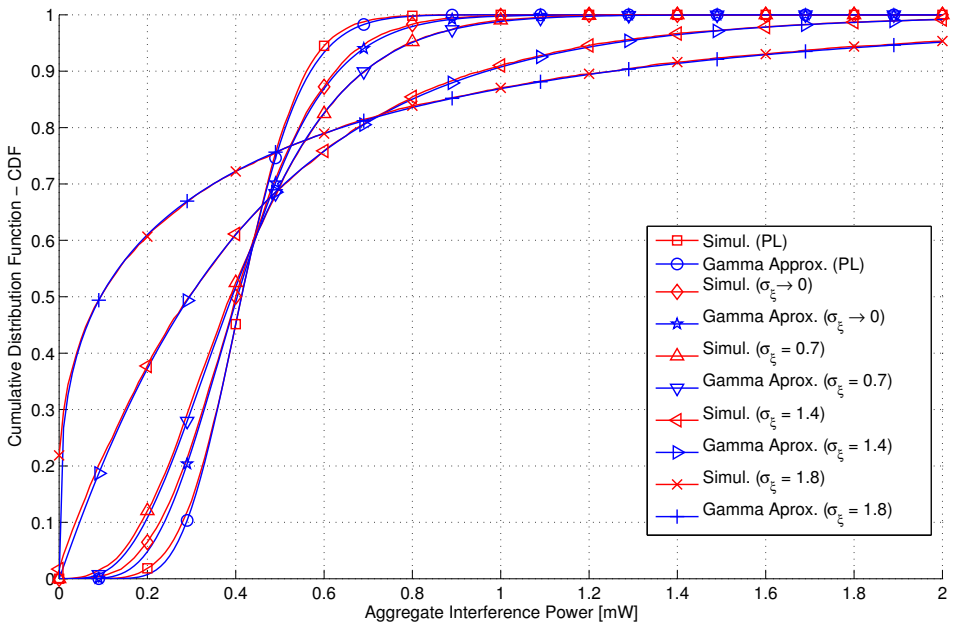


Figure 3.9: CDF of the aggregate interference and the Gamma approximation for different values of $\sigma_\xi$ ($P_T = 20$ dB, $R_i^l = 50$ m, $R_o^l = 70$ m, $\tau = 2 \times 10^{-3}$ nodes/m$^2$ and $\alpha = 2$).

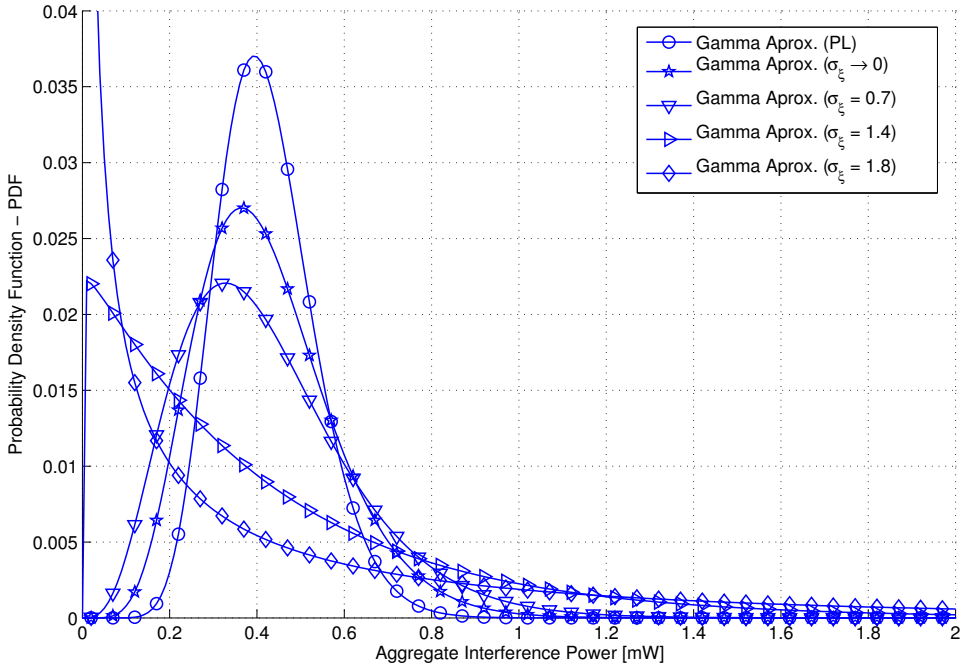


Figure 3.10: PDF of the aggregate interference and the Gamma approximation for different values of $\sigma_\xi$ ($P_T = 20$ dB, $R_i^l = 50$ m, $R_o^l = 70$ m, $\tau = 2 \times 10^{-3}$ nodes/m$^2$ and $\alpha = 2$).

distribution when only path loss is considered. The same is observed when only path loss and Rayleigh fading is considered, i.e. without considering shadowing ($\sigma_\xi \to 0$). These observations suggest that the CLT would be appropriate to model the aggregate interference in these cases, and therefore a Gaussian distribution may accurately characterize the aggregate interference power. However, this assumption is no longer valid as the uncertainty of the shadowing increases.

### 3.5.3 PHY layer Model II

In this Subsection we assess the model proposed in Section 3.4. As in Subsection 3.5.1, a set of simulations and numerical results were performed to validate the probability of successful packet reception ($\mathrm{P}_{S_2}$ in (3.76)), as well as the average number of received packets ($E_{\mathrm{rcv}_2}$) in (3.77).

We considered a scenario formed by a receiver circled by $n$ transmitters located in the area $A = \pi\left((R_o^L)^2 - (R_i^1)^2\right)$, which were distributed according to the PDF in (3.6). Different fading ($\Psi_k$) and noise ($N_0$) realizations were used on each trial, being the receiving condition (3.3) observed for each transmitter $j$. The statistical results collected from the simulations included the expected number of received packets, $E_{\mathrm{rcv}_2}$, as well as the probability of successful packet reception, $\mathrm{P}_{S_2}$. Each simulation trial was performed as described in Subsection 3.5.1. The simulations were parameterized according to the data presented in Table 3.3 and were computed using the Matlab software package.

Table 3.3: Parameters adopted in the simulations for the PHY layer Model II validation.

| Number of trials | $1 \times 10^5$ | $P_T$ | 20 dB |
|---|---|---|---|
| $R_i^1$ | 10 m | $R_o^L$ | 100 m |
| $\alpha$ | 2 | $\sigma_{N_0}$ | 1 (0 dB) |
| $\sigma_\xi$ | 0.7 | | |

Figures 3.11 and 3.12 illustrate the individual reception probability and the average number of received packets given $n$ transmitters, for different values of $b$. The curves identified as "Simul." represent the data obtained through simulation, while the ones identified as "Teor." were obtained by numerically computing (3.76) and (3.77), for the case of $\mathrm{P}_{S_2}$ and $E_{\mathrm{rcv}_2}$, respectively. In order to compare the accuracy of the model for different number of annuli, we have considered $L = \{1, 10\}$. To compute $\mathrm{P}_{S_2}$ in (3.76) we have first computed $f_\epsilon(x)$ in (3.73) using the FFT algorithm (to compute (3.73) the domain of $x$ was set to $[-200, 200]$ and a step of $61 \times 10^{-4}$ was adopted in the FFT algorithm).

From Figure 3.11 we observe that the numerical values of $\mathrm{P}_{S_2}$ closely follow the results obtained by simulation. As seen in the previous subsection, the figure shows that the probability of successful packet reception decreases as $n$ increases. This is because the SINR associated to each reception decreases as the number of nodes increases, and a lower SINR leads to a smaller probability of successful packet reception. Finally, the numerical results of the probability of successful packet reception were also validated for multiple threshold values ($b$). Regarding the

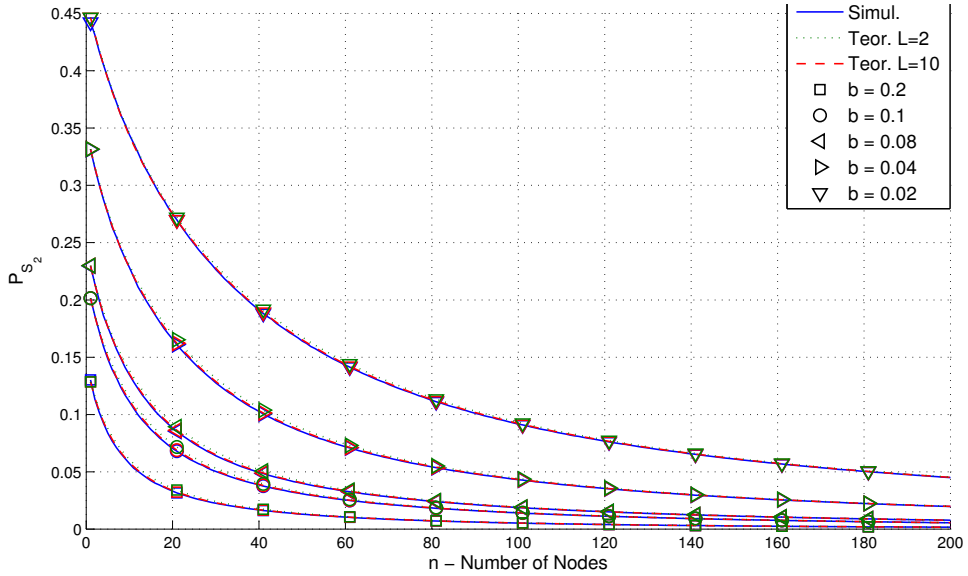


Figure 3.11: Packet reception probability ($P_{S_2}$) given $n$ transmitters.

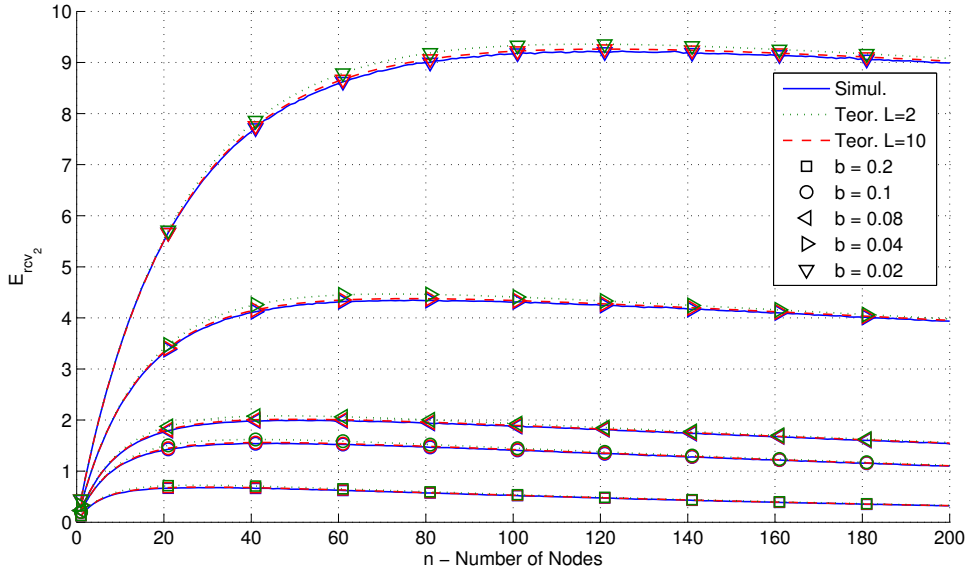


Figure 3.12: Average number of received packets ($E_{\mathrm{rcv}_2}$) given $n$ transmitters.

average number of successful received packets, plotted in the Figure 3.12, the numerical results are still close to the results obtained by simulation.

As can be seen, for each threshold value $b$ there is an optimal number of simultaneous transmitters that maximize the number of successful received packets. Another point to highlight is the higher accuracy of the model as the number of annuli ($L$) increases. By considering more annuli, the expectation of the interference caused by the nodes located on each annulus is more accurate, leading to a higher accuracy of the model.

## 3.6 Conclusions

The current chapter presents two mathematical models to characterize the performance of an MPR-based PHY layer to be adopted in the joint PHY/MAC cross-layer optimization. The performance of the MPR PHY layer is characterized by deriving the individual probability of successful packet reception ($\mathrm{P}_{S_1}$ and $\mathrm{P}_{S_2}$) and the average number of successful received packets ($E_{\mathrm{rcv}_1}$ and $E_{\mathrm{rcv}_2}$) when $n$ simultaneous transmissions occur. The computation of the probability takes into account the path loss effect, small and large-scale fading propagation effects, the decision threshold that characterizes the receiving system, and the influence of noise at the receiver side. In a first approach, a model was proposed to compute the $\mathrm{P}_{S_1}$ and $E_{\mathrm{rcv}_1}$ for near-field and far-field scenarios. In the second approach, a Gamma distribution approximation of the aggregate interference generated by the transmitters located in the annulus $l$ was explored. Considering the Gamma distribution approximation of the aggregate interference power, it was possible to derive the probability of successful packet reception ($\mathrm{P}_{S_2}$) when multiples transmitters are located in multiple annulus. In this approach the computational complexity of the model only depends on the number of considered annuli, contrarily to the first model that depends on the number of transmitters. To evaluate the accuracy of the two proposed models, the PHY layer performance was assessed for the different scenarios of near-field and far-field, considering different propagation effects. The results show that the Gamma distribution approximation can be adopted to model the aggregate power received from the transmitters located in a given annulus. Regarding the PHY layer performance characterized by the probability of successful packet reception and the average number of successful received packets, it was shown that the PHY layer performance is accurately characterized by the numerical results.

The proposed methodology to compute the numerical values of $\mathrm{P}_{S_1}$, $\mathrm{P}_{S_2}$, $E_{\mathrm{rcv}_1}$ and $E_{\mathrm{rcv}_2}$ effectively constitutes an advantage in terms of computational time due to the use of the FFT algorithm. Consequently, the proposed characterization is particularly useful to identify the optimal number of transmitters, which is an important parameter when cross-layer optimization techniques are adopted to jointly improve the efficiency of the PHY layer with the upper layers.

CHAPTER 4

# ILWNS' PERFORMANCE IN SHARED CHANNELS

## 4.1 Introduction

The ILWNs are characterized by the lack of wired infrastructure and pose unique challenges in the design of the PHY and MAC layers. Due to the distributed nature of these networks, and the fact that nodes simultaneously cooperate and compete for the network resources, the design of the MAC protocols plays an important role and has a large impact on the throughput of an ILWN [GLA+07a; GK00; GK03; Sad+10].

Nowadays several distributed protocols (such as IEEE 802.11 and IEEE 802.15.4) operate in shared Industrial Scientific Medical bands (e.g. 2.4 GHz). In such shared bands the interference level is usually high because they are utilized by different wireless technologies. One critical issue in ILWN operating in shared bands is the problem of dealing with Spatial Interference (as seen in the Subsection 2.2.2), which arises from the need of sharing the same wireless channel controlled in a decentralized way. In a shared channel multiple interferers may decrease the communication performance because they are not controlled by a central entity capable of mitigating the spatial interference. This fact is of particular importance as the density of nodes increase, because the nodes far away from the receiver may also cause non-negligible interference.

One of the solutions to avoid undesired levels of interference in shared channels consists on detecting the channel's interference level before starting the communication process. Suppose the node $SU_{Rx}$ represented in Figure 4.1 is the node responsible for receiving the information transmitted by a single (SPR) or multiple (MPR) $SU_{Tx}$ nodes. In the figure the node $SU_{Rx}$ has a given sensing range, which is limited by the radius $R_G$. In this chapter we consider that the $SU_{Tx}$ node(s) transmitting to the $SU_{Rx}$ node is(are) located within the sensing region. When the level of interference is high, the receiver and the transmitters may postpone the communication until lower interference levels are found in the channel. By doing so, the receiver node can increase

the probability of successfully receiving the packet(s). Simultaneously, the transmitters can also guarantee a certain level of protection to other communications (primary communications) that are already using the channel, which can be performed by the PU nodes indicated in the figure. Primary communications can be performed by:

- Nodes outside the sensing range of the receiver. These often occur in high density networks, and are represented in the figure by the PU nodes located in the gray zone;
- Nodes adopting different communication technologies located within the sensing region, or adopting the same technology but transmitting to a different node (not transmitting to $SU_{Rx}$). These primary communications may occur when the channel is shared by multiple nodes, and may be started by the PU nodes located within the sensing zone represented in the figure.

In Figure 4.1 the PU nodes may interfere with the communications performed between the $SU_{Rx}$ and the $SU_{Tx}$ nodes. We intentionally use the verb "may", because we assume that PUs access to the channel with a given probability.

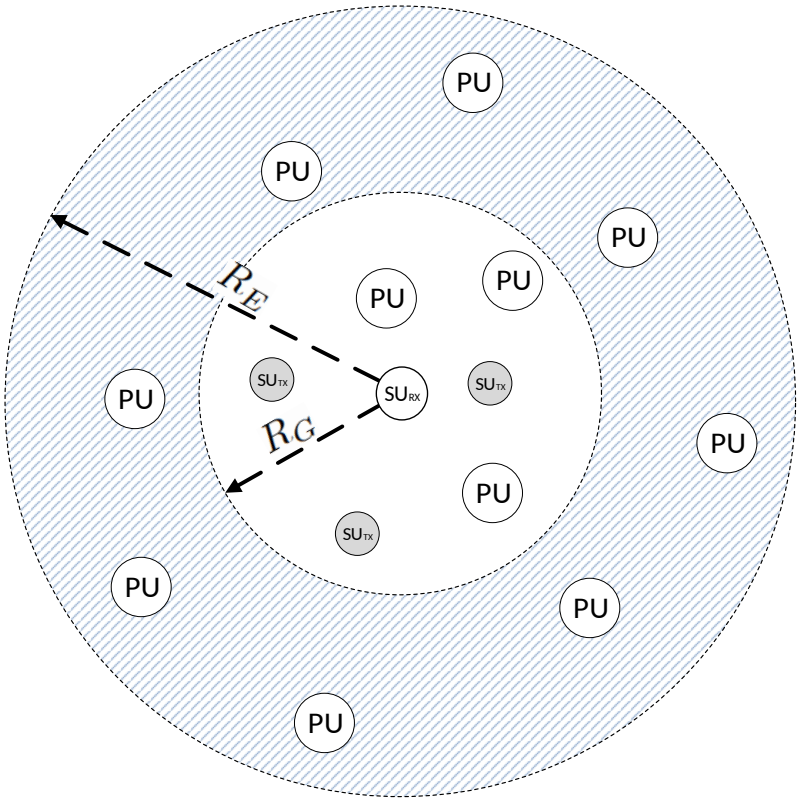


Figure 4.1: High density network scenario considered in the chapter.

The main motivation of this chapter is the characterization of the performance achieved by the receiving node $SU_{Rx}$ when it senses the channel as being idle and indicates to possible transmitters ($SU_{Tx}$) that they can start communicate. The performance is assessed through the throughput achieved by the SU nodes. The throughput is characterized for the case when the channel is idle (sensed and declared idle by the $SU_{Rx}$ node), since our goal is to consider that the nodes

only communicate after observing that condition. Over this chapter we adopt the terminology "conditional throughput" to indicate the throughput achieved after (or given that) the channel is sensed idle.

We highlight that from the perspective of the receiving node $SU_{Rx}$ and transmitting nodes $SU_{Tx}$, the scenario presented in Figure 4.1 includes several features that can be found in Cognitive Radio Networks (CRNs) [Hay05]. This is mainly because the SU nodes sense the channel and opportunistically access to the channel based on the sensing outcomes. Similarly, by postponing their transmissions the SU nodes protect the transmissions of the PU nodes. Due to this fact, the next subsection describes a few works on CRNs addressing different aspects that are useful for the scenario under consideration in this chapter.

### 4.1.1 Related Work on Cognitive Radio Networks

The nodes forming CRNs adopt cognitive radio practices and are usually denominated Secondary Users (SUs). Regularly, SUs represent unlicensed nodes, and consequently must be aware of the activity of the licensed users. The licensed users are denominated Primary Users (PUs). The SUs access the spectrum in an opportunistic way without causing to harmful interference the PUs. From the previous description we can easily find a similar behavior between the CRNs nodes and the SU nodes considered in the scenario depicted in Figure 4.1. From now on we adopt the acronyms SU and PU to represent the nodes of the scenario considered in this chapter (in Figure 4.1), as well as the nodes forming a CRN.

SUs ensure a level of protection to PUs by using Spectrum Sensing (SS) techniques. SS plays a central role in CRNs. The sensing aims at detecting the availability of vacant portions (holes) of spectrum and has been a topic of considerable research over the last years [YA09]. The traditional SS techniques include: Waveform-based Sensing (WBS) [ZG+12], a coherent technique that consists on correlating the received signal with *a priori* known set of different waveform patterns; Matched Filter-based Sensing (MFBS) [Bou+08], an optimal sensing scheme where the received signal is also correlated with a copy of the transmitted one; and Cyclostationarity-based Sensing (CBS) [AH+10], a technique that exploits the periodic characteristics of the received signals, *i.e.*, carrier tones, pilot sequences, etc. Additionally, several sensing techniques have been recently proposed, and briefly summarized in [Mas+13] and [Sun+13]. MFBS assumes prior knowledge of the primary's signal, while WBS assumes that the received signal matches with one of the patterns previously known. This means that these sensing techniques are not feasible in some bands, where several communication technologies may operate without *a priori* knowledge. On other hand, CBS is impracticable for signals that do not exhibit cyclostationarity properties.

Energy-Based Sensing (EBS) is the simplest spectrum sensing technique. The energy-based detection principle employed in EBS was first studied by Urkowitz, who formulated the problem as a binary hypothesis testing for the detection of deterministic signals considering white [Urk67] and colored [Urk69] Gaussian noise. The analysis of energy-based detection was extended by Kostylev [Kos02] to signals with random amplitude caused by fading effects. Similar analysis of energy-based detection was also considered in [Dig+07], which provides a closed-form expression for the

probability of detection for Rayleigh, Nakagami and Rician fading channels. Similar assumptions were formally treated in a different way in [Her+11] and [GS07]. [Sof+13] presents an analysis of energy detection performance considering generalized $\kappa - \mu$ extreme fading channels. The previous works have considered fast fading channels. [Sun+10] derives an approximation used to compute the probability of detection in slow fading channels. EBS has been studied in several CR scenarios, namely on local and cooperative sensing schemes [YA09]. More recently, several EBS schemes adopting sub-nyquist sampling have been proposed, which are advantageous in terms of the sensing duration [Sun+13]. It is well known that EBS can exhibit low performance in specific comparative scenarios [BM10], or when noise's variance is unknown or very large. In this chapter we consider that SU nodes adopt EBS. This assumption is based on the advantage that EBS does not need any *a priori* knowledge of PU's signal.

In the aforecited papers a single PU is considered. The methodology to write the probabilities of detection and false alarm is based on the assumption that the distribution of both hypotheses is Gaussian. While relying on the CLT, the number of samples required to observe this assumption is generally high, and its impact on the SUs' throughput can not be negligible. The detection and false alarm probabilities are used to define the decision threshold. The majority of works simply compute the decision threshold for a required probability of detection or false alarm [GS07], which is known as the constant false alarm ratio criterion. But another parameterization criteria can be found in the literature: [LA08] proposes a decision threshold parameterization imposing the probabilities of detection and false alarm that maximize the SUs' medium access probability for a given probability of channel availability. More parameterization criteria were presented and compared in [Lui+12].

Independently of the criteria rationale, the SUs parameterize the SS technique to ensure that the PUs located in a certain sensing region have a given level of protection. SU's sensing range is usually parameterized to detect the farthest PU that would not tolerate the interference caused when the SU transmits. By doing so, a SU can detect the farthest PU to which the SU may interfere with, and the SU is only granted to access the channel when no PU is detected. However, there are several scenarios where one or more PUs located outside the sensing region can be detected by a SU. In this case a SU cancels its transmission, reducing its performance. This effect of a SU misinterpreting a non-interfering PU was firstly studied in [Han+11], who have named it as the Spatial False Alarm (SFA) problem.

In SFA the characterization of the interference caused by the PUs outside the sensing region is of particular importance. [Chi97; Gul+12; PW10a; PW10b; Win+09] present several analytical approaches to model the aggregate interference in static networks. However, due to the considered assumptions, the aggregate distribution of the interference can not be approximated by a Gaussian distribution, which increases the analytical characterization complexity of the sensing performance.

[Han+11] introduced the SFA problem, showing that it is caused by the deviation of test statistics of the received PU signal and occurs for various sensing techniques. By characterizing the probability of detection of a single PU when it is located inside and outside a defined SU's sensing region, the authors have concluded that it is inevitable that a PU could be sensed by a SU even when located outside the sensing region. The impact of neglecting the SFA problem

in the throughput of a SU is also characterized. The work in [Han+11] was recently extended in [Han+13], where the authors characterize the SU's probability of accessing the channel considering the existence of multiple PUs. From the theoretical analysis the authors derive a general upper and lower bounds of the SU's sensing performance. [Han+11] also shows that the constant false alarm rate criterion, usually employed to parametrize the spectrum sensing, should act on the spatial false alarm probability instead of the conventional false alarm probability. This is due to the fact that multiple PUs may be active outside the sensing region. In this chapter we follow the recommentation in [Han+11], i.e., we consider the spatial false alarm probability to parametrize the spectrum sensing method.

### 4.1.2 Contributions

This chapter characterizes the performance of an ILWN network operating in a shared band where each SU may adopt an SPR or an MPR-based PHY layer. The performance is assessed in terms of the conditional throughput achieved by the SUs. From the point of the view of the SU nodes, the spectrum is always sensed before transmitting. In this way the receiver node can postpone the transmission(s) intended to it when high levels of interference are sensed in the channel. Our work takes into account the number of samples needed to perform the spectrum sensing with a given probability of detection. Additionally to SPR communications assumption, we also consider MPR communications. In the MPR scenario the average number of successful receptions when $n$ SUs' transmissions simultaneous occur is computed by the MPR model proposed in Chapter 3.

The analysis presented in this chapter is particularly focused on the impact of the path loss. This is because the path loss is the major effect related with the spatial interference. Path loss also deeply impacts on the SFA effect and on the MPR performance. We present several results showing the impact of the path loss on the probabilities of detection and false alarm and on the average number of successful receptions and conditional throughput achieved by the SUs.

Apart from the contributions above, this chapter also introduces several contributions related with the methodology proposed to characterize the probabilities of detection and false alarm, as well as the throughput achieved by the SUs. These are summarized as follows:

- A Gaussian approximation is first derived for the distribution of the aggregate interference caused by the PUs located in an annulus and its accuracy is assessed through simulation;

- Considering that the PUs are spatially distributed according to a 2D Poisson point process, and are active with probability $\rho_{ON}$, we derive the SU's probability of detecting and erroneously detecting (false alarm) PU's activity within the sensing region. These probabilities are then used to formulate a solution to parameterize the energy detector decision threshold;

- Using the distribution of the aggregate interference generated within and outside the sensing region to parametrize the decision threshold, we propose an optimization problem to find the minimum number of samples required to meet the PUs' protection level;

- Different results are presented for the probabilities of PUs' detection and false alarm in different propagation scenarios, and considering different number of channel samples. The results presented in this work show that depending on the path loss coefficient and on the number of samples to support the channel's occupancy decision (spectrum sensing), the SFA effect may be attenuated and/or almost neglected;
- In the characterization of the MPR-based PHY layer performance we have considered the aggregate interference caused by the PUs transmitting outside the sensing region.
- Finally, numerical results are provided, which represent an upper bound of the conditional throughput achieved by the ILWN considered in Figure 4.1, where each SU is equipped with a single radio capable of performing spectrum sensing. The bound captures the impact of the SFA on the spectrum sensing detection probability, and on the interference caused to the MPR communication process by the PUs located outside the sensing region.

### Chapter Contents

- **Section 4.2**: This section introduces the ILWN network and the basic concepts associated with the communication process of the SUs, including the needs to support the spectrum sensing;
- **Section 4.3**: Multiple aspects of the spectrum sensing are derived here. The amplitude of the aggregate interference of the PUs located outside the sensing area is studied in Subsection 4.3.1. The amplitude of the aggregate interference is used in Subsection 4.3.2 to derive the spectrum sensing detection and false alarm probabilities. The parametrization of the spectrum sensing decision threshold is finally addressed in Subsection 4.3.3;
- **Section 4.4**: This section characterizes the performance of an MPR-based PHY layer adopted by the considered ILWN where nodes also adopt the spectrum sensing studied in Subsection 4.3.
- **Section 4.5**: Describes the evaluation of the proposed methodology through the comparison of numerical and simulated results. These include different comparisons related with the spectrum sensing process and the ILWN's conditional throughput;
- **Section 4.6**: Ends the chapter by providing final remarks.

## 4.2 System Description

The chapter considers the coexistence of two wireless networks as illustrated in Figure 4.1, which share the same channel. One of the wireless networks is composed by PUs, which act as interferers to the SUs' communications. This network is named primary network. The other wireless network is seen as the network of interest formed by SUs, which opportunistically access the channel in the absence of PUs. This network is named secondary network.

Regarding the secondary network, we consider that $n^{SU}$ $\mathrm{SU_{Tx}}$ nodes take advantage of the MPR-based PHY layer to transmit data simultaneously to a single SU (the receiver $\mathrm{SU_{Rx}}$), as represented in Figure 4.1. The $\mathrm{SU_{Rx}}$ have a given range of sensing, which is limited by the radius $R_G$. Within the sensing region $\mathcal{A}_{in}$, with area $A_{in} = \pi(R_G)^2$ (white zone in the figure), an active PU must be detected with a given probability $P_D$ to guarantee that the receiver node $\mathrm{SU_{Rx}}$ avoids communicating when the interference level is high. Simultaneously, the other SU nodes guarantee a certain level of protection to the PUs. PUs are also located outside the sensing region (gray zone), causing interference to the SUs sensing the spectrum.

Each PU and SU is equipped with an omni-directional antenna and the PUs share the same frequency band. Time is divided into equal size slots, which are grouped into frames.

Single radio SUs are considered, meaning that SUs are equipped with a single transceiver. Therefore, the SUs are unable to sense and transmit simultaneously. Due to this limitation, SUs adopt an operation cycle where sensing and transmission operations occur in a consecutive manner. $\mathrm{SU_{Rx}}$ start to sense the spectrum during a fixed amount of time (sensing period) and, depending on the output of the sensing, the SUs wiling to transmit are allowed to jointly transmit in the sensed band during a fixed amount of time (transmission period). SUs repeat the operation cycle periodically to minimize the amount of interference caused to PUs and mitigate the interference caused to SUs. In this way, each SU may access the channel opportunistically, when one or more PUs do not use the channel, as considered in [Lui+13]. SUs adopt an EBS technique. SU's sensing and transmitting period durations are denoted by $T_S^{SU}$ and $T_D^{SU}$, respectively, as illustrated in Figure 4.2. Without loss of generality, we assume that all SUs are synchronized.

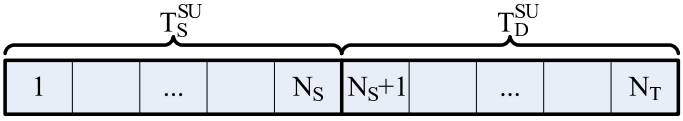


Figure 4.2: SU's time frame structure.

The time frame of the SUs is divided into $N_T$ slots where each slot duration is given by the channel sampling period adopted by the energy detector. The first $N_S$ slots are allocated to the spectrum sensing task (for channel sampling) and the remaining ones ($N_S + 1$ to $N_T$) are used to access the channel (for transmission, whenever possible).

The PUs are distributed within a certain area $A^{PU} = \pi(R_E)^2$ encircling the SU transmitter. The number of PUs is represented by a RV $X_l^{PU}$. In this work it is considered that the PUs are distributed according to a 2D Poisson point process, with distribution,

$$\mathrm{P}[X_l^{PU} = x] = \frac{(\rho_{ON}\tau^{PU}A_l)^x}{x!}e^{-\rho_{ON}\tau^{PU}A_l}, x = 0, 1, ..., \tag{4.1}$$

where $\tau^{PU}$ is the PU's spatial density, $\rho_{ON}$ is the probability of finding a PU active and $A_l$ represents the area where the PUs are distributed (e.g., for the total area where the PUs are distributed $A_l = A^{PU}$).

Regarding the spatial distribution of the SUs, we consider the presence of $n^{SU}$ SUs uniformly distributed within the area $A_{in} = \pi(R_G)^2$ encircling the receiver (considered in the PDF (3.6)

presented in the previous chapter). The power received by the node $SU_{Rx}$ from the $k$-th SU's transmitter, $P_k^{SU}$, is given by

$$P_k^{SU} = P_T^{SU} \Psi_k \left(R_k^l\right)^{-\alpha}, \tag{4.2}$$

where $P_T^{SU}$ is a constant representing the transmitted power adopted by all SUs, and no power control is applied. $\Psi_k$ is a RV that represents the fading observed in the channel between the receiver and the $k$-th SU. The RV $R_k^l$ represents the distance between the $k$-th SU's transmitter and the receiver, and $\alpha$ is the path loss coefficient. Similarly, the power received by the node $SU_{Rx}$ from the $k$-th PU, $P_k^{PU}$, is given by

$$P_k^{PU} = P_T^{PU} \Psi_k \left(R_k^l\right)^{-\alpha}, \tag{4.3}$$

where the transmitting power $P_T^{PU}$ is constant and no power control is applied. In this chapter it is assumed deterministic fading ($\Psi_k = 1$). The PDF of $R_k^l$ in both (4.2) and (4.3) follows a uniform distribution as defined in (3.6).

## 4.3 Spectrum Sensing

As described in [Han+11] and [Han+13], the SFA problem is due to the interference caused by the PUs located outside the sensing region, which may be erroneously detected as being active when no active PU is within the sensing region. The spectrum sensing should reflect the activity detected within the sensing region. Consequently, the SFA effect represents an abnormal sensing situation. Because EBS is assumed, the characterization of the interference caused by multiple PUs located outside a desired sensing region is of particular importance. In this way, this section characterizes the aggregate power received by a SU ($SU_{Rx}$) from the PUs located within a given annulus. While the proposed method can be generalized for any circular annulus, the annulus considered in the approach is the outer circular annulus illustrated in Figure 4.1 (gray ring). The PUs located in this annulus are outside the sensing region, and because of that, these are denoted as interferers. Following the same rationale, the aggregate power received from these nodes is denoted as interference.

### 4.3.1 Amplitude of the Aggregate Interference

The $SU_{Rx}$ performing the sensing task only aims at detecting the PUs inside the sensing region $\mathcal{A}_{in}$. The PUs located outside the sensing region are said to be located in the interference region, represented by the area given by $A_{out} = \pi\left((R_E)^2 - (R_G)^2\right)$, since they may interfere with the sensing performed by the SU. This subsection characterizes the envelope signal of the aggregate interference observed at the receiver $SU_{Rx}$ when PU nodes located within the area $A_l = \pi\left((R_E)^2 - (R_G)^2\right)$ are transmitting. The aggregate interference power received at the SU performing the sensing is expressed by

$$I_l^{PU} = \sum_{k=1}^{n^{PU}} P_k^{PU}, \tag{4.4}$$

where $P_k^{PU}$ is the interference caused by the $k$-th PU, (4.3). $n^{PU}$ is a RV that represents the total number of PUs located in the area $A_l$ and is distributed according to (4.1).

In Subsection 3.4.1 the total interference power caused by nodes located within an annulus $l$ is approximated through a Gamma distribution. Likewise, the interference caused by multiple PU nodes located within a area $A_l$ can be approximated by a Gamma distribution. Therefore, the parameters of the Gamma distribution are obtained by employing a moment matching method, [AAY10]. As in Subsection 3.4.1, the shape and the scale parameters of the Gamma distribution that characterizes the aggregate interference caused by the transmitters located within a area $A_l$ are respectively given by

$$\begin{aligned} k_l^{PU} &\approx \frac{\mathrm{E}_{I^{PU}}[I_l^{PU}]^2}{\mathrm{Var}_{I_l^{PU}}[I_l^{PU}]}, \\ \theta_l^{PU} &\approx \frac{\mathrm{Var}_{I_l^{PU}}[I_l^{PU}]}{\mathrm{E}_{I_l^{PU}}[I_l^{PU}]}. \end{aligned} \tag{4.5}$$

Since $X_l^{PU}$ follows a Poisson distribution, its expected value and variance are given by [PP02]

$$\mathrm{E}_{X_l^{PU}}\left[X_l^{PU}\right] = \mathrm{Var}_{X_l^{PU}}\left[X_l^{PU}\right] = \rho_{ON}\tau^{PU}A_l. \tag{4.6}$$

By using (3.63) and (4.6), the expected value of the aggregate power is given by

$$\begin{aligned} \mathrm{E}_{I_l^{PU}}[I_l^{PU}] &= \mathrm{E}_{X_l^{PU}}\left[X_l^{PU}\right]\mathrm{E}_{P_k^{PU}}\left[P_k^{PU}\right] \\ &= \rho_{ON}\tau^{PU}A_l\frac{\partial M^l_{P_k^{PU}}(0)}{\partial s}, \end{aligned} \tag{4.7}$$

and, using (3.64) and (4.6), the variance of the aggregate power is given as follows

$$\begin{aligned} \mathrm{Var}_{I_l^{PU}}[I_l^{PU}] &= \mathrm{E}_{X_l^{PU}}\left[X_l^{PU}\right]\mathrm{E}_{P_k^{PU}}\left[\left(P_k^{PU}\right)^2\right] \\ &= \rho_{ON}\tau^{PU}A_l\frac{\partial^2 M^l_{P_k^{PU}}(0)}{\partial s^2}. \end{aligned} \tag{4.8}$$

$M^l_{P_k^{PU}}(s)$ represents the MGF of $P_k^{PU}$, the power received from the $k$-th PU interferer located within the area $A_l$, given by

$$M^l_{P_k^{PU}}(s) = \mathrm{E}_{P_k^{PU}}[e^{sP_k^{PU}}]. \tag{4.9}$$

Using (4.3) and the PDF of the PU's spatial distribution, (3.6), (4.9) is rewritten as follows

$$M^l_{P_k^{PU}}(s) = \int_{R_G}^{R_E} e^{sP_k^{PU}} f_{R_k^l}(r)\,\mathrm{d}r. \tag{4.10}$$

By using the CF of the individual power for the far-field scenario derived in Subsection 3.2.2, and knowing that for a RV $X$ the MGF can be obtained from its CF, i.e. $M_X(s) = \varphi_X(-is)$, (4.10) can be written as follows

$$M^l_{P_k^{PU}}(s) = \frac{2}{\alpha\left({R_E}^2 - {R_G}^2\right)}\left[{R_E}^2\mathrm{Ei}\left(1+\frac{2}{\alpha}, -sP_T^{PU}{R_E}^{-\alpha}\right) - {R_G}^2\mathrm{Ei}\left(1+\frac{2}{\alpha}, -sP_T^{PU}{R_G}^{-\alpha}\right)\right]. \tag{4.11}$$

Note that (4.11) is obtained from (3.26) with $t = -is$ and $x = 1$ since only path loss effect is considered.

Using (4.11), $\mathrm{E}_{I^{PU}}[I^{PU}]$ in (4.7) and $\mathrm{Var}_{I^{PU}}[I^{PU}]$ in (4.8) are given as follow

$$\begin{aligned}\mathrm{E}_{I_l^{PU}}[I_l^{PU}] &= 2\pi\rho_{ON}\tau^{PU}P_T^{PU}\left(\frac{R_E^{2-\alpha}-R_G^{2-\alpha}}{2-\alpha}\right),\\ \mathrm{Var}_{I_l^{PU}}[I_l^{PU}] &= \pi\rho_{ON}\tau^{PU}{P_T^{PU}}^2\left(\frac{R_E^{2-2\alpha}-R_G^{2-2\alpha}}{1-\alpha}\right).\end{aligned} \tag{4.12}$$

By knowing $\mathrm{E}_{I_l^{PU}}[I_l^{PU}]$ and $\mathrm{Var}_{I_l^{PU}}[I_l^{PU}]$ the shape and the scale parameters of the Gamma distribution in (4.5) can be derived. The Gamma distribution represents the aggregate interference power received by $\mathrm{SU_{Rx}}$ from the PUs located within the area $A_I$. The envelope signal (amplitude) of the aggregate interference, $s_l^{PU}$, is given by the square root of a Gamma distributed RV, which is given by a Generalized Gamma distribution with the following parameters [Wal96],

$$f_{s_l^{PU}}(x) \approx \frac{2/a^d x^{(d-1)}e^{-\frac{x}{a}^2}}{\Gamma(d/2)}, \tag{4.13}$$

where $a$, $d$ are given by $\sqrt{\theta_l^{PU}}$ and $2k_l^{PU}$ respectively.

Since a Gamma distribution, with shape $k_l^{PU}$ and scale $\theta_l^{PU}$, is the sum of $k_l^{PU}$ Exponential$(1/\theta_l^{PU})$ distributions, using the CLT, when $k_l^{PU}$ is large, the Generalized Gamma distribution can be approximated by a Normal distribution [Joh+94]. In these conditions the amplitude of the aggregate interference can be also approximated by a Normal distribution represented by

$$s_l^{PU} \sim \mathcal{N}\left(\sqrt{\theta_l^{PU}}\frac{\Gamma(k_l^{PU}+1/2)}{\Gamma(k_l^{PU})}, \theta_l^{PU}\left(\frac{\Gamma(k_l^{PU}+1)}{\Gamma(k_l^{PU})} - \frac{\Gamma(k_l^{PU}+1/2)^2}{\Gamma(k_l^{PU})^2}\right)\right). \tag{4.14}$$

The amplitude of the aggregate interference can be approximated by a Normal distribution when the number of PUs is enough to observe the CLT conditions and the considered $R_G$ value is according to the far-field scenario.

### 4.3.2 Detection and False Alarm Probabilities

The interference formulation presented in the previous subsection is now used to characterize the probabilities of detection and false alarm. Since the amplitude of the interference caused by several PUs outside the sensing region is approximated by a Gaussian distribution when deterministic fading is assumed, the traditional binary hypothesis testing can be employed to detect the activity of the PUs within the sensing region. The hypothesis testing was used in several works (e.g [GS07; Kos02; Lui+13; Tan05]) by considering the hypotheses of only observing noise or signal plus noise to indicate a vacant channel or an occupied channel, respectively. In this subsection we follow the same methodology but considering different hypotheses. Due to the interference caused by the PUs located outside the sensing region, a channel is now considered vacant when only noise and a given amount of interference generated by PUs located outside the sensing region is observed; or a channel is declared occupied when in addition to noise and to the interference generated outside the sensing region, the PUs within the sensing region become active.

To distinguish between occupied and vacant spectrum bands, SUs sample the channel during the sensing period $T_S^{SU}$, and for the $N_S$ samples two hypotheses can be distinguished

$$\begin{aligned} &\mathcal{H}_0 : s_{rec}(m) = w(m) + s_{out}^{PU}(m) && m = 1, 2, ..., N_S, \\ &\mathcal{H}_1 : s_{rec}(m) = w(m) + s_{out}^{PU}(m) + s_{in}^{PU}(m) && m = 1, 2, ..., N_S, \end{aligned} \tag{4.15}$$

where $s_{rec}(m)$ is a RV representing the signal received by $\mathrm{SU_{Rx}}$.

The first condition, $\mathcal{H}_0$, represents the hypothesis corresponding to the absence of PUs inside the sensing region, while the second condition, $\mathcal{H}_1$, indicates the occurrence of PUs' activity within the sensing region. $s_{out}^{PU}(m)$ and $s_{in}^{PU}(m)$ are RVs that represent the amplitude of the aggregate interference caused by PUs located outside and within the sensing region, i.e., the aggregate interference generated by the PUs located within the areas $A_{out} = \pi({R_E}^2 - {R_G}^2)$ and $A_{in} = \pi {R_G}^2$, respectively. As shown in the Subsection 4.3.1, $s_{out}^{PU}(m)$ and $s_{in}^{PU}(m)$ may be approximated by Normal RVs as in (4.14). The mean and variance of $s_{in}^{PU}(m)$ and $s_{out}^{PU}(m)$ are respectively denoted by $\mu_{in}$, $\sigma_{in}^2$ and $\mu_{out}$, $\sigma_{out}^2$. $w(m)$ is assumed to be a zero-mean AWGN with unit variance ($\sigma_{N_0}^2 = 1$), *i.e.*, $w(m) = \mathcal{N}(0, 1)$. $m$ represents the sample index.

EBS relies on the classical energy detector [Urk67]. During the detection period ($T_S^{SU}$), the receiver $\mathrm{SU_{Rx}}$ determines the amount of energy received in $N_S$ samples, given by

$$Y_S = \sum_{m=1}^{N_S} |s_{rec}(m)|^2, \tag{4.16}$$

and compares it with the energy threshold $\eta$ to decide whether a PU is detected in the sensing region.

In order to apply the CLT, the variance of the RV $S_{rec}$ is normalized, i.e., $S_{rec}^{'} = S_{rec}/\sigma_{rec}$ is considered instead of $S_{rec}$, where $\sigma_{rec}$ is the standard deviation of the RV $S_{rec}$ and is represented by

$$\sigma_{rec} = \begin{cases} \sigma_{\mathcal{H}_0} = \sqrt{\sigma_{out}^2 + 1}, & \mathcal{H}_0, \\ \sigma_{\mathcal{H}_1} = \sqrt{\sigma_{out}^2 + \sigma_{in}^2 + 1}, & \mathcal{H}_1. \end{cases} \tag{4.17}$$

Consequently, $S_{rec}^{'}$ is distributed according to the following Normal distribution,

$$S_{rec}^{'} \sim \begin{cases} \mathcal{N}\left(\dfrac{\mu_{out}}{\sqrt{\sigma_{out}^2 + 1}}, 1\right), & \mathcal{H}_0, \\ \mathcal{N}\left(\dfrac{\mu_{out} + \mu_{in}}{\sqrt{\sigma_{out}^2 + \sigma_{in}^2 + 1}}, 1\right), & \mathcal{H}_1. \end{cases} \tag{4.18}$$

$Y_S^{'}$ is introduced to denote the amount of energy received in $N_S$ samples when the normalized variable ($S_{rec}^{'}$) is assumed. Under the hypotheses $\mathcal{H}_0$ and $\mathcal{H}_1$, $Y_S^{'}$ follows a non-central Chi-square

distribution with $N_S$ degrees of freedom, and a non centrality parameter $\lambda_S$ [PP02], represented by

$$\lambda_S = \begin{cases} \lambda_{\mathcal{H}_0} = N_S \left( \dfrac{\mu_{out}}{\sqrt{1+\sigma_{out}^2}} \right)^2, & \mathcal{H}_0, \\ \lambda_{\mathcal{H}_1} = N_S \left( \dfrac{\mu_{out}+\mu_{in}}{\sqrt{1+\sigma_{out}^2+\sigma_{in}^2}} \right)^2, & \mathcal{H}_1. \end{cases} \tag{4.19}$$

When the number of samples $N_S$ is large enough, it is possible to use the CLT to approximate the Chi-square distribution to a Gaussian distribution [Tan05], as follows

$$Y_S^{'} \sim \begin{cases} \mathcal{N}\left(N_S + \lambda_{\mathcal{H}_0}, 2(N_S + 2\lambda_{\mathcal{H}_0})\right), & \mathcal{H}_0, \\ \mathcal{N}\left(N_S + \lambda_{\mathcal{H}_1}, 2(N_S + 2\lambda_{\mathcal{H}_1})\right), & \mathcal{H}_1. \end{cases} \tag{4.20}$$

Since we have considered $S_{rec}^{'}$ instead of $S_{rec}$, the RV $Y_S$ is obtained as follows

$$Y_S = \sum_{m=1}^{N_S} S_{rec}^2 = \sigma_{rec}^2 Y_S^{'}. \tag{4.21}$$

Consequently, $Y_S$ can be approximated by the following Normal distribution

$$Y_S \sim \begin{cases} \mathcal{N}\left(\sigma_{\mathcal{H}_0}^2(N_S + \lambda_{\mathcal{H}_0}), 2\sigma_{\mathcal{H}_0}^4(N_S + 2\lambda_{\mathcal{H}_0})\right), & \mathcal{H}_0, \\ \mathcal{N}\left(\sigma_{\mathcal{H}_1}^2(N_S + \lambda_{\mathcal{H}_1}), 2\sigma_{\mathcal{H}_1}^4(N_S + 2\lambda_{\mathcal{H}_1})\right), & \mathcal{H}_1. \end{cases} \tag{4.22}$$

Therefore, for a SU, the probabilities of detection ($P_D$) and false alarm ($P_{FA}$) are represented by

$$P_{FA} = \mathbb{Q}\left( \frac{\eta - (N_S + \lambda_{\mathcal{H}_0})\sigma_{\mathcal{H}_0}^2}{\sqrt{(2N_S + 4\lambda_{\mathcal{H}_0})\sigma_{\mathcal{H}_0}^4}} \right), \tag{4.23}$$

and

$$P_D = \mathbb{Q}\left( \frac{\eta - (N_S + \lambda_{\mathcal{H}_1})\sigma_{\mathcal{H}_1}^2}{\sqrt{(2N_S + 4\lambda_{\mathcal{H}_1})\sigma_{\mathcal{H}_1}^4}} \right), \tag{4.24}$$

where $\mathbb{Q}(x) = \frac{1}{\sqrt{2\pi}} \int_x^\infty e^{-\frac{u^2}{2}} du$ is the complementary distribution function of the standard Normal. By observing (4.23) and (4.24) we can see that $P_{FA}$ and $P_D$ depend on the number of samples ($N_S$), the energy threshold ($\eta$), and the mean and variance of the aggregate interference caused by the PUs located within and outside the sensing region.

### 4.3.3 Spectrum Sensing Decision Threshold

This subsection introduces a simple criterion to parameterize the energy detector threshold in order to guarantee a level of protection to the PUs located within the sensing region and, consequently avoid SUs transmissions to occur. The rationale behind the parameterization criterion is to define

an energy threshold that takes into account the case when the average of the received energy can be generated by both PUs located within and outside the sensing region ($\Theta_{\mathcal{H}_1}$) or only generated by PUs located outside the sensing region ($\Theta_{\mathcal{H}_0}$).

Under the hypotheses $\mathcal{H}_0$ and $\mathcal{H}_1$, the expectation of the total energy collected during the $N_S$ samples ($Y_S$) is given by (4.22). Following (4.22), the average of the energy received by a $\mathrm{SU_{Rx}}$ due to the transmissions of the PUs located within the sensing region is given by

$$\Theta_{\mathcal{H}_1} = \left(N_S + \lambda_{\mathcal{H}_1}\right)\sigma^2_{\mathcal{H}_1}. \tag{4.25}$$

Similarly, when the received energy is only generated by PUs outside the sensing region, its average is given by

$$\Theta_{\mathcal{H}_0} = \left(N_S + \lambda_{\mathcal{H}_0}\right)\sigma^2_{\mathcal{H}_0}. \tag{4.26}$$

Taking into account the received energy in both cases, the decision threshold ($\eta$) can be simply defined as being located in the middle of the two averages $\Theta_{\mathcal{H}_1}$ and $\Theta_{\mathcal{H}_0}$, i.e,

$$\eta = \frac{\Theta_{\mathcal{H}_1} + \Theta_{\mathcal{H}_0}}{2}. \tag{4.27}$$

The decision threshold adopted in the following criterion defines the minimum number of samples ($N_S^*$) that guarantees a required level of protection to the PUs,

$$\begin{aligned} N_S^* = \quad & \min N_S \\ \text{s.t.} \quad & \\ & P_D = \chi, \\ & N_S > 2WT_S^{SU}, \\ & \eta = \frac{\Theta_{\mathcal{H}_1} + \Theta_{\mathcal{H}_0}}{2}, \end{aligned} \tag{4.28}$$

where $N_S^*$ is the minimum number of samples to obtain the expected level of protection $\chi$. The constraint $N_S > 2WT_S^{SU}$ imposes the Nyquist sampling rate ($W$ represents the bandwidth of the sensed band).

## 4.4 ILWNs Performance in Shared Channels

In this section we characterize the performance of the SU's MPR-based PHY layer and the throughput of the considered ILWN. The PHY layer with MPR capabilities of the SUs is characterized by the individual probability of successful reception and the average number of received packets when $n^{SU}$ simultaneous transmissions occur.

### 4.4.1 Probability of Successful Packet Reception

Taking into account the SUs' operation cycle, we highlight that the SUs start to sense the spectrum during a fixed amount of time $T_S^{SU}$ and can transmit in the sensed band during a fixed amount of time $T_D^{SU}$. In this section we consider that the receiver $\mathrm{SU_{Rx}}$ decides if the transmitters can

proceed or postpone their transmission according to the spectrum sensing outcome. Moreover, we assume that during the transmission period $T_D^{SU}$ no PUs' transmission occur within the sensing region when SUs transmitters communicate with the receiver $\mathrm{SU_{Rx}}$. This assumption represents the best performance scenario, when SUs' transmission is not suffering interference from the PUs located within the sensing region.

As assumed in Section 3.2, the power of the signals is considered as being i.i.d. RVs. The total interference power received at the $\mathrm{SU_{Rx}}$ regarding the transmissions of the PUs located outside the sensing region is expressed by

$$I_{out}^{PU} = \sum_{k=1}^{n^{PU}} P_k^{PU}, \tag{4.29}$$

where $P_k^{PU}$ is the RV representing the power received from one of the $n^{PU}$ PU interferers.

The total aggregate power received from the multiple transmissions is given by

$$\Lambda^{SU} = N_0 + I_{out}^{PU} + \sum_{k=1}^{n^{SU}} P_k^{SU}, \tag{4.30}$$

where $P_k^{SU}$ is the RV representing the power received from one of the $n^{SU}$ SU transmissions. $N_0$ is a RV representing the noise power at the receiver.

Considering (4.30), the SINR associated to the signal received from SU node $j$ is defined by

$$\gamma_j^{SU} = \frac{P_j^{SU}}{\Lambda^{SU} - P_j^{SU}}. \tag{4.31}$$

Starting from the capture condition of the MPR receiver defined in (3.3), and using (4.31), the necessary condition for successful reception of the signal from node $j$ is given as

$$P_j^{SU} > b'\Lambda^{SU}. \tag{4.32}$$

where $b' = \frac{b}{b+1}$.

From (4.32), the probability of successful reception may be written as follows

$$\mathrm{P}_{S_3} = 1 - \mathrm{P}[P_j^{SU} - b'\Lambda^{SU} \leq 0]. \tag{4.33}$$

Considering the auxiliary RV $\beta_1 = P_j - b'\Lambda^{SU}$, and using (4.30), it follows

$$\beta_1 = \frac{P_j^{SU}}{b+1} - b' \sum_{k=1, k\neq j}^{n^{SU}} P_k^{SU} - b' I_{out}^{PU} - b' N_0, \tag{4.34}$$

and the CF of $\beta_1$ is given by

$$\varphi_{\beta_1}(t) = \varphi_{P_j^{SU}}\left(\frac{t}{b+1}\right) \cdot \prod_{k=1, k\neq j}^{n^{SU}} \varphi_{P_k^{SU}}(-b't) \cdot \varphi_{I_{out}^{PU}}(-b't) \cdot \varphi_{N_0}(-b't). \tag{4.35}$$

$\varphi_{\beta_1}(t)$ in (4.35) is similar to $\varphi_{\beta}(t)$ in (3.35). The CF $\varphi_{N_0}(t)$ is defined in (3.10). $\varphi_{P_j^{SU}}(t)$ corresponds to the CF of the the individual power when only path loss effect is considered. That is, $\varphi_{P_j^{SU}}(t)$ is obtained using (3.16) with $x = 1$ and is given as follows

$$\varphi_{P_j^{SU}}(t) = \varphi_{P_k^{SU}}(t) = \frac{2}{\alpha (R_G)^2} \left[(1+R_G)^2 \mathrm{Ei}\left(1+\frac{2}{\alpha}, -itP_T^{SU}(R_G+1)^{-\alpha}\right) - \mathrm{Ei}\left(1+\frac{2}{\alpha}, -itP_T^{SU}\right) - -(1+R_G)\mathrm{Ei}\left(1+\frac{1}{\alpha}, -itP_T^{SU}(R_G+1)^{-\alpha}\right) + \mathrm{Ei}\left(1+\frac{1}{\alpha}, -itP_T^{SU}\right)\right]. \tag{4.36}$$

By assuming that each individual power $P_k^{SU}$ is i.i.d., the PDF of the aggregate power given a total of $n^{SU}$ active transmitters is the convolution of the PDFs of each $P_k^{SU}$. Thereby, the CF of the SUs' aggregate power is given by

$$\prod_{k=1, k\neq j}^{n^{SU}} \varphi_{P_k^{SU}}(t) = \left(\varphi_{P_k^{SU}}(t)\right)^{n^{SU}-1}. \tag{4.37}$$

The CF of the aggregate interference power caused by PU located outside of the sensing region, $\varphi_{I_{out}^{PU}}(t)$, is characterized by the Gamma approximation described in Subsection 4.3.1 and is given as

$$\varphi_{I_{out}^{PU}}(t) = \left(1 - \theta_{out}^{PU} it\right)^{-k_{out}^{PU}}, \tag{4.38}$$

where $k_{out}^{PU}$ and $\theta_{out}^{PU}$ are the shape and the scale parameters of the Gamma distribution, respectively, which are defined in (4.5).

The distribution $f_{\beta_1}(x)$ in (4.35), can be obtained by the inverse CF, as follows

$$f_{\beta_1}(x) = \frac{1}{2\pi} \int_{-\infty}^{\infty} \mathrm{e}^{-ixt} \varphi_{\beta_1}(t)\, \mathrm{d}t. \tag{4.39}$$

From (4.33), the probability of successful packet reception can be written as

$$\mathrm{P}_{S_3} = 1 - \mathrm{P}[\beta_1 \leq 0], \tag{4.40}$$

and, using (4.39) and (4.35), we obtain

$$\mathrm{P}_{S_3} = 1 - \int_{-\infty}^{0} \frac{1}{2\pi} \int_{-\infty}^{\infty} \mathrm{e}^{-ixt} \varphi_{P_j}(t) \cdot \varphi_{P_k^{SU}}(-bt)^{(n^{SU}-1)} \cdot \varphi_{I_{out}^{PU}}(-bt) \cdot \varphi_{N_0}(-bt)\, \mathrm{d}t \mathrm{d}x. \tag{4.41}$$

Finally, the average number of received packets ($E_{\mathrm{rcv}_3}$) is approximated by

$$E_{\mathrm{rcv}_3} \approx n^{SU} \cdot \mathrm{P}_{S_3}. \tag{4.42}$$

### 4.4.2 Conditional Throughput

The performance of the ILWN with MPR capability is characterized in this subsection. In this case, the definition of the average number of nodes successfully transmitting packets during the transmission period depends on the MPR-based PHY layer performance and on the EBS performance, as EBS influences the access of the SUs during the transmission stage.

The throughput achieved by the $SU_{Rx}$ located in the center of the sensing region (as illustrated in Figure 4.1) is represented by the effective usage of the channel during the transmission period $T_D^{SU}$ when the energy detector correctly identifies a transmission opportunity with probability $1 - P_{FA}$ and with an average number of received packets of $E_{\text{rcv}_3}$ given $n^{SU}$ transmissions.

Consequently, the utilization of the channel by the $SU_{Rx}$ lasts on average $T_D^{SU}(1-P_{FA})$ when no activity of PUs is sensed within the sensing region. Considering Figure 4.2, a SU senses the channel during a $T_S^{SU}$ period followed by a transmission period $T_D^{SU}$. Hence, the conditional throughput achieved by a SU, given that no PU is active within the sensing region, is defined as the ratio between the expected utilization of the channel during the transmitting period ($T_D^{SU}(1-P_{FA})E_{\text{rcv}_3}$) and the frame's duration ($T_S^{SU} + T_D^{SU}$). Thus, the conditional throughput is defined as follows

$$S^{SU} = \frac{T_D^{SU}(1-P_{FA})E_{\text{rcv}_3}}{T_S^{SU} + T_D^{SU}}. \tag{4.43}$$

## 4.5 Performance Analysis

This section describes a set of simulations and numerical results to validate the aggregate interference approximation described in Subsection 4.3.1, as well as the probabilities of detection and false alarm proposed in (4.23) and (4.24). Subsection 4.5.3 presents simulation results that shows the impact of considering fading channels in the characterization of the interference. Subsection 4.5.4 evaluates the proposed criterion to parameterize the energy detector threshold. Finally, the impact of the spectrum sensing performance on the MPR PHY layer's throughput is studied in Subsection 4.5.5.

### 4.5.1 Validation of the Aggregate Interference Distribution

We have considered a scenario formed by a network of PUs distributed according to a 2D Poisson point process and a single SU, $SU_{Rx}$, as illustrated in Figure 4.1. The spectrum sensing is performed by the $SU_{Rx}$ node. Figure 4.3 illustrates the CDF of the aggregate interference caused by the PUs positioned within an annulus with area $A = \pi\left((R_E)^2 - (R_G)^2\right)$, for different values of $\tau^{PU}$. The curve identified as "Simu." represents the data obtained through simulations, while Gamma and Normal approximations were obtained by computing the distributions (4.13) and (4.14).

The Generalized Gamma and Normal approximations in Figure 4.3 are close enough to the aggregate interference obtained through simulation. It is observed that for higher densities ($\tau^{PU}$), the Normal approximation leads to more accurate results due to the fact that a higher density of PUs is considered, which increases the accuracy of the CLT assumption. As can be seen from the figure, the aggregate interference can be successfully approximated by the methodology proposed in Subsection 4.3.1 and the Generalized Gamma distribution parameterized with the parameters in (4.13) approximates the aggregate interference for different density values.

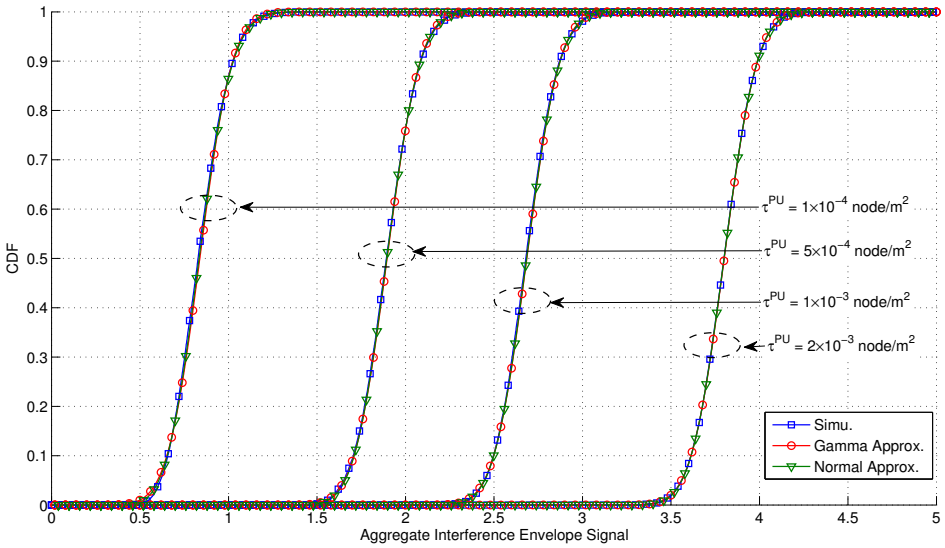


Figure 4.3: CDF of the aggregate interference amplitude and the Generalized Gamma and Normal approximations for different values of $\tau^{PU}$ ($P_T^{PU} = 30$ dB, $\rho_{ON} = 0.5$, $R_G = 50$ m, $R_E = 500$ m and $\alpha = 2$).

### 4.5.2 Validation of $P_D$ and $P_{FA}$

This subsection compares the theoretical results obtained with (4.23) and (4.24) with simulation results. Departing from the same simulation scenario described in Subsection 4.5.1, we consider that the $\text{SU}_{\text{Rx}}$ is equipped with an energy detector. As seen in the previous subsection the amplitude of the aggregate interference is approximated by a Normal distribution. The approximation is valid assuming a far-field scenario. In the results presented hereafter we have considered that the individual distance between each PU transmitter and the SU receiver was randomly chosen using a uniform distribution in the interval $[5\text{ m}, R_E]$.

Figures 4.4 and 4.5 illustrate the theoretical probabilities of detection and false alarm along with the simulation for different values of PU's transmission power ($P_T^{PU} = 20$ dB and $P_T^{PU} = 30$ dB). As shown in both figures, the theoretical probabilities of detection and false alarm are successfully validated by the simulation results. In Figure 4.4 we observe that due to the lower transmission power (20 dB) adopted by the PUs and number of sensing samples, $N_S$, $P_D$ and $P_{FA}$ curves are close to each other, meaning that the energy detector can not operate near the optimal point of operation, where $P_D \approx 1$ and $P_{FA} \approx 0$. Figure 4.5 plots the same curves for better operation conditions of the energy detector, i.e. $P_T^{PU} = 30$ dB. In this case the descending zone of $P_{FA}$ and $P_D$ are more distant, meaning that the optimal operating region was extended when compared to the case when $P_T^{PU} = 20$ dB.

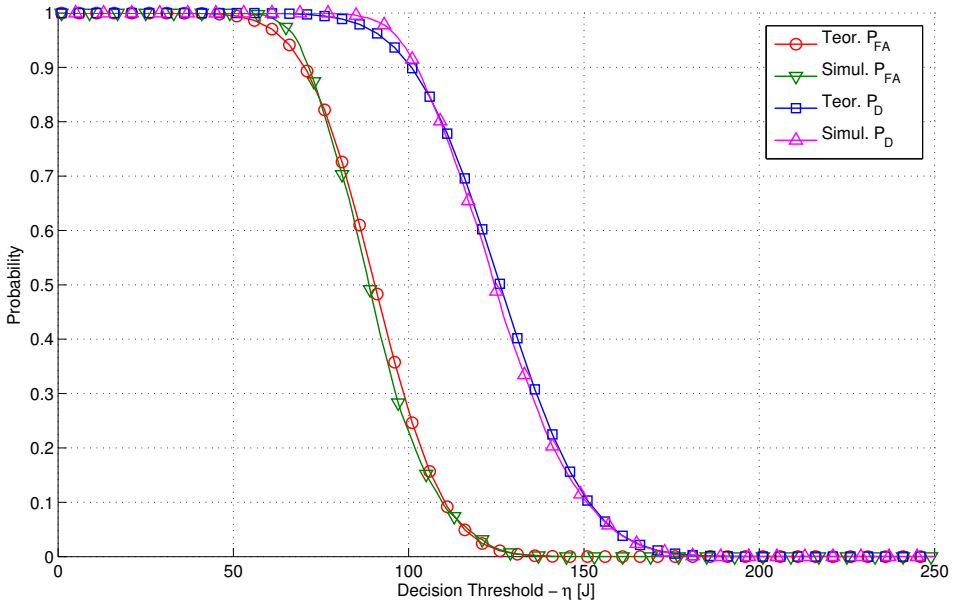


Figure 4.4: $P_D$, $P_{FA}$ for different thresholds $\eta$ ($P_T^{PU} = 20$ dB, $\rho_{ON} = 0.5$, $\tau^{PU} = 0.001$ node/m$^2$, $N_S = 60$ samples, $R_G = 100$ m, $R_E = 500$ m).

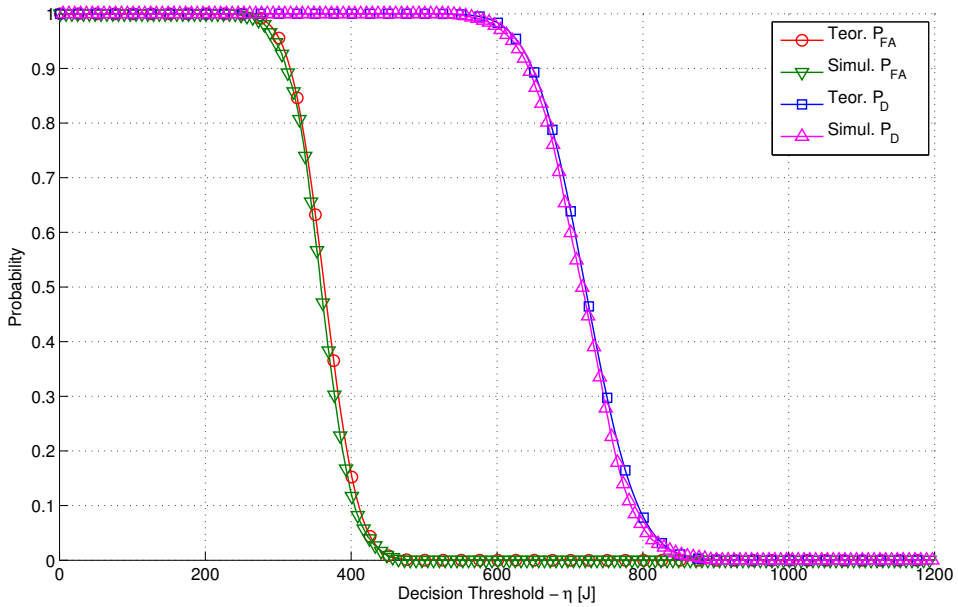


Figure 4.5: $P_D$, $P_{FA}$ for different thresholds $\eta$ ($P_T^{PU} = 30$ dB, $\rho_{ON} = 0.5$, $\tau^{PU} = 0.001$ node/m$^2$, $N_S = 60$ samples, $R_G = 100$ m, $R_E = 500$ m).

### 4.5.3 Impact of Fading Channels

The results presented in the previous subsection only assume path loss as the main cause of PUs' signal attenuation, neglecting the effects of fading channels. This section evaluates the impact of assuming fading effects.

When SFA is considered, the sensing parameterization achieves the required detection probability by increasing the number of samples ($N_S$), which allows the assumption of the CLT in (4.22). In this way the two Gaussian distributions representing the signal $s_{rec}(n)$ in hypotheses $\mathscr{H}_0$ and $\mathscr{H}_1$ are farther apart (they overlap very little). By increasing $N_S$, the impact of the fading channel in the probabilities of detection and false alarm is marginal when the fading samples are i.i.d. (as considered in [Dig+07; Her+11; Kos02; Sun+10]). To show this effect, we have conducted several simulations using the data presented in Table 4.1, and considering different fading scenarios:

**(a)** only path loss (as considered in the results depicted in Figure 4.5);

**(b)** path loss and Rayleigh fading (Exp($2\sigma_\zeta^2 = 1$));

**(c)** path loss, Rayleigh fading (Exp($2\sigma_\zeta^2 = 1$)) and Lognormal shadowing ($\ln\mathcal{N}(\mu_\xi = -{\sigma_\xi}^2/2, \sigma_\xi = 0.7)$).

Table 4.1: Parameters used for performance evaluation under different propagation effects.

| | | | |
|---|---|---|---|
| $P_T^{PU}$ | 30 dB | $\alpha$ | 2.25 |
| $\rho_{ON}$ | 0.5 | $\tau^{PU}$ | 0.001 node/m$^2$ |
| $R_G$ | 30 m | $R_E$ | 500 m |

The probabilities of detection and false alarm were obtained for different $N_S$ values and are illustrated in Figure 4.6. As can be seen, the detection probability obtained with the different propagation effects decreases as more uncertainty is considered. However, as $N_S$ increases, the probabilities obtained with fading channels (cases (b) and (c)) approach the probabilities obtained when only path loss is considered. This observation was the main reason to not consider fading channels in this work because, for realistic $N_S$ values (i.e. $N_S$ values that assure a high practical level of protection to PUs), the probabilities of detection and false alarm considering fading channels are close to the ones obtained when only path loss is assumed.

### 4.5.4 Evaluation of the Sensing Parametrization Criterion

This subsection evaluates the criterion to parameterize the energy detector threshold, proposed in Subsection 4.3.3. To characterize the proposed criterion, we have numerically solved the parameterization problem (4.28), using the data described in Table 4.2.

Figure 4.7 shows $N_S^*$ and $P_{FA}$ obtained for a given level of protection $P_D$ when the parameterization criterion (4.28) is used. As can be seen, the number of samples $N_S^*$ increases with the required level of protection $P_D = \chi$. For almost full protection to PUs ($P_D \approx 1$), the results clearly

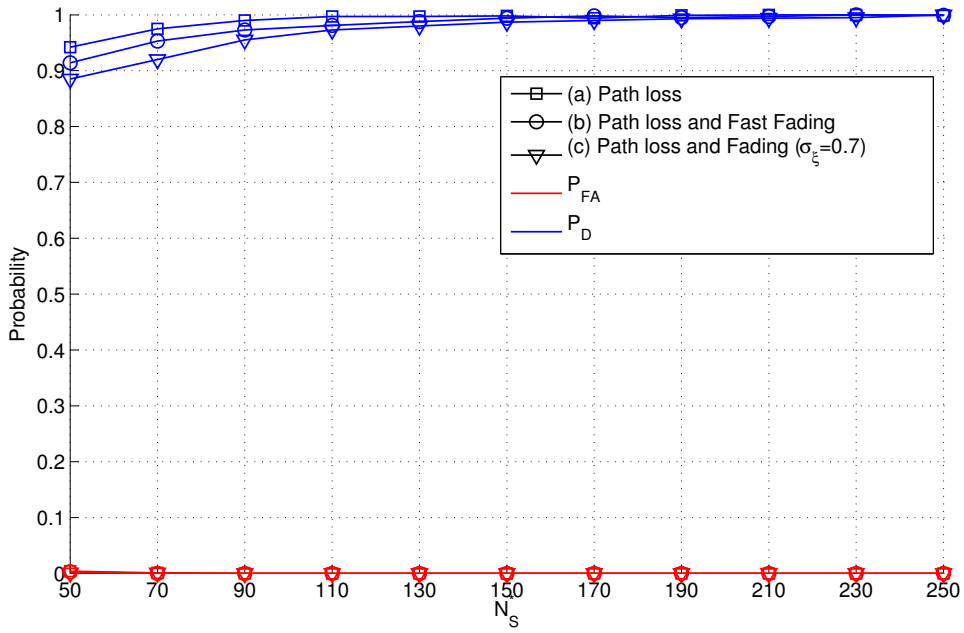


Figure 4.6: $P_D$, $P_{FA}$ for different $N_S$ values. $\eta$ is given by (4.27) for each $N_S$ value.

Table 4.2: Parameters used for performance evaluation of the energy detector.

| | | | |
|---|---|---|---|
| $W$ | 100 kHz | Sampling Rate | 5 $\mu$s |
| $T_F^{SU} = T_S^{SU} + T_D^{SU}$ | 10 $ms$ | $P_T^{PU}$ | 30 dB |
| $\rho_{ON}$ | 0.5 | $\tau^{PU}$ | 0.001 node/m$^2$ |
| $R_G$ | 30 m | $R_E$ | 500 m |

show that the SFA effect can be neglected ($P_{FA} \approx 0$) if $N_S$ is high. However, for lower levels of protection (e.g. $0.8 < P_D < 1$) the SFA occurs ($P_{FA} > 0$).

While the results depicted in Figure 4.7 consider a path loss coefficient $\alpha = 2.5$, Figure 4.8 presents results for different path loss coefficients and applying the same criterion (4.28) and the same scenario described in Table 4.2. As can be seen, more samples are required as the path loss coefficient increases. This is due to the high attenuation of the signal received from the sensing region, which requires a higher number of samples to improve the accuracy of the decision. Regarding the SFA, it is shown that when $P_D$ is close to 1 the SFA may be neglected ($P_{FA} \approx 0$).

### 4.5.5 Evaluation of the ILWNs Performance in Shared Channels

The results in this subsection characterize the performance of SU's network under different channel sensing condition (i.e. for different path loss coefficients). The results include the average number of received packets ($E_{\text{rcv}_3}$) given $n^{SU}$ transmitters, and the throughput of the secondary network.

To evaluate the impact of the SFA effect on an ILWN we first assess the network throughput to capture the impact of both $P_{FA}$ and $N_S$ in the network performance for the same simulation scenario from Subsection 4.5.4. The conditional throughput achieved by a SU was characterized

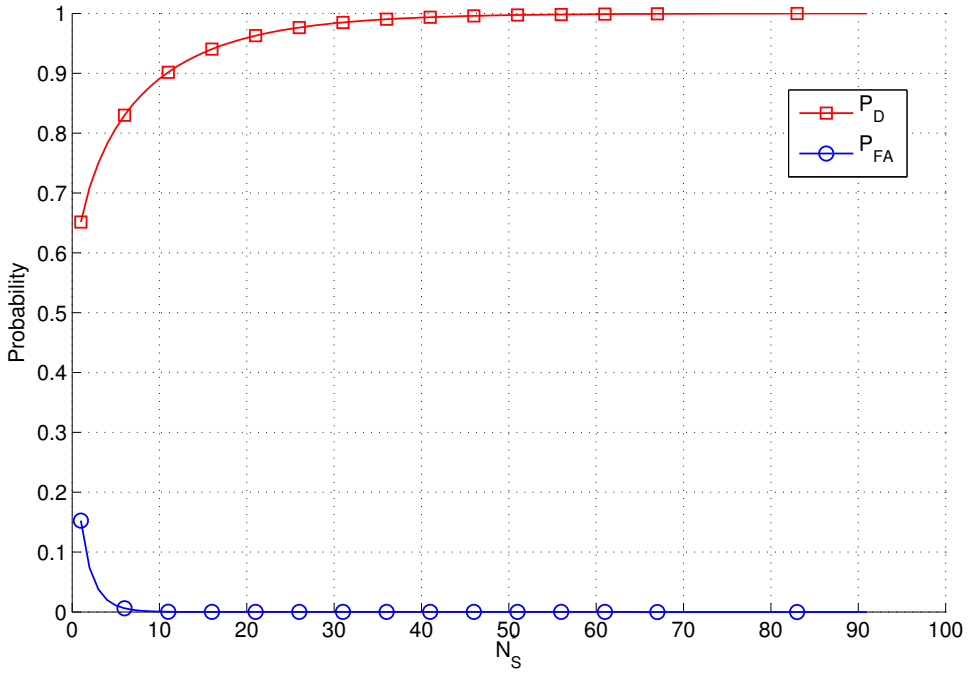


Figure 4.7: $P_{FA}$ obtained for a level of protection $P_D$ when the parameterization criterion (4.28) is adopted ($\alpha = 2.5$).

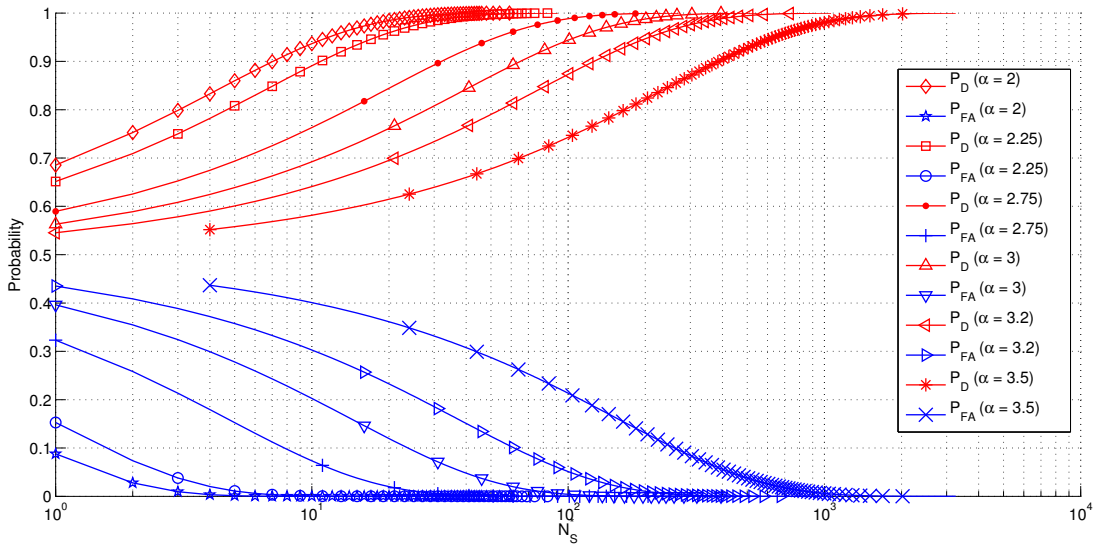


Figure 4.8: $P_D$ and $P_{FA}$ for different $\alpha$ values and levels of protection ($P_D$).

without considering the performance of ILWN's MPR communication (i.e. in (4.43) $E_{\text{rcv}_3}$ is equal to 1). $S^{SU}$ results are depicted in Figure 4.9. As can be seen, for $\alpha = 2.25$ a SU may fully explore the spectrum opportunities within the sensing region, as the conditional throughput may reach 100% while guaranteeing full protection to the PUs ($S^{SU} \approx 1$ when $P_D \approx 1$). But as the the path loss coefficient increases, the increase on the number of samples required to guarantee the level of protection to the PUs decreases the throughput. In this case (say for $\alpha > 3$ in Figure 4.9), a SU may never reach 100% of conditional throughput and no full protection is guaranteed to the PUs within the sensing region ($P_D < 1$) when the throughput of the SU is non-null.

While the throughput results in Figure 4.9 were obtained for an SPR scenario, next we consider an MPR scenario where the $\text{SU}_{\text{Rx}}$ can receive multiple packets simultaneously whenever the outcome of the spectrum sensing indicate the channel as being idle. We consider the scenario formed by a SU receiver circled by SUs and PUs. Regarding the ILWN, we considered $n^{SU}$ SUs transmitters located in the area $A = \pi R_G^2$, which were distributed according to the PDF in (3.6). The PUs were distributed according to a 2D Poisson point process. Assuming that the $\text{SU}_{\text{Rx}}$ senses the channel as vacant, it will receive $n^{SU}$ transmissions plus the total number of transmissions from the PUs located outside the sensing region (i.e. $A_{out} = \pi({R_E}^2 - {R_G}^2)$). Different noise ($N_0$) realizations were used on each trial, being the receiving condition (4.32) observed for each SU transmitter $j$. The expected number of received packets, $E_{\text{rcv}_3}$ was computed from the simulations' data.

The simulations were parameterized according to the data presented in Table 4.3. Regarding

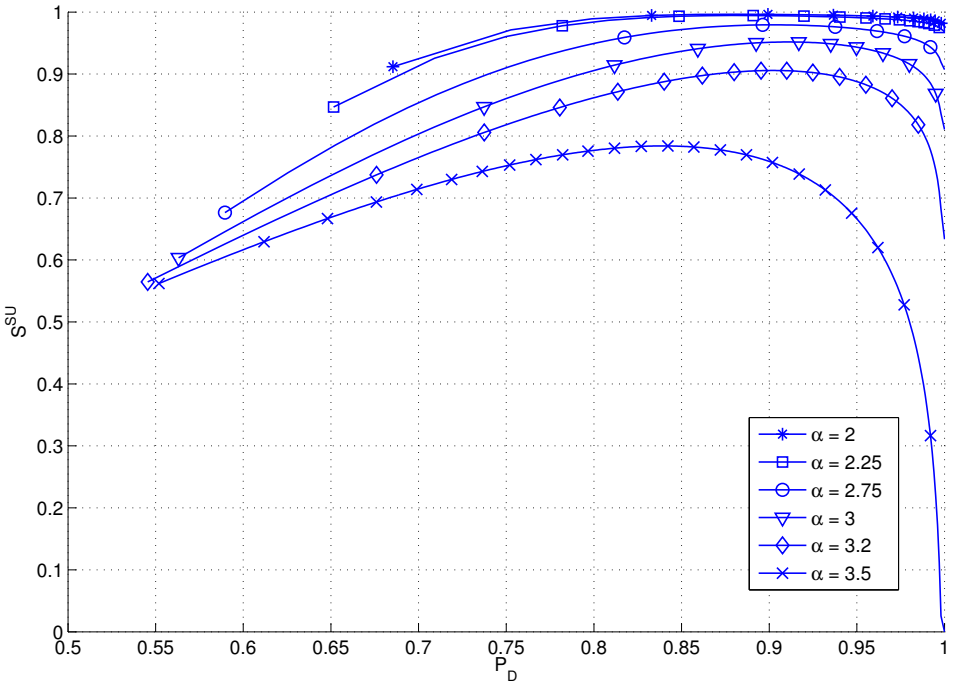


Figure 4.9: Conditional throughput ($S^{SU}$) achieved by SU equipped with an SPR-based PHY layer and given that no PUs are active within the sensing region.

the computation of $P_{S_3}$ in (4.41) we have adopted the FFT algoritm with domain $x$ set to $[-10, 10]$ and a step of $3 \times 10^{-4}$.

Table 4.3: Parameters used for performance evaluation of the ILWN in Shared Channels.

| | | | |
|---|---|---|---|
| $W$ | 100 kHz | Sampling Rate | 5 $\mu s$ |
| $T_F^{SU} = T_S^{SU} + T_D^{SU}$ | 10 $ms$ | $P_T^{SU}$ and $P_T^{PU}$ | 30 dB |
| $\rho_{ON}$ | 0.5 | $\tau^{PU}$ | 0.001 node/m$^2$ |
| $R_G$ | 30 m | $R_E$ | 500 m |
| $\sigma_{N_0}$ | 1 (0 dB) | $b$ | 0.04 |

Figure 4.10 illustrates the average number of received packets given $n^{SU}$ transmitters, for different values of path loss coefficient. The curves identified as "Simul." represent the data obtained through simulation, while the ones identified as "Teor." were obtained by numerically computing (4.42). The curves identified as "Simul. without sensing" were achieved for a scenario where the $SU_{Rx}$ does not perform spectrum sensing, and as consequence, the SUs are allowed to transmit, even when the PUs located within the sensing region transmit.

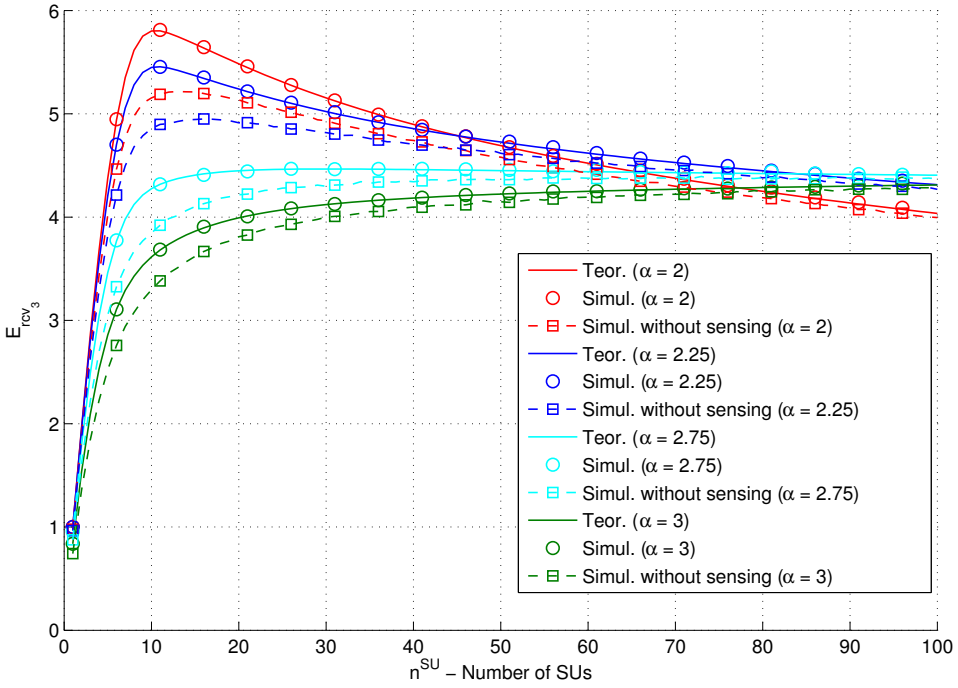


Figure 4.10: Average number of received packets ($E_{\text{rcv}_3}$) given $n^{SU}$ transmitters and different values of $\alpha$.

From Figure 4.10 we observe that the numerical values of $E_{\text{rcv}_3}$ closely follow the results obtained by simulation. The figure shows the maximum point of operation of the MPR-based PHY layer. After that point $E_{\text{rcv}_3}(n^*)$ decreases as $\alpha$ increases. The decrease is because with the increase of $\alpha$ more the power propagation losses increase with the distance increase, meaning that the SUs further away from the $SU_{Rx}$ receiver will experience a lower probability of successful

transmission. Finally, by comparing the results of the average number of received packets for the cases with and without the spectrum sensing, we observe that the average number of received packets increases when spectrum sensing is adopted. By using spectrum sensing the $SU_{Rx}$ achieves a better performance regarding the MPR communication, due to the fact that the interference caused by the PUs' transmissions located in the sensing region is avoided.

Figures 4.11(a), (b) and (c) represent the conditional throughput by computing (4.43) against different values of $n^{SU}$ and different parameterization of $P_D$, for $\alpha$ equal to 2, 2.25 and 2.75, respectively. Figure 4.11 (d) represents the conditional throughput, $S^{SU}$, for different values of $P_D$ and different values of $\alpha$ and considering $n^{SU}$ equal to 10 nodes. As already observed in Figures 4.10 and 4.9, in Figures 4.11(a), (b), (c) and (d) we observe that the conditional throughput achieved by the SU's network decreases as the path loss coefficient increases. The conditional throughput decreases due to two reasons: 1) the sensing period that guarantees an optimal operation of the EBS technique (i.e., $P_{FA} \approx 0$ and $P_D \approx 1$) increases as $\alpha$ increases; 2) optimal number of simultaneous transmitters that maximize the number of successful received packets increases as $\alpha$ increases.

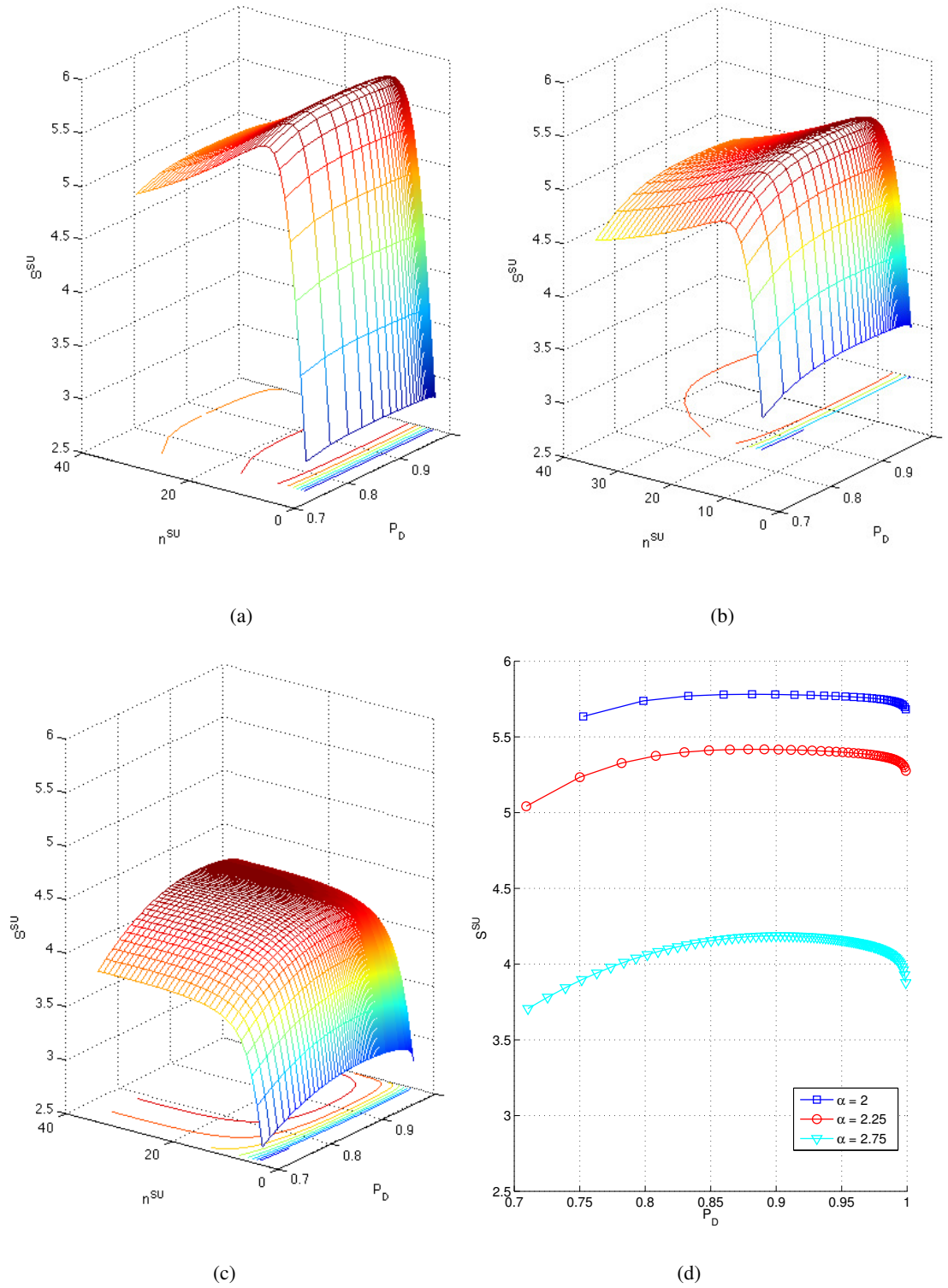


(a) (b) (c) (d)

Figure 4.11: Conditional throughput ($S^{SU}$) achieved by SU versus $P_D$ and $n^{SU}$, for $\alpha = 2$, $\alpha = 2.25$ and $\alpha = 2.75$, respectively, (a), (b) and (c); (d) Conditional throughput ($S^{SU}$) achieved by SU versus $P_D$, for $n^{SU} = 10$ nodes and $\alpha = \{2, 2.25, 2.75\}$.

## 4.6 Conclusions

In this chapter we evaluate the performance of an ILWN operating in shared channels, considering that each SUs uses the EBS as the spectrum sensing technique and adopts a PHY layer with SPR or MPR capabilities. The amplitude of the aggregate interference caused by multiple PUs located outside the sensing region was characterized. We have started with the characterization of the aggregate interference observed by a single SU, concluding that the amplitude of the interference can be approximated by a Generalized Gamma distribution. Moreover, we assumed that it can also be approximated by a Normal distribution, showing results that validate the proposed assumption. The interference formulation was used to derive the probabilities of detection ($P_D$) and false alarm ($P_{FA}$), and closed-form expressions are presented. Several results evaluate the accuracy of the computation of $P_D$ and $P_{FA}$, when compared with simulation results. By proposing a simple decision threshold criterion, this work shows that the SFA can be almost neglected, but its price in terms of number of samples required to meet the level of PUs' protection decreases the conditional throughput achieved by the SUs. The chapter ends up showing that the path loss coefficient effectively impacts on the network performance. Both the average number of packets successfully received and the throughput decrease with the increase of the path loss coefficient. The indicates that a substantial decrease of network throughput is observed in worst propagation conditions. Finally, the chapter also identifies the advantages of adopting a spectrum sensing behavior to avoid the interference caused by PUs that transmit within the sensing region.

CHAPTER 5

# DISTRIBUTED PHY/MAC CROSS-LAYER DESIGN FOR ILWNS

## 5.1 Introduction

MAC schemes take huge responsibility when handling the medium access control and coordination over wireless channels. In ILWNs adopting MPR-based PHY layer the receiver is able to decode multiple overlapping packets transmitted concurrently. This fact changes the underlying assumption about the PHY layer and demands for a new approach in designing MAC protocols, which encourages concurrent transmissions rather than discouraging them to take the full advantage of the MPR capability of the PHY layer.

For decades, the majority of wireless communication systems have considered the collision channel model, where multiple packets transmitted at the same time are lost (they are treated as noise). In the collision channel model any receiver can successfully decode at most one packet at a time, which is usually designated as an SPR behavior. The SPR behavior, usually found in most of the PHY layers proposed so far for wireless systems, has motivated the design of MAC protocols that avoid packet collisions. These include the well-known Aloha, S-ALOHA and other CSMA protocols [Abr70; KL75; KT75; LK75; Rob73]. These traditional MAC protocols when used with an MPR-based PHY layer underestimate the channel capacity, leading to inefficient use of the channel.

Nowadays, recent advances in PHY layer design are enabling the reception of multiple packets transmitted at the same time from different sources. Currently, different MPR techniques are already available for the PHY layer of distributed networks, including but not limited to MIMO MPR [Ma+08] and CDMA MPR [Ngo+08]. Other MPR technologies can be found in operation, including the time-slotted uplink random access of IEEE 802.16e systems [Biba], radio systems adopting the 3GPP LTE standard [GPP], or the MU-MIMO PHY layer implemented in the IEEE 802.11ac devices [Bibd]. As described in Chapter 2, the peculiar characteristics of ILWNs increase

the complexity of MAC protocols that should be able to take full advantage of the MPR capabilities even in highly dynamic environments. In a decentralized MPR transmission scheme the problem of scheduling the requested transmissions is more challenging. This is mainly because the number of captured packets in MPR schemes is greater than one and the transmissions must be coordinated in a distributed way to maximize the number of captured packets.

Several efforts have been recently devoted to investigate the design of innovative distributed MAC schemes not requiring a central coordinating node. [BC10] investigated the problems involved in the introduction of an MPR-based PHY layer in asynchronous IEEE 802.11 networks, admitting the IEEE 802.11 DCF MAC designed for SPR PHY layers. [Cel+10] characterized a new policy to adapt the medium access probability in a distributed way depending on the spatial position of the nodes and not considering power control. [JL11] proposed a decentralized access based on the IEEE 802.11 DCF to be adopted in MU-MIMO PHY layers. [Jun+12] extended the work in [JL11] to the scenario where the transmitters can asynchronously access the medium depending on the number of nodes already transmitting. [AV17] proposed a IEEE 802.11 DCF-based MAC protocol for Wireless Local Area Network (WLAN) with nodes equipped MPR-based PHY layers. The protocol modifies the backoff mechanism of the IEEE 802.11 DCF so that the backoff process quickly adapts to the prevailing traffic conditions while leveraging MPR.

Although being proposed for distributed MPR operation, [AV17; Cel+10; JL11; Jun+12] are not optimized in a cross-layered manner, and consequently the MAC operation is not adequately adapted to the real-time MPR performance observed in the PHY layer. In this chapter, we consider the use of an integrated cross-layer design approach to optimize the performance of the ILWN. To that end, we endeavor to develop cross-layer methodologies where the wireless link conditions and Quality of Service (QoS) requirements are shared between the PHY and the MAC layer. Such information is then used to design efficient methods for dynamic allocation of the network resources. This chapter focuses on decentralized MAC design protocols for MPR radio systems. We propose three decentralized MAC schemes to be adopted in distributed MPR-based wireless networks.

The main contribution of this chapter is the design and the characterization of the MAC layer and PHY layer performance for distributed networks with MPR capabilities. By jointly characterizing the MAC and PHY layers it is possible to study the overall performance and throughput gain arising from different parameterization of the MAC and PHY layers.

In Chapter 3 and Chapter 4, we have proposed a model to characterize the PHY layer performance. The proposed model is capable of approximating the average number of packets successfully received for a given number of simultaneous transmissions and considering several parameters associated with the propagation effects and the receiver sensibility (capture threshold). The average number of packets successfully received can be approximated by a rational function adopting an interpolation process that uses the numerical results obtained with the model. The proposed solution is valid for any spatial distribution of transmitters and any propagation model, as long as the received signals from the multiple transmitters are independent and i.i.d.. The generic PHY layer is used to study the performance of the PHY/MAC cross-layer design.

Regarding the MAC schemes, we evaluate different distributed MAC policies and protocol

designs. Theses include: a MAC Protocol with SPR Reservation (MAC-SPRR); a MAC Protocol with MPR Reservation (MAC-MPRR); and a MAC Protocol with Maximization of the MPR Reservation (MAC-MMPRR). These MAC schemes are designed to work in a distributed way, i.e. without requiring a central node that coordinates the medium access. Basically, the proposed schemes are divided in two stages. In the first stage the nodes indicate their willingness to transmit by adopting an SPR or MPR PHY layer. In the second stage the nodes jointly transmit taking advantage of the MPR-based PHY layer. In the MAC-SPRR scheme an SPR-based PHY layer is considered in the first stage. On other hand, an MPR-based PHY layer is considered in the MAC-MPRR and MAC-MMPRR schemes.

Different from what is usually found in the literature, both MAC and PHY layers are considered in the characterization of the throughput achieved by the proposed schemes. The results obtained numerically and through simulation indicate the advantages of our solution (in terms of throughput), identifying optimal points of operation.

The main contributions of this chapter include:

- The formal characterization of the throughput achieved by the PHY/MAC cross-layer scheme. The MAC behavior is modeled in order to characterize the number of competing nodes at a given instant, which is an input of a model that approximates the performance of the MPR-based PHY layer. In this way, we quantify the average number of packets successfully received as a function of the multiple parameters that compose the PHY/MAC cross-layer design;
- The identification of the optimal parameters that maximize the throughput. This contribution encompasses a first step where the medium access probability of the nodes is regulated in order to obtain the optimal number of successful received packets on each reservation slot. In a second step the optimal number of reservation slots is computed in order to maximize the throughput;
- The design of a two-stage MAC protocol particularly tailored to benefit from the MPR advantages. This includes an innovative reservation stage, where the nodes adopt different medium access probabilities according to the reservation slot they are trying to access. In this way, the optimal number of competing nodes transmitting data packets in the second stage can be reached quickly;
- Simulation and numerical results, which highlight the advantages of the proposed design (in terms of throughput), identifying optimal points of operation.

### Chapter Contents

- **Section 5.2**: The description of the system, including the system assumptions and the principle of operation of the proposed MAC schemes, is presented in this section;
- **Section 5.3**: Considering the PHY layer performance characterization derived in Chapters 3 and 4, this section approximate the expected number of successful receptions when $r$ simultaneous transmissions occur by a rational function which is computed by an interpolation

process. The rational function approximation is validated for different capture thresholds $b$ and fading uncertainty $\sigma_\xi$;

- **Section 5.4**: The proposed MAC-SPRR and MAC-MPRR schemes are analyzed. This section presents the characterization of the reservation stage (first stage) in a generic way. The performance of the MAC-SPRR and MAC-MPRR schemes are characterized in Subsections 5.4.2 and 5.4.3, respectively. The performance of the proposed MAC schemes in different scenarios is evaluated in Subsection 5.4.4;

- **Section 5.5**: The proposed MAC-MMPRR scheme is assessed in this Section. Subsection 5.5.2 presents the methodology to maximize the throughput of the proposed cross-layer scheme. The performance of the proposed MAC-MMPRR scheme is evaluated and analyzed for different scenarios in Subsection 5.5.3;

- **Section 5.6**: This section summarizes the chapter's conclusions.

## 5.2 System Description

The system characterization adopted to evaluate the performance of the proposed MAC protocols is presented in this section. Subsection 5.2.1 introduces the system assumptions and Subsection 5.2.2 describes the operation of the different protocols.

### 5.2.1 System Assumptions

This chapter considers the network scenario represented in Figure 5.1. $n$ nodes ($\mathrm{Tx}_1$, $\mathrm{Tx}_2$,...,$\mathrm{Tx}_n$) compete for the medium to transmit data to the Rx node, which is capable of adopting an MPR PHY layer. The proposed MAC scheme works in a distributed way, without being coordinated by a central node. It is assumed that nodes associate to the Rx node before start transmitting, similar to the association mechanism adopted in IEEE 802.11 standard.

While the proposed schemes can be adopted in a scenario where each node transmits to a random destination, this chapter considers that the transmitters always transmit to a fixed destination, which is referred to as the node Rx, as illustrated in Figure 5.1. Initially, the Rx node assumes the synchronization task if it does not receive synchronization information during a pre-defined time interval. This is similar to the synchronization schemes already proposed in several distributed MAC schemes for wireless sensor networks, where any node can start transmitting a SYNC packet [Ye+02]. For the sake of simplicity, we consider that the Rx node is always responsible for the synchronization of the $n$ transmitters. Regarding the MPR-communication task it is adopted the capture model characterize in Chapter 3.

### 5.2.2 Protocol Description

Figure 5.2 illustrates the transmission cycle adopted in the proposed MAC schemes. The transmission cycle is defined as the time interval needed to complete an MPR transmission.

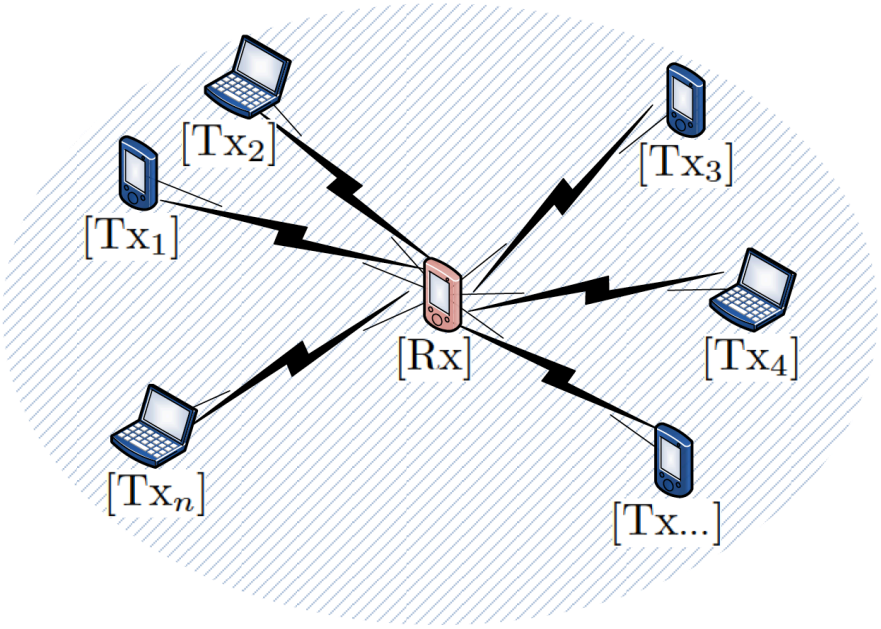


Figure 5.1: $n$ nodes competing for the medium to transmit data to the Rx node.

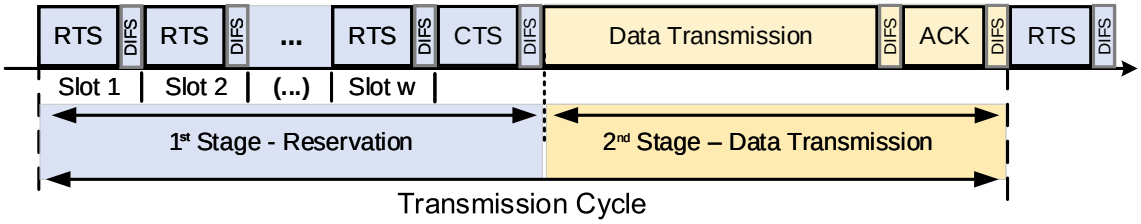


Figure 5.2: Double stage MAC Protocol.

In the first stage (reservation stage) of the transmission cycle, the multiple nodes competing for the channel may transmit a Request To Send (RTS) packet whenever they have an MPR packet to transmit. Within the reservation stage each node transmits the RTS packet with probability $p$ in at most one of the $w$ slots. The duration of each slot includes the duration of the RTS packet plus the Distributed Inter-Frame Space (DIFS) time interval. The DIFS interval avoids an overlap of consecutive RTS packets due to the propagation delay. Each RTS packet contains the addresses of the source and destination node.

The reservation stage finishes with the transmission of a Clear to Send (CTS) packet, which is transmitted by the destination node and indicates the addresses of the transmitters allowed to transmit in the second stage. CTS packets may also contain power control information (when used). From the description above, the reservation stage duration is defined as

$$D_{stg_1} = w(D_{RTS} + DIFS) + (D_{CTS} + DIFS), \tag{5.1}$$

where $D_{RTS}$ and $D_{CTS}$ represent the duration of the RTS and CTS packets, respectively.

The transmitters advertised in the CTS packet transmit their data packet in the second stage (Data transmission). The transmitters copy their data packets to the channel at the beginning of the second stage and an MPR technique is adopted at the PHY layer to decode the multiple and simultaneous transmissions at the receiver side. After receiving the multiple data packets (these packets are transmitted in the "Data Transmission" interval illustrated in Figure 5.2), the receiver node confirms the packets successfully received by transmitting back an acknowledged packet (ACK). The duration of the second stage is given by

$$D_{stg_2} = (D_{PKT} + DIFS) + (D_{ACK} + DIFS), \tag{5.2}$$

where $D_{PKT}$ and $D_{ACK}$ represent the duration of the data and ACK packets, respectively.

In this chapter we propose and evaluate three MAC protocols adopting the transmission cycle represented in Figure 5.2, being described as follows:

MAC Protocol with SPR Reservation (MAC-SPRR) - In this scheme it is assumed an SPR-based PHY layer during the first stage of the transmission cycle. Figure 5.3 (a) illustrates an example of the operation of the MAC-SPRR scheme. From the figure, in the first slot of the reservation stage, $\mathrm{Tx}_1$ and $\mathrm{Tx}_3$ simultaneously transmit an RTS packet to the receiver Rx. Since an SPR-based PHY layer is admitted in the reservation stage neither $\mathrm{Tx}_1$ or $\mathrm{Tx}_3$ transmissions succeed during the reservation stage and, consequently, they are unable to transmit on the second stage of transmission. On the other hand, the RTS transmission of $\mathrm{Tx}_2$ and $\mathrm{Tx}_4$ do not collide at the receiver with RTS transmissions of other nodes. The receiver sends a CTS packet in order to inform $\mathrm{Tx}_2$ and $\mathrm{Tx}_4$ that they are allowed to start their data transmission during the second stage of the transmission cycle. At the end of the transmission cycle the receiver Rx sends an ACK to inform which data packets were successfully received. We highlight that when SPR is adopted, instead of MPR, an RTS packet is successfully received if it implies an exclusive use of the channel by a single transmitter. This scheme may be particularly useful when a receiver successfully decodes an RTS packet and wants to measure the power received from the source node, which allows the adoption of power control schemes or other advanced signal processing techniques required by some MPR techniques. As stated above, during the second stage of transmission it is assumed an MPR-based PHY layer. The total number of nodes that will access to the MPR transmission phase corresponds to the total number of RTS packets that were successfully received during reservation phase.

MAC Protocol with MPR Reservation (MAC-MPRR) - Contrarily to the previous scheme, in this scheme it is assumed that the nodes adopt an MPR-based PHY layer during both stages (Reservation and Data transmission). A certain average number of received packets, $E_r$, is admitted when $r$ simultaneous transmissions occur, either in the reservation phase (sending the RTS packet) or in the transmission phase (see the example scenario of operation in Figure 5.3). Thus, one or more successful transmissions are expected to occur at each slot of the

first stage of transmission. $E_r$ can be characterized by $E_{rcv_1}$ or $E_{rcv_2}$ derived in Chapter 3 or by $E_{rcv_3}$ derived in Chapter 4. The number of nodes that are allowed to transmit in the transmission phase is determined by the sum of the RTS successfully transmitted in the $w$ slots of the reservation phase. This scheme have the benefit of taking advantage of the MPR capabilities not only during the second stage but also during the reservation stage.

MAC Protocol with Maximization of the MPR Reservation (MAC-MMPRR) - This scheme differs from the previous one in only one aspect: the probability of access, $p$, varies during the reservation stage. While in the previous schemes it is assumed that $p$ is maintained constant during the $w$ RTS slots, in this scheme different access probabilities are adopted on each slot. This modification in the design of the MAC scheme improves the MPR communication process, by adapting the value of $p$ to control the average number of nodes that simultaneously

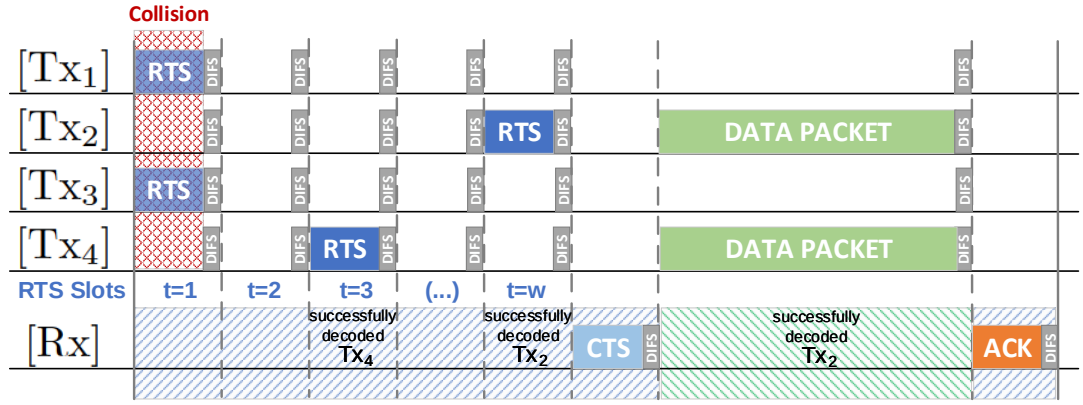


(a)

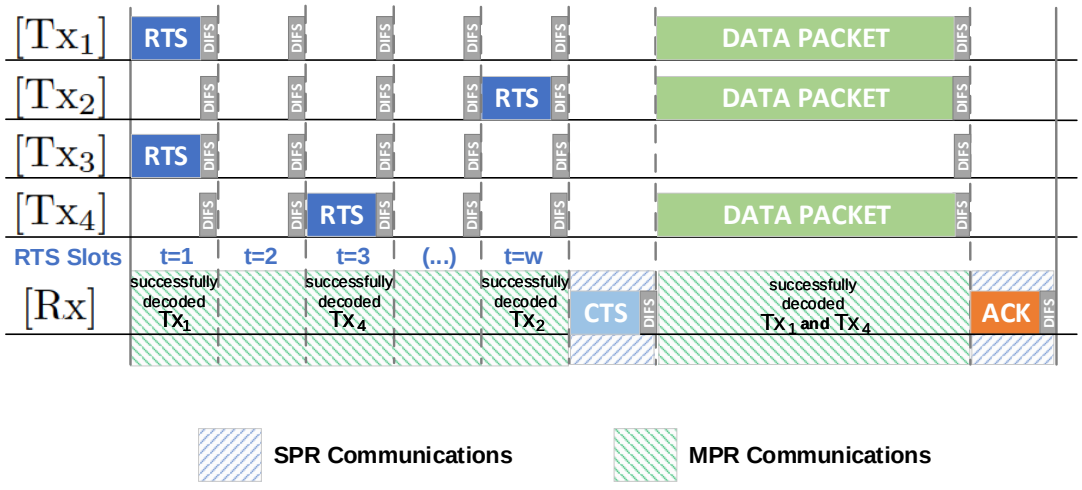


(b)

Figure 5.3: MAC schemes: (a) MAC-SPRR; (b) MAC-MPRR and MAC-MMPRR.

transmit. The adoption of $p$ in the design of the MAC scheme is particularly advantageous when the overall system is optimized in a cross-layer manner, taking into account the joint performance of the PHY and MAC layer.

## 5.3 PHY layer Performance

In Chapters 3 and Chapter 4 we have characterized the performance of the MPR-based PHY layer under different propagation characteristics of the medium, spatial distribution of the nodes scattered in the network and scenarios considering and neglecting interference. Moreover, the performance of the MPR-based PHY layer was characterized by the average number of received packets given the number of nodes simultaneous transmitting (e.g. $E_{rcv_1}$ and $E_{rcv_2}$ in Chapter 3, or $E_{rcv_3}$ in Chapter 4), which have been numerically computed by using the FFT algorithm. In Chapter 3 and Chapter 4 we have concluded that the individual probability of successful packet reception and the average number of successful received packets are important performance metrics.

This section aims to decrease the mathematical complexity of the average number of received packets computed in the models presented in Chapter 3. For that, we approximate the curve that characterizes the average number of received packets by a mathematical function to be adopted in the joint PHY/MAC cross-layer optimization.

Lets start by considering a similar network configuration as discussed in Chapter 3. We consider that each transmitter adopts an MPR PHY layer and $r$ nodes simultaneously transmit data to the Rx node. We assume that the multiple signals received by the Rx node are independent and identically distributed (i.i.d.) RVs with PDF $f_{P_k}$. The total power received from the multiple transmissions is expressed by $\Lambda = \sum_{k=1}^{r} P_k + N_0$, where $P_k$ and $N_0$ are RVs that represent the power received by the $k$-th transmitter and the noise power at the receiver, respectively. The receiver node Rx acts as an MPR receiver where the SINR, regarding the signal received from node $\mathrm{Tx}_j$, is defined by $\gamma_j = \frac{P_j}{\Lambda - P_j}$.

Considering the capture condition adopted in (3.3), the signal received from node $\mathrm{Tx}_j$ is successfully received whenever the capture condition $\gamma_j > b$ holds. The capture threshold $b$ is a parameter that characterizes the type of PHY layer, including the type of modulation and the sensitivity of the receiver (see Section 3.2).

The performance of a generic MPR-based PHY layer can be evaluated using the capture condition in (3.3) to define the probability of a successful reception, which is written as

$$\mathrm{P}_S = \mathrm{P}[\gamma_j > b]. \tag{5.3}$$

Assuming that the powers of the received signals ($P_k$) from the multiple transmitters are i.i.d., and suffer the propagation effects described in Section 3.2, it is possible to characterize the average number of successfully received packets ($E_r$) when $r$ simultaneous transmissions occur,

$$E_r = r \cdot \mathrm{P}_S. \tag{5.4}$$

To capture the performance of a generic MPR PHY layer in a formal way, we have computed the model from Section 3.3 varying the number of transmitters ($r$) and considering the propagation

conditions described in Subsection 3.2 parametrized with the values in Table 5.1. To compute $P_S$ in (3.43) we have first computed $f_\beta(x)$ in (3.41) through the FFT algorithm (the domain $x$ was set to $[-500, 500]$ and a step of $7.6 \times 10^{-3}$ was adopted in the FFT algorithm).

Table 5.1: Parameters adopted in the simulations of the PHY layer performance.

| | | | |
|---|---|---|---|
| $P_T$ | 20 dB | $D$ | 10 m |
| $\alpha$ | 2 | $\sigma_{N0}$ | 1 (0 dB) |

The pairs of values $(r, E_r)$ obtained by deriving the model were used in a rational function interpolation process to identify the parameters of a rational function that describes the PHY layer performance function $h_{MPR}(x)$ for a given capture threshold $b$ and for a given fading uncertainty ($\sigma_\xi$). Although different interpolation functions were adopted (e.g. spline interpolation), the rational function exhibited the lowest fitting error for the different sets of data. In light of this, the rational function adopted in the interpolation process was

$$E_r(r) \sim h_{MPR}(r) = \frac{p_1 r + p_0}{q_2 r^2 + q_1 r + q_0}. \tag{5.5}$$

The interpolation and model results are compared in Figures 5.4 and 5.5 for different number of nodes ($r$), capture threshold ($b$) values and multiple fading propagation effects. The rational function parameters determined in the interpolation process are presented in Tables 5.2 and 5.3 which correspond to the results illustrated in Figures 5.4 and 5.5, respectively. As it can be seen from the results presented in both figures, the rational curve fitting results are close to the results obtained with the model considering the values of $r$ between 1 and $r^*$ ($r^*$ is the coordinate of the maximum of each curve, $E_r$). For $r$ higher than $r^*$ it is noticeable that the error between the rational curve fitting results and the results obtained with the model increase as $r$ increases (particularly for $\sigma_\xi = 0.2$ in Figure 5.5). Still, these results allow us to use the rational function in the PHY/MAC layer characterization and optimization, since the domain of $r$ that reflects a good MPR performance is approximated. Although not treated in the thesis, the parameters of the rational function can be estimated, being an useful technique to predict the real-time performance of the MPR-based PHY layer, namely due to the time-varying nature of the radio propagation.

Table 5.2: Coefficients of the rational functions for $\sigma_\xi = 0.7$

| $b$ | $p_1$ | $p_0$ | $q_2$ | $q_1$ | $q_0$ |
|---|---|---|---|---|---|
| 0.10 | 237.23 | −58.40 | 1.00 | 48.18 | 199.55 |
| 0.08 | 362.14 | −91.96 | 1.00 | 62.37 | 315.53 |
| 0.04 | 1293.17 | −186.37 | 1.00 | 121.50 | 1360.43 |
| 0.02 | 4454.42 | 949.63 | 1.00 | 211.67 | 5533.07 |

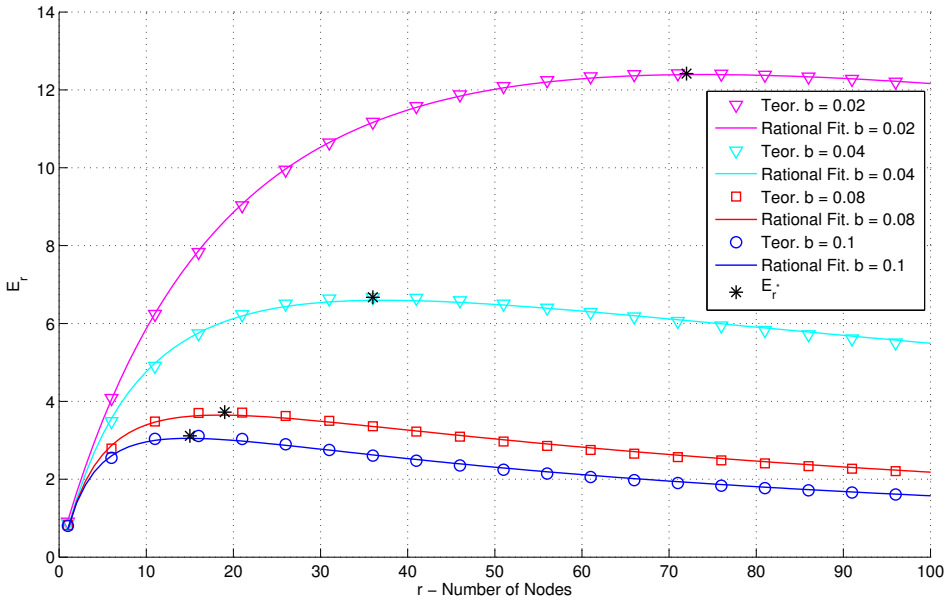


Figure 5.4: Average number of successfully received packets ($E_r$) as a function of the number of transmitters ($r$) for multiple capture thresholds ($b$) and $\sigma_\xi = 0.7$.

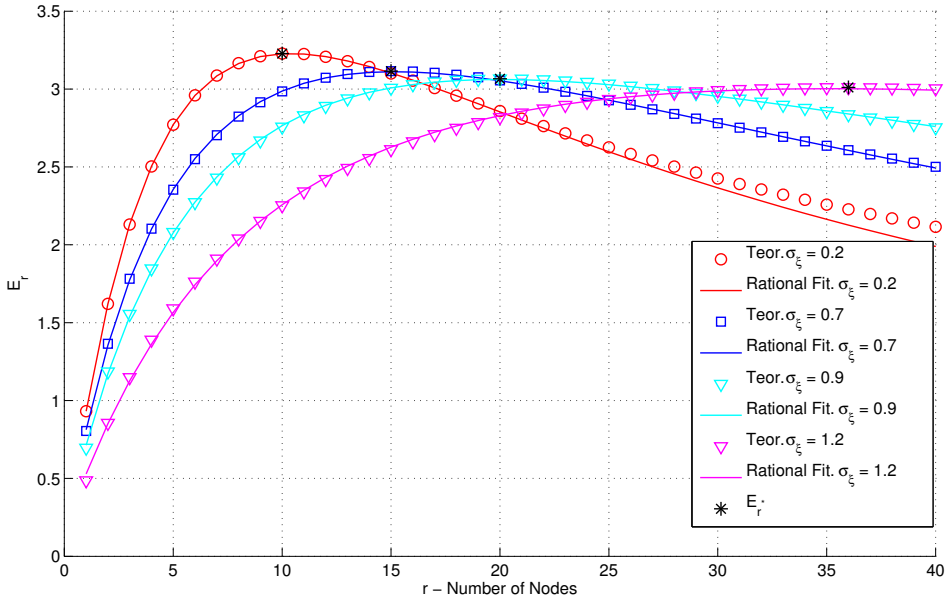


Figure 5.5: Average number of successfully received packets ($E_r$) as a function of the number of transmitters ($r$) for multiple fading propagation effects ($\sigma_\xi$) and $b = 0.1$.

Table 5.3: Coefficients of the rational functions for $b = 0.1$

| $\sigma_\xi$ | $p_1$ | $p_0$ | $q_2$ | $q_1$ | $q_0$ |
|---|---|---|---|---|---|
| 0.2 | 158.07 | −62.34 | 1.00 | 30.05 | 83.89 |
| 0.7 | 237.23 | −58.40 | 1.00 | 48.18 | 199.55 |
| 0.9 | 313.31 | −29.79 | 1.00 | 64.33 | 375.84 |
| 1.2 | 540.32 | 195.68 | 1.00 | 110.40 | 1275.46 |

## 5.4 Distributed MAC Protocols

In the following subsection, the reservation stage is characterized in a generic way. After the reservation stage characterization, we study the throughput achieved by the proposed MAC-SPRR and MAC-MPRR schemes.

### 5.4.1 Characterization of the Reservation Stage

Denoting $N$ as a RV representing the number of nodes transmitting an RTS packet in a reservation slot

$$N \in \{0, 1, ..., n\},$$

where $n$ corresponds to the total number of nodes that are attempting to transmit an RTS and being $X$ a RV representing the slot where the RTS is transmitted,

$$X \in \{1, 2, ..., w\},$$

the probability of a node transmitting an RTS packet in the slot $t \in \{1, 2, ..., w\}$ is given by a geometric distribution as follows

$$P[X = t] = p \cdot (1 - p)^{t-1}, \tag{5.6}$$

because each node only transmits a single RTS in the $w$ available reservation slots.

The probability of $N = n_t$ nodes transmitting an RTS in a slot $X = t$ is given by the binomial distribution

$$\begin{aligned} P[N = n_t, X = t] = &\binom{n}{n_t} \cdot (P[X = t])^{n_t} \cdot \\ &\cdot (1 - P[X = t])^{n-n_t}, \end{aligned} \tag{5.7}$$

and using (5.6) we have

$$\begin{aligned} P[N = n_t, X = k] = &\binom{n}{n_t} \cdot \left(p \cdot (1 - p)^{t-1}\right)^{n_t} \cdot \\ &\cdot \left(1 - p \cdot (1 - p)^{t-1}\right)^{n-n_t}. \end{aligned} \tag{5.8}$$

Being $m$ the maximum number of nodes that may transmit an RTS packet in a slot, the expected number of nodes transmitting an RTS packet in the slot $t$ is given by

$$E_t(m) = \sum_{i=1}^{m} i \cdot P[N = i, X = t]. \tag{5.9}$$

Note that $m$ may be limited to one in order to represent a successful transmission event when an SPR communication model is adopted in the reservation phase.

### 5.4.2 MAC-SPRR

In this subsection we characterize the network throughput of the MAC scheme with SPR reservation. The average number of nodes, $E_{rts}^{spr}$, successfully transmitting an RTS packet during the first stage of the transmission cycle, is given by

$$E_{rts}^{spr} = \sum_{t=1}^{w} E_t(1). \tag{5.10}$$

Given $E_{rts}^{spr}$, the average number of nodes, $E_{data}^{spr}$, that succeed in the second stage of transmission depends on the MPR-based PHY layer. In Section 5.3 we study the performance of the MPR PHY layer, where we define a rational function ($h_{MPR}(r)$) to indicate the expected number of successfully received packets when $r$ simultaneous transmissions occur. Defining $E_{data}^{spr}$ as a function of $E_{rts}^{spr}$,

$$E_{data}^{spr} = h_{MPR}(E_{rts}^{spr}), \tag{5.11}$$

the system network throughput is given by

$$S^{spr} = \frac{E_{data}^{spr} T_{PKT}}{T_a + w}, \tag{5.12}$$

which corresponds to the ratio between the average amount of time that the channel is successfully used by the nodes transmitting during the MPR transmission stage and the duration of the transmission cycle, where

- $T_{PKT}$ represents the average amount of time during which the channel is successfully used by the nodes transmitting the MPR packet, and is given by,

$$T_{PKT} = \frac{D_{PKT}}{D_{RTS} + DIFS}. \tag{5.13}$$

  Note that $T_{PKT}$ is expressed in multiples of time slot duration, i.e. multiples of $D_{RTS}+DIFS$;

- $(T_a + w)$ represents the duration of the transmission cycle (in Figure 5.2), and $T_a$ is given by

$$T_a = \frac{D_{stg2} + D_{CTS} + DIFS}{D_{RTS} + DIFS}. \tag{5.14}$$

  Note that $T_a$ is also expressed in multiples of time slot duration.

### 5.4.3 MAC-MPRR

The performance of the MAC scheme with MPR reservation is characterized in this subsection. In this case, the definition of the average number of nodes successfully transmitting an RTS packet

during the first stage of the transmission cycle ($E_{rts}^{mpr}$), depends on the MPR PHY layer capability indicated by the $h_{MPR}(r)$ function. Consequently, $E_{rts}^{mpr}$ is given by

$$E_{rts}^{mpr} = \sum_{t=1}^{w} h_{MPR}(E_t(n_t)), \tag{5.15}$$

where $n_t$ denotes the maximum number of nodes that may transmit an RTS packet in a given slot, which is equal to the total number of nodes competing in the reservation phase.

The average number of nodes that achieve success in the second stage of transmission depends again on the MPR PHY layer capability and is given as follows,

$$E_{data}^{mpr} = h_{MPR}(E_{rts}^{mpr}). \tag{5.16}$$

The throughput of the overall system network is finally given by

$$S^{mpr} = \frac{h_{MPR}(E_{rts}^{mpr})T_{PKT}}{T_a + w}. \tag{5.17}$$

### 5.4.4 Performance Evaluation

This subsection presents a set of performance results of the proposed MAC-SPRR and MAC-MPRR schemes. The models presented in Subsection 5.4.1, Subsection 5.4.2 and Subsection 5.4.3 are evaluated in Subsection 5.4.4.1. Regarding the MAC-MPRR protocol, the optimal throughput of the overall network system is analyzed in Subsection 5.4.4.2.

#### 5.4.4.1 Model Validation and Performance Analysis

We have considered a single-hop network where $n$ nodes adopt the proposed MAC-SPRR and MAC-MPRR schemes. The network scenario is formed by a receiver circled by $n$ transmitters within a radius $D$, which were distributed according to the PDF in (3.6). Different fading ($\Psi_k$) and noise ($N_0$) realizations were used on each trial. The MAC schemes were implemented adopting the capture condition in (3.3) to determine the number of successful MPR data packets transmitted in each transmission cycle. The simulations were parametrized according to the data presented in Table 5.4. The performance results were characterized for two receiving thresholds, $b = 0.1$ and $b = 0.04$.

Next we present results obtained for MAC-SPRR and MAC-MPRR schemes. Figures 5.6 depicted the average number of RTS packets successfully received, during the reservation stage. The average number of data packets is depicted in Figure 5.7. The throughput achieved by the schemes is represented in Figure 5.8. The results are plotted for different values of n (total number of nodes attempting transmission). The curves “Simul.” and “Teor.” represent the simulated and the numerical results obtained with the theoretical model, respectively, for the MAC-SPRR and MAC-MPRR schemes. Regarding the number of slots for reservation, $w = 10$ slots were adopted in the MAC-MPRR scheme, while 20 slots were adopted in the MAC-SPRR. In both MAC schemes the probability of access, $p$, is parameterized to 0.15.

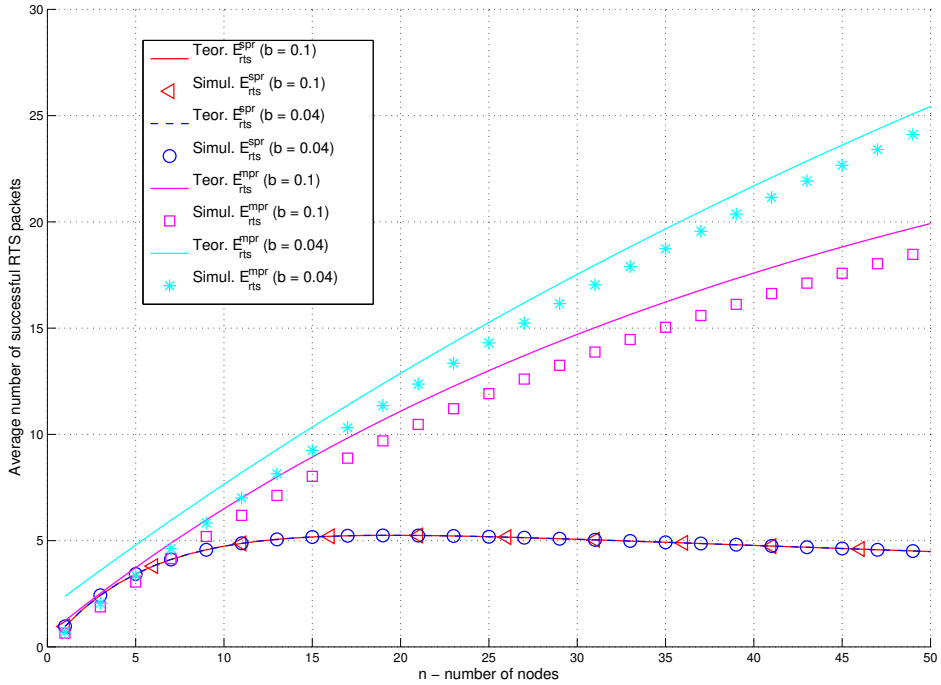


Figure 5.6: Average number of successful RTS packets decoded for multiple competing nodes when the number of RTS slots is constant ($w = 20$ for MAC-SPRR and $w = 10$ for MAC-MPRR).

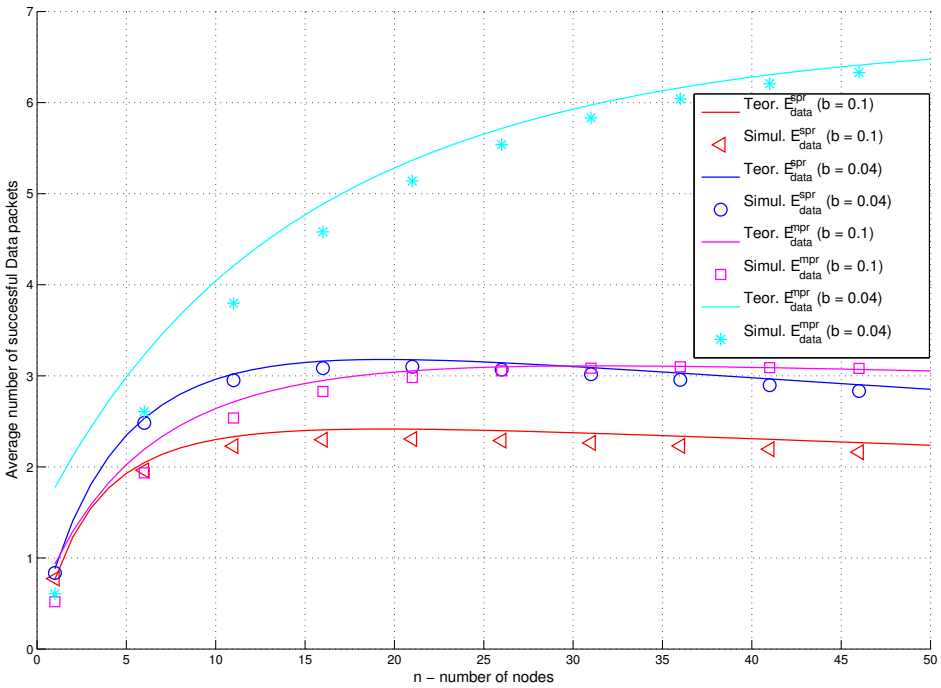


Figure 5.7: Average number of successful Data packets decoded for multiple competing nodes when the number of RTS slots is constant ($w = 20$ for MAC-SPRR and $w = 10$ for MAC-MPRR).

Table 5.4: Parameters adopted in the simulations regarding the evaluation of MAC-SPRR and MAC-MPRR.

| | | | |
|---|---|---|---|
| Slot duration | 20 $\mu s$ | $P_T$ | 20 dB |
| DIFS | 50 $\mu s$ | $\alpha$ | 2 |
| $D_{\text{RTS}}$ | 352 $\mu s$ | $D$ | 10 m |
| $D_{\text{CTS}}$ | 304 $\mu s$ | $\sigma_{N0}$ | 1 (0 dB) |
| $D_{\text{PKT}}$ | 8000 $\mu s$ | $\sigma_{\xi}$ | 0.7 |
| $D_{\text{ACK}}$ | 304 $\mu s$ | Number of trials | $5 \times 10^5$ |

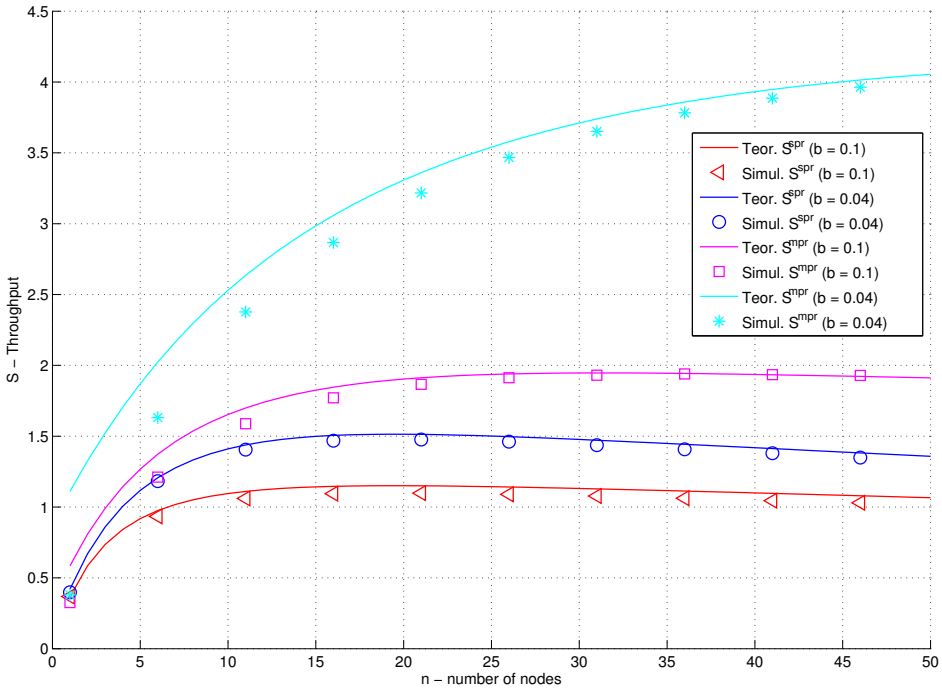


Figure 5.8: Throughput achieved for multiple competing nodes when the number of RTS slots is constant ($w = 20$ for MAC-SPRR and $w = 10$ for MAC-MPRR).

For all the scenarios, the numerical results are close to the values obtained through simulation. The deviation between the simulation results and the numerical results is mainly due to the fact that the MPR-based PHY layer performance is approximated by the rational function proposed in Section 5.3. Despite the gap between the "Simul." and "Teor." curves the throughput curves have identical maxima and minima with $n$. Since in mathematical optimization the goal is to find a global maxima and minima, the proposed modeling approach can be used for optimization purposes.

From the results plotted in Figure 5.7, the $E_{data}$ values in each scenario have a maximum equal to $E_{r^*}$. This point corresponds to the case when the number of nodes arriving at the second stage of the transmission cycle is equal to $r^*$ (i.e. the maximum MPR capacity of the PHY layer). After this point, as the number of nodes transmitting in the second transmission stage increases, the

average number of successful Data packets decoded decrease because the descending part of the MPR-based PHY layer performance curve is reached.

From the results plotted in Figure 5.8, we observe that the proposed MAC scheme with MPR capabilities in the first stage of the transmission cycle leads to a better performance when compared to the case when SPR-based PHY layer is used in the reservation stage. Note that in comparable conditions, the $E_{data}$ values of the MAC-SPRR scheme are greater than the values observed in the MAC-MPRR scenario. However, in terms of throughput values, the MAC-MPRR scheme achieves higher values than the MAC-SPRR scheme, due to the fact that the number of RTS slots, $w$, is higher for MAC-SPRR scheme ($w = 20$ in MAC-SPRR and $w = 10$ in MAC-MPRR).

#### 5.4.4.2 Numerical Optimization

MAC-MPRR was optimized to achieve the maximum system network throughput. For that, MAC-MPRR was optimized for different number of nodes, $n$, by finding the optimal number of reservation slots ($w$) and the optimal probability of access ($p$).

Assuming a given MPR-based PHY layer the system network throughput achieved by MAC-MPRR is optimized as follows:

$$\begin{aligned} \max_{p,w} \quad & S^{mprr}, \\ \text{s.t.} \quad & 0 < p < 1 \\ & 1 \leq w \leq w_{max}. \end{aligned}$$

Basically, the optimal throughput is computed taking into account two constraints: $w$ is limited to the maximum number of reservation slots that a frame can hold, and $p$ is limited to a value between 0 and 1.

The scenario considered for the protocol's optimization was the same as considered in the previous subsection. MAC-MPRR consists of two transmission stages. As explained in Subsection 5.4.4.1, the first stage is used to regulate the number of nodes competing in the second stage of the transmission cycle in order to maximize the MPR-based PHY layer performance in the second stage of the transmission cycle. If we take into consideration (5.16), and based on the aforementioned explanation, we can see that MAC-MPRR achieves the highest PHY layer performance when the average number of nodes transmitting in the second stage of transmission is equal to $r^*$, that corresponds to the maximum of the rational function in (5.5). However, in order to guarantee a certain number of nodes transmitting in the second stage of transmission we may increase or decrease the number of $w$ RTS slots which consequently may decrease or increase the overall system throughput.

The solution of the optimization problem indicates that the number of $w$ RTS slots and the probability of access $p$ should be parameterized in order to guarantee the optimal trade-off between the time spent in the reservation stage and the number of nodes transmitting in the second stage of transmission. In order to sustain the previous analysis, Figure 5.9 shows for $n = 65$ and $n = 125$ the theoretical results of the throughput achieved by the network, obtained with (5.17), considering different values of $w$ and $p$ a assuming $w_{max} = 20$.

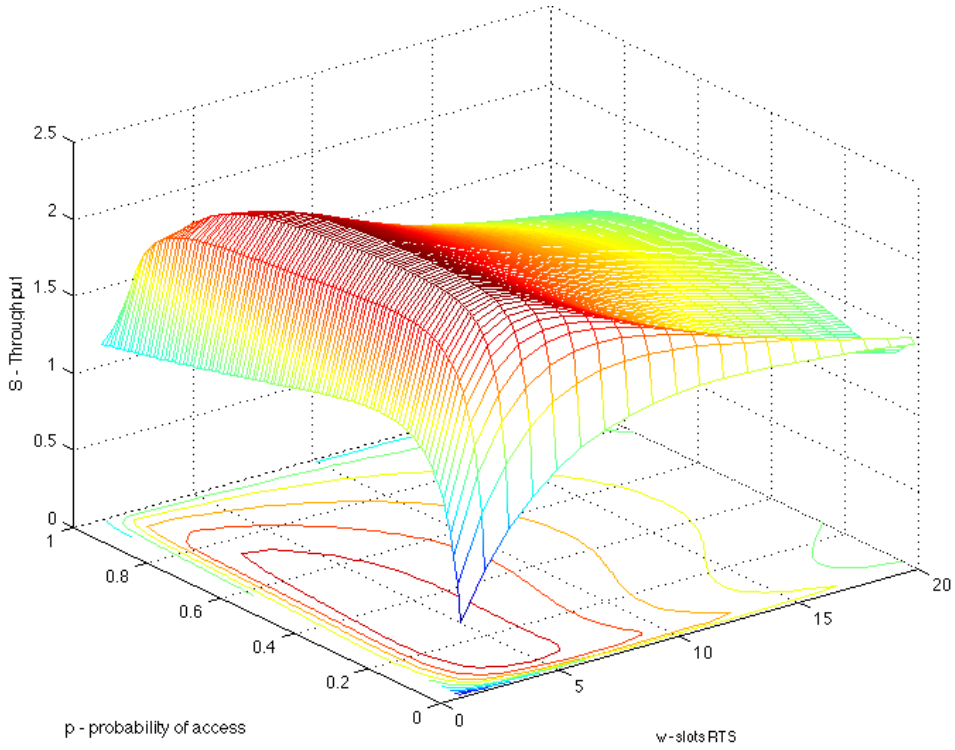


(a) $n = 65$.

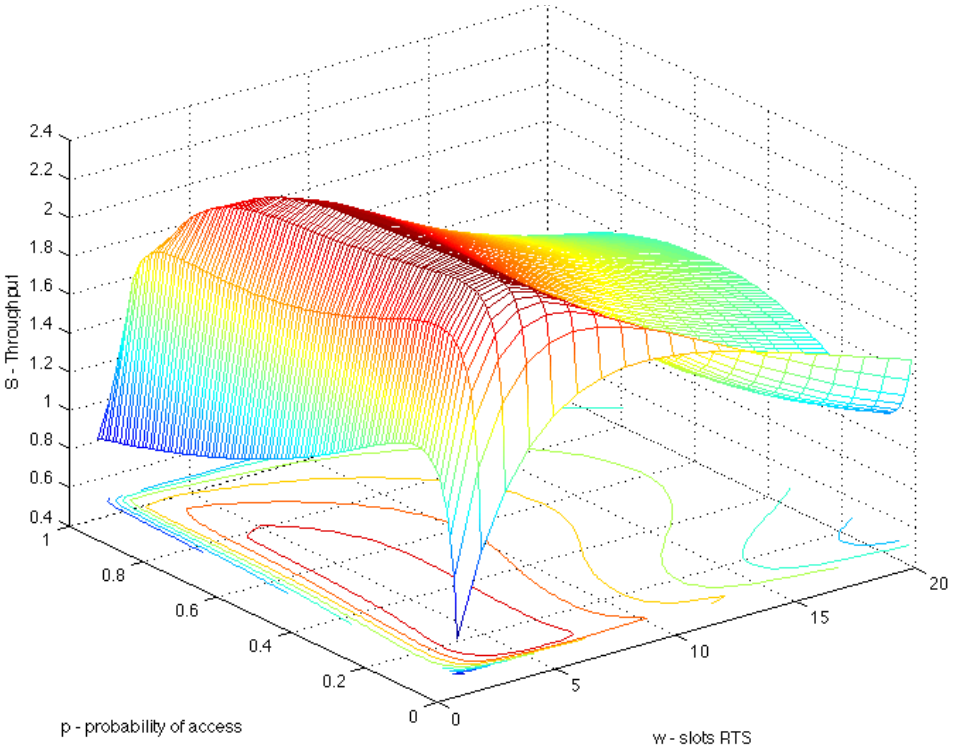


(b) $n = 125$.

Figure 5.9: Throughput achieved for multiple competing nodes for different values of $w$ and $p$ and $n$.

We can see that for $n = 65$, the highest throughput is achieved when the probability of access $p$ is close to 0.3 and the number of slots allocated to RTS transmissions is close to 4. As $n$ increases, the probability of access $p^*$ decreases and $w^*$ remains the same (see Figure 5.9 for $n = 125$). This means that $w^*$ guarantees the optimal trade-off between the time spent in the reservation stage and the number of nodes transmitting in the second stage of transmission. Moreover, the probability of access $p^*$ decreases as $n$ increases in order to maximize the performance of the MPR-based PHY layer during the reservation stage.

Table 5.5 contains the optimal values of $w^*$ and $p^*$ that maximize the throughput of system network $S^{mpr}$, as well as the average number of nodes successfully transmitting an RTS packet, $E_{rts}^{mpr}$, and successfully transmitting a Data packet $E_{data}^{mpr}$, for $b = 0.1$.

Table 5.5: MAC-MPRR protocol: optimal values of $w$ and $p$ for different number of nodes, as well as the optimal throughput, the average number of nodes successfully transmitting an RTS packet, $E_{rts}^{mpr}$, and successfully transmitting a Data packet $E_{data}^{mpr}$.

| | Number of nodes - $n$ | | | | | | | | | | | | |
|---|---|---|---|---|---|---|---|---|---|---|---|---|---|
| | 5 | 15 | 25 | 35 | 45 | 55 | 65 | 75 | 85 | 95 | 105 | 115 | 125 |
| $S^{mpr}$ | 1.49 | 2.09 | 2.25 | 2.31 | 2.34 | 2.36 | 2.37 | 2.37 | 2.37 | 2.38 | 2.38 | 2.38 | 2.38 |
| $w^*$ | 4 | 4 | 4 | 4 | 4 | 4 | 4 | 4 | 4 | 4 | 4 | 4 | 4 |
| $p^*$ | 0.53 | 0.42 | 0.38 | 0.35 | 0.32 | 0.29 | 0.27 | 0.25 | 0.22 | 0.20 | 0.18 | 0.16 | 0.15 |
| $E_{rts}^{mpr}$ | 3.5 | 7.0 | 9.0 | 10.2 | 11.0 | 11.5 | 11.8 | 12.0 | 12.1 | 12.2 | 12.3 | 12.3 | 12.3 |
| $E_{data}^{mpr}$ | 1.9 | 2.7 | 2.9 | 3.0 | 3.0 | 3.1 | 3.1 | 3.1 | 3.1 | 3.1 | 3.1 | 3.1 | 3.1 |

## 5.5 Optimal PHY/MAC Scheme

In this section we characterize the reservation stage and throughput achieved by the MAC-MMPRR scheme described in 5.2. Considering the MAC schemes with MPR-based PHY layer during the reservation stage, the rational to define the optimal probabilities of transmitting the RTS packet on each reservation slot $t$, $t \in \{1,..,w\}$, is based on the optimal number of transmissions ($r^*$) that maximize the number of received packets according to the features of the MPR PHY layer. Because the nodes only transmit at most in one slot of the reservation phase, the number of competing nodes decreases over the reservation phase. Consequently, to maintain the optimal number of transmissions equal to $r^*$ on each slot, the probabilities $p_t$ should increase over the $w$ slots. In the MAC-MPRR scheme studied in the previous section, we have considered a constant probability of transmitting the RTS packet during the $w$ slots of reservation. But in MAC-MMPRR a variable probability is adopted instead. Figure 5.10 illustrates the results of the MPR communication performance for each $t$-th slot of the $w$ RTS slots available in the MAC-MPRR scheme. In the figure, the number of RTS transmissions per slot decreases with $t$. Moreover, in the first and second slots the number of RTS transmissions is higher than the optimal number of transmissions ($r^*$) that maximize the MPR performance. Therefore, in this section we modify the design of the MAC scheme with MPR-based reservation by considering that the probability of transmitting an RTS

packet in the $t$-th slot, $p_t$, varies during the $w$ reservation slots in order to maximize the MPR performance for each slot. Furthermore, in this section we proposed an optimization method that jointly optimizes the PHY/MAC cross-layer performance.

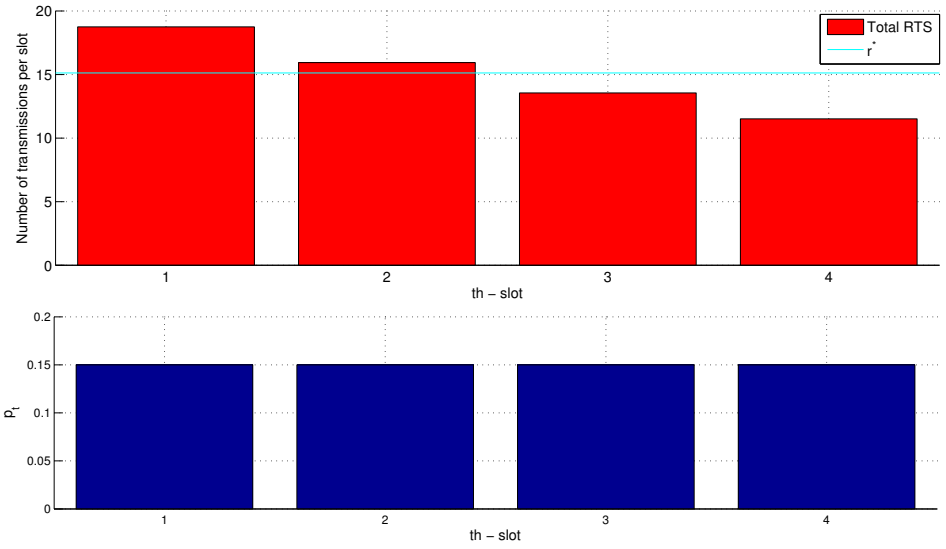


Figure 5.10: Average number of RTS packets transmitted in the $t$-th slot and the probability of access $p_t$ considering the design of the MAC-MPRR scheme and assuming the scenario from Subsection 5.4.4.2 with $n = 125$.

### 5.5.1 System Analysis

Again, $N \in \{0, 1, ..., n\}$ and $X \in \{1, 2, ..., w\}$ denote the RVs of the number of nodes transmitting an RTS packet in a reservation slot and the slot where the RTS is transmitted, respectively. The probability of a node transmitting an RTS packet in the slot $t$ is given by

$$P[X = t] = \begin{cases} p_1, & t = 1 \\ p_2(1 - p_1), & t = 2 \\ p_3(1 - p_1)(1 - p_2), & t = 3 \\ \vdots & \\ p_w(1 - p_1) \times ... \times (1 - p_{w-1}), & t = w \end{cases} \tag{5.18}$$

which can be simplified to

$$P[X = t] = \begin{cases} p_t \prod_{i=1}^{t-1}(1 - p_i), & 1 < t \leq w, \\ p_t, & t = 1 \end{cases}. \tag{5.19}$$

The probability of $N = n_t$ nodes transmitting an RTS in a slot $X = t$ is given by the Binomial

distribution

$$P[N = n_t, X = t] = \binom{n}{n_t} \cdot (P[X = t])^{n_t} \cdot \tag{5.20}$$

$$\cdot (1 - P[X = t])^{n - n_t}. \tag{5.21}$$

Denoting $m$ as the maximum number of nodes that may transmit an RTS packet in a slot, the expected number of nodes transmitting an RTS packet in the slot $t$ is given by

$$E_t(m) = \sum_{i=1}^{m} i \cdot P[N = i, X = t]. \tag{5.22}$$

But the number of RTS packets successfully received by the destination node depends on the MPR-based PHY layer, which is given as follows

$$E_{MPR} = h_{MPR}(E_t(m)). \tag{5.23}$$

Consequently, the average number of nodes successfully transmitting an RTS packet during the first stage of the transmission cycle, $E_{rts}^{mmpr}$, is given by

$$E_{rts}^{mmpr} = \sum_{k=1}^{w} h_{MPR}(E_t(n)), \tag{5.24}$$

where $n$ denotes the maximum number of nodes that may transmit an RTS packet in a given slot, which is equal to the total number of nodes competing in the reservation phase.

The average number of nodes that achieve success in the second stage of transmission depends again on the MPR PHY layer capability. Therefore, $E_{data}^{mmpr}$ is given as follows

$$E_{data}^{mmpr} = h_{MPR}\left(E_{rts}^{mmpr}\right). \tag{5.25}$$

By using (5.25), the throughput of the overall system network is finally given by

$$S^{mmpr} = \frac{h_{MPR}(E_{rts}^{mmpr}) T_{PKT}}{T_a + w}, \tag{5.26}$$

which represents the ratio between the average amount of time that the channel is successfully used by the nodes transmitting the MPR packets and the duration of the transmission cycle.

### 5.5.2 Optimization

In this subsection, we show how the probability of RTS transmission, $p_t$, and the number of slots of the reservation phase, $w$, can be parameterized to maximize the throughput of the MAC-MMPRR scheme.

#### 5.5.2.1 Throughput Optimization - optimal $p_t$

The rational to define the optimal probabilities of transmitting the RTS packet on each reservation slot $t$, $t \in \{1,..,w\}$, is based on the optimal number of transmissions ($r^*$) that maximize the number of received packets according to the features of the MPR-based PHY layer. Because the nodes transmit at most one RTS packet on each reservation phase, the number of competing nodes decreases over the reservation phase. Consequently, to maintain the optimal number of transmissions equal to $r^*$ on each slot, the probabilities $p_t$ are increased over the slots.

Therefore, assuming a wireless network with a large number of nodes ($n \geq wr^*$) and considering (5.19), the optimal condition to define $p_t$ is stated as follows

$$nP[X = t] = r^*, \tag{5.27}$$

where $n$ is the total number of nodes competing in the reservation phase. Replacing (5.19) in (5.27), $p_t$ is given by

$$p_t = \begin{cases} \dfrac{r^*}{n}, & t = 1 \\ \dfrac{r^*}{n - r^*}, & t = 2 \\ \dfrac{r^*}{n - 2r^*}, & t = 3 \\ \vdots & \\ \dfrac{r^*}{n - (w-1)r^*}, & t = w \end{cases} \tag{5.28}$$

which can be simplified to

$$p_t = \frac{r^*}{n - (t-1)r^*}, 1 \leq t \leq w. \tag{5.29}$$

From (5.29) we confirm that the probability $p_t$ increases with the slot index $t$.

Finally, we highlight that (5.29) is only valid as far as $n \geq wr^*$. Otherwise, the optimal number of transmissions per slot is lowered to $n/w$, to uniformly distribute the transmissions over the available slots. This fact is written as follows

$$p_t = \begin{cases} \dfrac{r^*}{n - (t-1)r^*}, & wr^* \leq n < \infty \\ \dfrac{n/w}{n - (t-1)n/w}, & 0 < n < wr^* \end{cases}. \tag{5.30}$$

#### 5.5.2.2 Throughput Optimization - optimal $w$

The MPR PHY layer performance reaches the optimal point of operation for $E_{r^*} = h_{MPR}(r^*)$. So during the reservation stage, the probability $p_t$ of a given slot $t$ should be parameterized in order to have an average number of RTS packets simultaneously transmitted equal to $r^*$. In this way, the maximum MPR-based PHY layer performance is obtained during the reservation stage. In each slot of the reservation stage, the average number of RTS packets successfully received is constant and equal to $E_{r^*}$. Consequently, the average number of nodes that will compete in the second stage is given by

$$E_{data}^{mmpr} = wE_{r^*}. \tag{5.31}$$

The throughput defined in (5.26) can be rewritten as

$$S^{mmpr} = \frac{h_{MPR}(wE_{r^*})T_{PKT}}{T_a + w}, \tag{5.32}$$

and replacing the rational function (5.5) in (5.32) we obtain

$$S^{mmpr} = \frac{T_{PKT}(p_0 + E_{r^*}p_1 w)}{(Ta + w)(q_0 + E_{r^*}q_1 w + E_{r^*}^2 q_2 w^2)}. \tag{5.33}$$

Departing from (5.33), the goal is now centered on determining the optimal number of slots $w$, denoted as $w^*$, that maximizes the system throughput. (5.33) represents a rational function and can be maximized by applying the Lagrange multipliers optimization process. The maximization of a rational function is equivalent to the following problem [JH02, Theorem 2.1.]

$$\sup \delta$$

subject to

$$N(S^{mmpr}(w)) - \delta D(S^{mmpr}(w)) \geqslant 0,$$

where $N(\cdot)$ and $D(\cdot)$ represent the numerator and denominator of the rational function in (5.33). The Lagrangian is given by,

$$\mathcal{L} = \delta - \lambda(N(S^{mmpr}(w)) - \delta D(S^{mmpr}(w))), \tag{5.34}$$

where $\lambda$ represents the Lagrange multiplier. Next, we set the gradient of $\mathcal{L}$ equal to the zero vector,

$$\nabla_{\delta,w,\lambda}\mathcal{L}(\delta, w, \lambda) = \left(\frac{\partial \mathcal{L}}{\partial \delta}, \frac{\partial \mathcal{L}}{\partial w}, \frac{\partial \mathcal{L}}{\partial \lambda}\right) = 0. \tag{5.35}$$

The solution for the maximization of $S^{mmpr}$ is found by solving the following system of equations

$$\nabla_{\delta,w,\lambda}\mathcal{L}(\delta, w, \lambda) = \begin{cases} \dfrac{\partial \mathcal{L}}{\partial \delta} = 0 \\ \dfrac{\partial \mathcal{L}}{\partial w} = 0 \Leftrightarrow \\ \dfrac{\partial \mathcal{L}}{\partial \lambda} = 0 \end{cases} \tag{5.36}$$

$$\Leftrightarrow \nabla_{\delta,w,\lambda}\mathcal{L}(\delta, w, \lambda) = \begin{cases} 1 - \lambda\,(T_a + w)A = 0 \\ \lambda\Big(E_{r^*}p_1 T_{PKT} - \delta\,(T_a + w)\Big(E_{r^*}q_1 + 2E_{r^*}^2 q_2 w\Big) - \delta A\Big) = 0 \\ T_{PKT}\,(p_0 + E_{r^*}p_1 w) - \delta\,(T_a + w)A = 0 \end{cases}$$

where

$$A = \Big(q_0 + E_{r^*}q_1 w + E_{r^*}^2 q_2 w^2\Big).$$

From (5.36), the optimal number of RTS slots, $w^*$, is computed. $w^*$ is the optimal trade-off between minimization of the time spent in the reservation stage (MAC coordination cost) and the maximization of number of the successful transmissions during the second stage of transmission.

### 5.5.3 Model Validation and Performance Analysis

This subsection describes a set of simulations and numerical results to validate and analyze the MAC-MMPRR scheme performance characterization and the optimization method proposed in Subsection 5.5.2.

As in Section 5.4, we considered a single-hop network where $n$ nodes adopt the proposed MAC scheme. The network scenario is formed by a receiver Rx circled by $n$ transmitters uniformly distributed in the area $\pi D^2$. Different fading ($\Psi_k$) and noise ($N_0$) realizations were used on each trial. The MAC scheme was implemented adopting the SINR capture condition to determine the number of successful MPR data packets transmitted on each transmission cycle. The simulations were parametrized according to the data presented in Table 5.6.

Table 5.6: Parameters adopted in the simulations regarding the evaluation of MAC-MMPRR.

| | | | |
|---|---|---|---|
| Slot duration | 20 $\mu s$ | $P_T$ | 20 dB |
| DIFS | 50 $\mu s$ | $\alpha$ | 2 |
| $D_{\text{RTS}}$ | 352 $\mu s$ | $D$ | 10 m |
| $D_{\text{CTS}}$ | 304 $\mu s$ | $\sigma_{N0}$ | 1 (0 dB) |
| $D_{\text{PKT}}$ | 8000 $\mu s$ | $\sigma_\xi$ | $\{0.2, 0.7, 1.2\}$ |
| $D_{\text{ACK}}$ | 304 $\mu s$ | Number of trials | $5 \times 10^5$ |

The performance results were characterized for two capture capture thresholds, $b = \{0.1, 0.04\}$ and for three fading uncertainty scenarios, $\sigma_\xi = \{0.2, 0.9, 1.2\}$. In each scenario, we approximate the performance of the MPR-based PHY layer by the respective rational function which is parametrized with the coefficients described in Tables 5.2 and 5.3.

Figure 5.11, Figure 5.12 and Figure 5.13 illustrate the average number of RTS and Data packets successfully decoded by the node Rx, and the throughput achieved for different values of $w$ (number RTS slots of the reservation stage), respectively. The curves "Simul." and "Teor." represent the simulated and the numerical results, respectively. The numerical results of the average number of nodes successfully transmitting an RTS packet during the first stage of the transmission cycle, $E_{rts}^{mmpr}$, were computed through (5.24). The numerical results of the average number of nodes successfully transmitting a Data packet in the second stage of the transmission cycle, $E_{data}^{mmpr}$, were computed through (5.25). Regarding the total number of transmitters Tx in the network, we consider $n = 300$ nodes. Consequently, the condition $wr^* \leq n$ is guaranteed for the scenarios considered (i.e., $\sigma_\xi = \{0.2, 0.9, 1.2\}$ and $b = \{0.1, 0.04\}$) and the optimization method proposed in 5.5.2.2 to find $w^*$ can be employed. The numerical results of the throughput were computed using (5.33).

In Figures 5.11, 5.12 and 5.13 , we observe that for different receiving thresholds ($b$) and different levels of uncertainty ($\sigma_\xi$), the numerical results are close to the values obtained through simulation, which successfully validates the proposed modeling approach.

As can be seen in Figure 5.13, for each scenario considered there is an optimal number of $w$

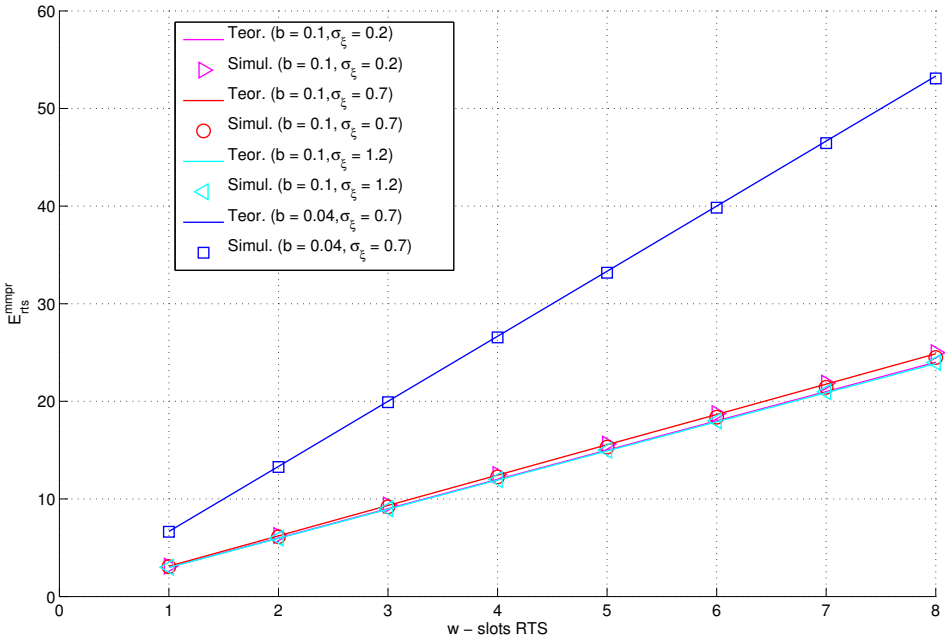


Figure 5.11: Average number of successful RTS packets decoded for multiple values of $w$, different levels of uncertainty ($\sigma_\xi$) and different capture thresholds $b$ ($n = 300$ nodes).

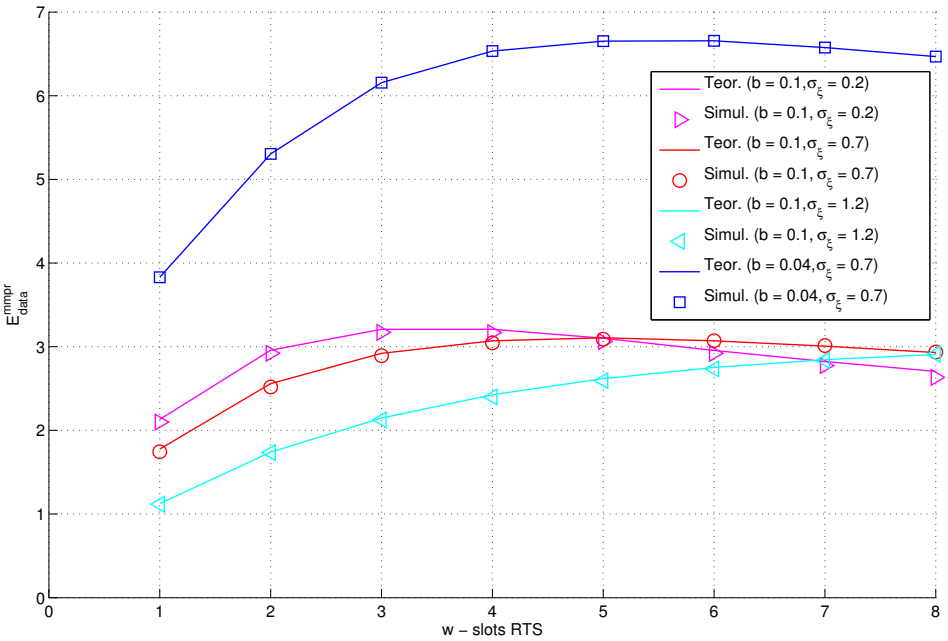


Figure 5.12: Average number of successful Data packets decoded for multiple sizes of $w$, different levels of uncertainty ($\sigma_\xi$) and different capture thresholds ($n = 300$ nodes).

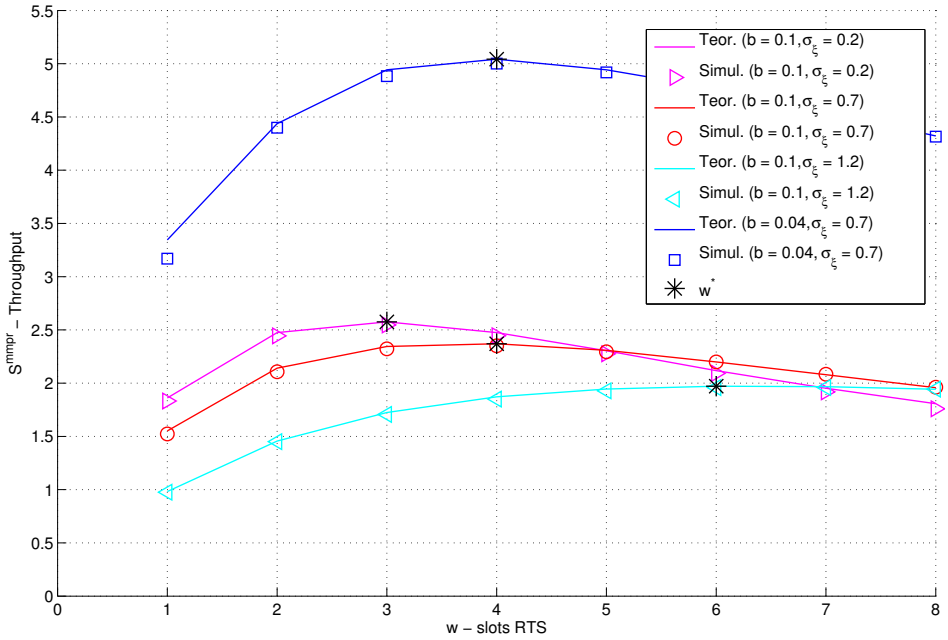


Figure 5.13: Throughput for multiple sizes of $w$, different levels of uncertainty ($\sigma_\xi$) and different capture thresholds ($n = 300$ nodes).

RTS slots that maximize the throughput achieved by the wireless network. Moreover, the throughput asymptotically converges to 0 as $w \to \infty$. The optimal number of slots, $w^*$ that maximizes the throughput $S^{mmpr}$ was determined by computing the Lagrange multipliers optimization method proposed in Subsection 5.5.2.2 and is represented in the figure by the markers "$w^*$". As can be seen, different levels of fading uncertainty require different parameterizations to achieve the optimal throughput. Note that the number of $w$ RTS slots that maximize system network throughput is lower than the $w$ that maximizes $E_{data}^{mmpr}$. For example, for $b = 0.1$ and $\sigma_\xi = 0.7$ the maximum $E_{data}^{mmpr}$ is reached for $w = 5$. However, the maximum throughput is reached for $w = 4$, which corresponds to the optimal trade-off between the time spent in the reservation stage and the number of nodes transmitting in the second stage of transmission.

Figure 5.14 represents the throughput achieved for different values of $n$ (total number of nodes attempting transmission). The numerical results were computed adopting the parameters described in Table 5.6. To evaluate the overall optimization scheme proposed in this section, we have numerically determined the optimal values of $w$ and $p_t$ that maximize (5.33). The curves "Teor MMPRR"represent the solutions found with the optimization process proposed in Subsection 5.5.2. The curves "Teor MPRR" represents the numerical results of the optimization of the MAC-MPRR scheme proposed in Section 5.4. The results plotted in Figure 5.14 show that the proposed PHY/MAC scheme can achieve higher throughput when optimized by the methodology proposed in Subsection 5.5.2. As $n$ increases the throughput increases until the average number of data transmitting nodes reaches $r^*$ (i.e.$Edata^{mmpr} = E_{r^*}$), which represents the maximum throughput achievable for the threshold $b$ and fading uncertainty $\sigma_\xi$.

Table 5.7 contains the optimal values of $w$ and $r$ that maximize the throughput of system

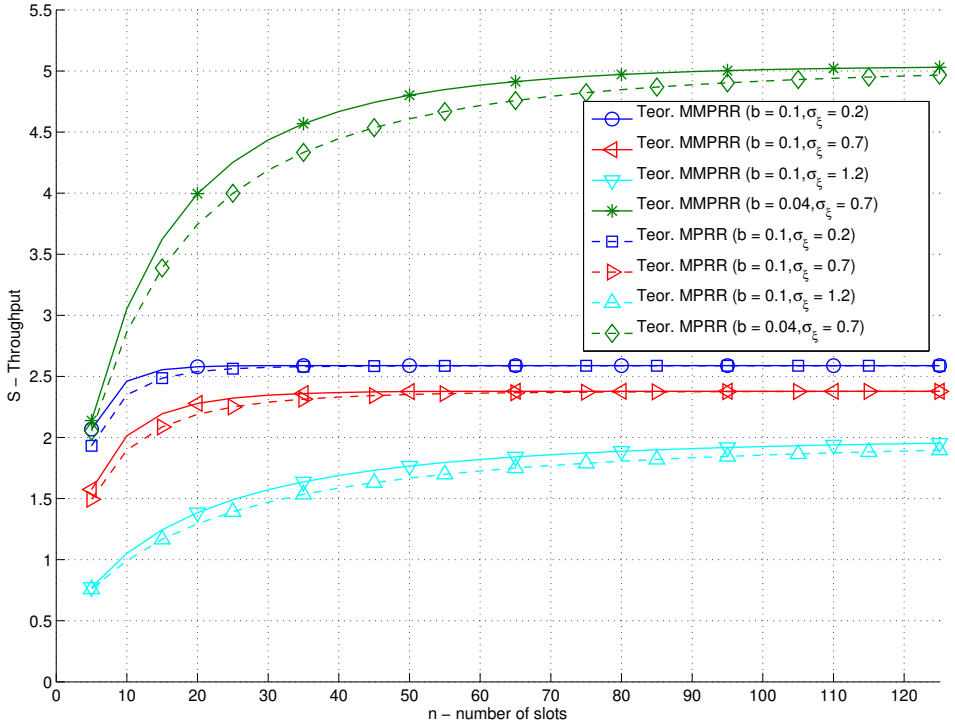


Figure 5.14: Throughput achieved for multiple competing nodes for different levels of uncertainty ($\sigma_\xi$) and different capture thresholds ($b$).

network $S^{mmpr}$, as well as the average number of nodes successfully transmitting an RTS packet, $E_{rts}^{mpr}$, and successfully transmitting a Data packet $E_{Data}^{mpr}$, when $b = 0.1$ and $\sigma_\xi = 0.7$.

Table 5.7: MAC-MMPRR protocol: optimal values of $w$ and $r^*$ for different number of nodes, $b = 0.1$ and $\sigma_\xi = 0.7$, as well as the optimal throughput, $E_{rts}^{mmpr}$ and $E_{Data}^{mmpr}$.

| | Number of nodes - $n$ | | | | | | | | | | | | |
|---|---|---|---|---|---|---|---|---|---|---|---|---|---|
| | 5 | 15 | 25 | 35 | 45 | 55 | 65 | 75 | 85 | 95 | 105 | 115 | 125 |
| $S^{mmpr}$ | 1.57 | 2.19 | 2.32 | 2.36 | 2.37 | 2.38 | 2.38 | 2.38 | 2.38 | 2.38 | 2.38 | 2.38 | 2.38 |
| $w^*$ | 4 | 4 | 4 | 4 | 4 | 4 | 4 | 4 | 4 | 4 | 4 | 4 | 4 |
| $r^*$ | 1.2 | 3.8 | 6.2 | 8.8 | 11.2 | 13.8 | 15.2 | 15.2 | 15.2 | 15.2 | 15.2 | 15.2 | 15.2 |
| $E_{rts}^{mmpr}$ | 3.8 | 8.1 | 10.4 | 11.6 | 12.2 | 12.4 | 12.4 | 12.4 | 12.4 | 12.4 | 12.4 | 12.4 | 12.4 |
| $E_{Data}^{mmpr}$ | 2.0 | 2.8 | 3.0 | 3.1 | 3.1 | 3.1 | 3.1 | 3.1 | 3.1 | 3.1 | 3.1 | 3.1 | 3.1 |

## 5.6 Final Remarks

In this chapter we have presented three different decentralized PHY/MAC cross-layer schemes to coordinate the medium access of multiple transmitters adopting an MPR-based PHY layer. The transmission cycle of three MAC schemes is divided into two stages: Reservation stage and Data Transmission stage. The Reservation stage of the transmission cycle accommodates an SPR-based

PHY layer in the MAC-SPRR scheme and an MPR-based PHY layer in the MAC-MPRR and MAC-MMPRR schemes. By adopting a generic model for the PHY layer, we formally characterized the throughput achieved by the proposed MAC-SPRR, MAC-MPRR and MAC-MMPRR schemes when both MAC and PHY layers are considered.

Regarding the PHY layer characterization, we approximate the expected number of successful receptions when $r$ simultaneous transmissions occur by a rational function through an interpolation process. The characterization of the PHY layer performance takes into account the path loss effect, small and large-scale fading propagation effects, the decision threshold adopted in the receiving MPR system and the influence of noise at the receiver side. Several results obtained through simulation were compared to assess the accuracy of the proposed rational function approximation.

For the MAC-MMPRR scheme, we proposed an optimal parameterization of the MAC parameters taking the joint PHY/MAC interaction into account. We show that the number of RTS slots used in the reservation stage and the access probability $p_t$ adopted on each slot may be set to achieve the maximum throughput. Different results show that the proposed PHY/MAC scheme can achieve higher throughput when optimized by the methodology proposed in Subsection 5.5.2. The results confirm that different uncertainty levels associated with the fading effects require specific MAC parameters to achieve throughput optimality. Finally, several results obtained through simulation were compared to assess the accuracy of the proposed modeling methodology, as well as the effectiveness of the proposed optimization scheme to maximize the throughput.

CHAPTER 6

# CONCLUSIONS AND FUTURE WORK

## 6.1 Conclusions

This thesis investigates the adoption of MPR techniques at the PHY layer of distributed wireless networks. In an initial stage we have investigated the adoption of MPR techniques at the PHY layer of distributed wireless networks. A generic MPR performance model was derived, which allows to determine optimal points of operation for different radio conditions. The model was derived for both near and far-field propagation scenarios and was validated for different scenarios, by comparing simulation results with numerical results obtained with the theoretical model. This stage was described in Chapter 3. We have considered an ILWN scenario where $n$ nodes transmit data simultaneously to a single receiver with MPR capabilities and the PHY layer performance was characterized by modeling the individual probability of successful packet reception and the average number of successful received packets when $n$ simultaneous transmissions occur. Two modeling approaches were considered. In the first one a far-field and a near-field scenario was considered. The individual probability of successful packet reception and the average number of successful received packets were modeled base on the CF of the individual received power of each transmitter and on the CF of the noise at the receiver side. Regarding the second modeling approach, a Gamma distribution approximation was proposed to characterize the aggregate interference generated by the transmitters located in the annulus $l$. The total aggregate interference power caused by transmitters that are located in multiple annulus was approximated by the product of Gamma Characteristic Functions (CFs). This approximation was then used to derive the probability of successful packet reception and the average number of successful received packets. In both approaches path loss effects and small and large-scale fading propagation effects were considered. Results showed that the aggregate power received from the transmitters located in a given annulus can be approximated by a Gamma distribution. Regarding the PHY layer performance characterization it was shown that the first modeling approach is accurately characterized by the numerical results. The results

of the second approach were less accurate when considering a small number of annuli.

The model proposed in Chapter 3 was used to study the performance of ILWNs in high density of transmitters and when the spectrum can be sensed a priori (i.e. before each transmission). Based on the theoretical analysis developed in the thesis, we show that depending on the propagation conditions the spectrum sensing can reduce the network throughput to a level where its use should be avoided. Chapter 4 describes the performance evaluation of an ILWN operating in shared channels. The transmitters adopt a EBS as the spectrum sensing technique. First the performance of the EBS was characterized by deriving the probabilities of detection and false alarm. Based on these probabilities we have proposed a decision threshold criterion and derived the conditional throughput achieved by the SUs. Next, considering that MPR is adopted, we have characterized the performance of the PHY layer by deriving the average number of packets successfully received. Results showed that the SFA can be almost neglected, but as path loss coefficient increases the conditional throughput achieved by the SUs decreases due to the huge number of samples required to meet the level of PUs' protection. Also, we showed that the average number of packets successfully received decrease with the increase of the path loss coefficient and the performance of the MPR-based PHY layer is better when spectrum sensing is used.

At the final stage, we proposed a cross-layered architecture that improves the capacity of an ILWN. Different MAC schemes for ILWNs adopting MPR communications were proposed and their performance was theoretically characterized and validated through simulation. The cross-layer optimization methodology considers the features of the MPR communication scheme together with the MAC performance. The proposed methodology improves the throughput of ILWNs and is described in Chapter 5. Three different decentralized PHY/MAC cross-layer schemes to coordinate the medium access of multiple transmitters adopting an MPR-based PHY layer were proposed: MAC-SPRR, MAC-MPRR and MAC-MMPRR. From the results regarding the MAC-SPRR and the MAC-MPRR schemes, it was possible to observe that the optimal reservation length strongly depends on the maximum performance of the PHY layer adopted in the data transmission. Moreover, in MAC schemes that uses MPR-based PHY layer in the reservation, the access policy should be continuously adapted in order to maximize the performance of the PHY layer. Based on these conclusions, we have proposed the MAC-MMPRR scheme. Taking into account the joint PHY/MAC interaction, we proposed an optimal parameterization of the reservation duration and the probability of access per slot. Different results show that the proposed PHY/MAC scheme can achieve higher throughput when optimized by the proposed optimization methodology. The results showed that different uncertainty levels associated with the fading effects require specific MAC parameters to achieve throughput optimality.

## 6.2 Future Work

This thesis represents a starting point in the research of decentralized PHY/MAC cross-layer schemes. Future research directions may include the study of different MAC protocols that may better accommodate the specifics of MPR communication systems. A more practical direction may also include the estimation of the MPR model parameters, in order to have a realistic approximation

of the performance achieved by the PHY layer in real-time. The estimation can also be useful to optimize the performance of both layers in real-time, depending on the radio propagation conditions and the properties of the MAC protocol.

# BIBLIOGRAPHY


[AK99] A. Abdi and M. Kaveh. "On the utility of gamma PDF in modeling shadow fading (slow fading)". In: *IEEE 49th Vehicular Technology Conference*. Vol. 3. 1999. ISBN: 0-7803-5565-2. DOI: 10.1109/vetec.1999.778479.

[Abd+01] A. Abdi, H. Barger, and M. Kaveh. "A simple alternative to the lognormal model of shadow fading in terrestrial and satellite channels". In: *IEEE IEEE 54th Vehicular Technology Conference. VTC Fall 2001.* Vol. 4. 2001. ISBN: 0-7803-7005-8. DOI: 10.1109/vtc.2001.957106.

[AS65] M. Abramowitz and I. Stegun. In: *Handbook of Mathematical Functions with Formulas, Graphs, and Mathematical Tables, New York: Dover* (1965).

[Abr70] N. Abramson. "THE ALOHA SYSTEM: Another Alternative for Computer Communications". In: *Proceedings of the November 17-19, 1970, Fall Joint Computer Conference*. AFIPS '70 (Fall). Houston, Texas, 1970, pp. 281–285. DOI: 10.1145/1478462.1478502.

[AAY10] S. Al-Ahmadi and H. Yanikomeroglu. "On the approximation of the generalized-K distribution by a gamma distribution for modeling composite fading channels". In: *IEEE Transactions on Wireless Communications* 9.2 (Feb. 2010), pp. 706–713. ISSN: 1536-1276. DOI: 10.1109/TWC.2010.02.081266.

[AH+10] A. Al-Habashna, O. Dobre, R. Venkatesan, and D. Popescu. "Cyclostationarity-Based Detection of LTE OFDM Signals for Cognitive Radio Systems". In: *Proceedings IEEE GLOBECOM 2010.* Dec. 2010, pp. 1–6.

[AY10a] M. Aljuaid and H. Yanikomeroglu. "Investigating the Gaussian Convergence of the Distribution of the Aggregate Interference Power in Large Wireless Networks". In: *IEEE Transactions on Vehicular Technology* 59.9 (Nov. 2010), pp. 4418–4424. ISSN: 0018-9545. DOI: 10.1109/TVT.2010.2067452.

[AY10b] M. Aljuaid and H. Yanikomeroglu. "Investigating the validity of the Gaussian approximation for the distribution of the aggregate interference power in large wireless networks". In: *25th Biennial Symposium on Communications (QBSC).* May 2010, pp. 122–125. DOI: 10.1109/BSC.2010.5472989.

[AV17] I. Arun and T. Venkatesh. "Design and performance analysis of a MAC protocol for wireless LANs supporting multipacket reception". In: *Journal of Network and Computer Applications* 87 (2017), pp. 223–236. ISSN: 1084-8045. DOI: 10.1016/j.jnca.2017.03.010.

[BC10] F. Babich and M. Comisso. "Theoretical analysis of asynchronous multi-packet reception in 802.11 networks". In: *IEEE Transactions on Communications* 58.6 (June 2010), pp. 1782–1794. ISSN: 0090-6778. DOI: 10.1109/TCOMM.2010.06.090186.

[BC13] F. Babich and M. Comisso. "Multi-Packet Communication in Heterogeneous Wireless Networks Adopting Spatial Reuse:Capture Analysis". In: *IEEE Transactions on Wireless Communications* 12.10 (Oct. 2013), pp. 5346–5359. ISSN: 1536-1276. DOI: 10.1109/TWC.2013.091113.130788.

[BC14] F. Babich and M. Comisso. "Capture analysis of mobile multi-packet networks adopting spatial reuse: An alternative study". In: *Global Communications Conference (GLOBECOM), 2014 IEEE*. Dec. 2014, pp. 3477–3482. DOI: 10.1109/GLOCOM.2014.7037346.

[BB09] F. Baccelli and B. Błaszczyszyn. "Stochastic Geometry and Wireless Networks: Volume II Applications". In: *Foundations and Trends® in Networking* 4.1–2 (2009), pp. 1–312. ISSN: 1554-057X. DOI: 10.1561/1300000026.

[Bel16] B. Bellalta. "IEEE 802.11ax: High-efficiency WLANS". In: *IEEE Wireless Communications* 23.1 (Feb. 2016), pp. 38–46. ISSN: 1536-1284. DOI: 10.1109/MWC.2016.7422404.

[Bet+03] C. Bettstetter, G. Resta, and P. Santi. "The node distribution of the random waypoint mobility model for wireless ad hoc networks". In: *IEEE Transactions on Mobile Computing* 2.3 (July 2003), pp. 257–269. ISSN: 1536-1233. DOI: 10.1109/TMC.2003.1233531.

[BM10] D. Bhargavi and C. Murthy. "Performance comparison of energy, matched-filter and cyclostationarity-based spectrum sensing". In: *Proceedings IEEE SPAWC 2010*. June 2010, pp. 1–5.

[Bou+08] A. Bouzegzi, P. Ciblat, and P. Jallon. "Matched Filter Based Algorithm for Blind Recognition of OFDM Systems". In: *Proceedings IEEE VTC 2008-Fall*. Sept. 2008, pp. 1–5.

[BS04] K. O. Bowman and L. R. Shenton. "Estimation: Method of Moments". In: *Encyclopedia of Statistical Sciences*. John Wiley & Sons, Inc., 2004. ISBN: 9780471667193. DOI: 10.1002/0471667196.ess1618.pub2.

[Bue+96] R. Buehrer, N. Correal, and B. Woerner. "A comparison of multiuser receivers for cellular CDMA". In: *Global Telecommunications Conference, 1996. GLOBECOM '96. 'Communications: The Key to Global Prosperity*. Vol. 3. Nov. 1996, 1571–1577 vol.3. DOI: 10.1109/GLOCOM.1996.591904.

[Cel+10] G. D. Celik, G. Zussman, W. F. Khan, and E. Modiano. "MAC for Networks with Multipacket Reception Capability and Spatially Distributed Nodes". In: *IEEE Transactions on Mobile Computing* 9.2 (Feb. 2010), pp. 226–240. ISSN: 1536-1233. DOI: 10.1109/TMC.2009.135.

[Cel+08] G. Celik, G. Zussman, W. Khan, and E. Modiano. "MAC for Networks with Multipacket Reception Capability and Spatially Distributed Nodes". In: *INFOCOM 2008, IEEE 27th Conference on Computer Communications*. Apr. 2008, pp. 2110–2118. DOI: 10.1109/INFOCOM.2008.202.

[CH01] C. C. Chan and S. Hanly. "Calculating the outage probability in a CDMA network with spatial Poisson traffic". In: *IEEE Transactions on Vehicular Technology* 50.1 (Jan. 2001), pp. 183–204. ISSN: 0018-9545. DOI: 10.1109/25.917918.

[Cha+13] D. Chan, T. Berger, and L. Tong. "Carrier Sense Multiple Access Communications on Multipacket Reception Channels: Theory and Applications to IEEE 802.11 Wireless Networks". In: *IEEE Transactions on Communications* 61.1 (Jan. 2013), pp. 266–278. ISSN: 0090-6778. DOI: 10.1109/TCOMM.2012.120512.110285.

[CB02] J. Cheng and N. Beaulieu. "Accurate DS-CDMA bit-error probability calculation in Rayleigh fading". In: *IEEE Transactions on Wireless Communications* 1.1 (Jan. 2002), pp. 3–15. ISSN: 1536-1276. DOI: 10.1109/7693.975440.

[Chi97] M. Chiani. "Analytical distribution of linearly modulated cochannel interferers". In: *IEEE Transactions on Communications* 45.1 (Jan. 1997), pp. 73–79. ISSN: 0090-6778. DOI: 10.1109/26.554288.

[Cou+04] M. Coupechoux, T. Lestable, C. Bonnet, and V. Kumar. "Throughput of the Multi-hop Slotted Aloha with Multi-packet Reception". English. In: Lecture Notes in Computer Science 2928 (2004). Ed. by R. Battiti, M. Conti, and R. Cigno, pp. 301–314. DOI: 10.1007/978-3-540-24614-5_22.

[Dig+07] F. Digham, M.-S. Alouini, and M. K. Simon. "On the Energy Detection of Unknown Signals Over Fading Channels". In: *IEEE Transactions on Communications* 55.1 (Jan. 2007), pp. 21–24. ISSN: 0090-6778. DOI: 10.1109/TCOMM.2006.887483.

[DN00] Z. Ding and T. Nguyen. "Stationary points of a kurtosis maximization algorithm for blind signal separation and antenna beamforming". In: *IEEE Transactions on Signal Processing* 48.6 (June 2000), pp. 1587–1596. ISSN: 1053-587X. DOI: 10.1109/78.845917.

[Din+04] R. Dinis, C. Lam, and D. Falconer. "On the impact of phase noise and frequency offsets in block transmission CDMA schemes". In: *1st International Symposium on Wireless Communication Systems*. Sept. 2004, pp. 95–99. DOI: 10.1109/ISWCS.2004.1407216.

[Din+09] R. Dinis, P. Montezuma, L. Bernardo, R. Oliveira, M. Pereira, and P. Pinto. "Frequency-domain multipacket detection: a high throughput technique for SC-FDE systems". In: *IEEE Transactions on Wireless Communications* 8.7 (July 2009), pp. 3798–3807. ISSN: 1536-1276. DOI: 10.1109/TWC.2009.081275.

[Biba] "Draft IEEE Standard for Local and Metropolitan Area Networks part 16: Air Interface for Fixed and Mobile Broadband Wireless Access Systems - Management Plane Procedures and Services". In: *IEEE Std P802.16g/D6, Nov 2006* (Nov. 2006).

[Dua+14] M. Duarte, A. Furtado, M. Luis, L. Bernardo, R. Dinis, and R. Oliveira. "Practical Assessment of Energy-Based Sensing through Software Defined Radio Devices". In: *Technological Innovation for Collective Awareness Systems*. Ed. by L. M. Camarinha-Matos, N. S. Barrento, and R. Mendonça. Berlin, Heidelberg: Springer Berlin Heidelberg, 2014, pp. 525–532. ISBN: 978-3-642-54734-8.

[EE99] J. Evans and D. Everitt. "On the teletraffic capacity of CDMA cellular networks". In: *IEEE Transactions on Vehicular Technology* 48.1 (Jan. 1999), pp. 153–165. ISSN: 0018-9545. DOI: 10.1109/25.740079.

[Fur+14a] A. Furtado, L. Irio, R. Oliveira, L. Bernardo, and R. Dinis. "Characterization of the Spatial False Alarm effect in Cognitive Radio Networks". In: *23rd International Conference on Computer Communication and Networks (ICCCN)*. Aug. 2014, pp. 1–8. DOI: 10.1109/ICCCN.2014.6911742.

[Fur+14b] A. Furtado, M. Luís, L. Irio, R. Oliveira, L. Bernardo, and R. Dinis. "Detection of licensed users' activity in a random access ultra wideband cognitive system". In: *IEEE International Conference on Ultra-WideBand (ICUWB)*. Sept. 2014, pp. 91–95. DOI: 10.1109/ICUWB.2014.6958957.

[Fur+16a] A. Furtado, R. Oliveira, R. Dinis, and L. Bernardo. "A distributed MAC protocol for multi-packet reception wireless networks". In: *IEEE 27th Annual International Symposium on Personal, Indoor, and Mobile Radio Communications (PIMRC)*. Sept. 2016, pp. 1–6. DOI: 10.1109/PIMRC.2016.7794791.

[Fur+16b] A. Furtado, L. Irio, R. Oliveira, L. Bernardo, and R. Dinis. "Spectrum Sensing Performance in Cognitive Radio Networks With Multiple Primary Users". In: *IEEE Transactions on Vehicular Technology* 65.3 (Mar. 2016), pp. 1564–1574. ISSN: 0018-9545. DOI: 10.1109/TVT.2015.2406254.

[Fur+16c] A. Furtado, R. Oliveira, R. Dinis, and L. Bernardo. "Successful Packet Reception Analysis in Multi-Packet Reception Wireless Systems". In: *IEEE Communications Letters* 20.12 (Dec. 2016), pp. 2498–2501. ISSN: 1089-7798. DOI: 10.1109/LCOMM.2016.2606105.

[Fur+17a] A. Furtado, D. Vicente, R. Oliveira, L. Bernardo, and R. Dinis. "Performance analysis of a distributed MAC scheme for Multi-Packet Reception wireless networks". In: *2017 13th International Wireless Communications and Mobile Computing Conference (IWCMC)*. June 2017, pp. 1706–1711. DOI: 10.1109/IWCMC.2017.7986541.

[Fur+17b] A. Furtado, D. Vicente, R. Oliveira, L. Bernardo, and R. Dinis. "Performance analysis of Multi-Packet Reception wireless systems in far-field region". In: *2017 13th International Wireless Communications and Mobile Computing Conference (IWCMC)*. June 2017, pp. 2045–2049. DOI: 10.1109/IWCMC.2017.7986598.

[Fur+18a] A. Furtado, R. Oliveira, L. Bernardo, and R. Dinis. "Decentralized PHY/MAC Design for the Uplink of Multi-Packet Reception Wireless Networks". In: *2018 14th International Wireless Communications and Mobile Computing Conference (IWCMC)*. June 2018, pp. 1–6.

[Fur+18b] A. Furtado, R. Oliveira, L. Bernardo, and R. Dinis. "Optimal Cross-Layer Design for Decentralized Multi-Packet Reception Wireless Networks". In: *2018 IEEE 87th Vehicular Technology Conference (VTC Spring)*. June 2018, pp. 1–5.

[Fur+13] A. Furtado, M. Luís, R. Oliveira, R. Dinis, and L. Bernardo. "Channel Availability Assessment for Cognitive Radios". In: *Technological Innovation for the Internet of Things*. Ed. by L. M. Camarinha-Matos, S. Tomic, and P. Graça. Berlin, Heidelberg: Springer Berlin Heidelberg, 2013, pp. 495–504. ISBN: 978-3-642-37291-9.

[Gan+12] F. Ganhao, R. Dinis, L. Bernardo, and R. Oliveira. "Analytical BER and PER Performance of Frequency-Domain Diversity Combining, Multipacket Detection and Hybrid Schemes". In: *IEEE Transactions on Communications* 60.8 (Aug. 2012), pp. 2353–2362. ISSN: 0090-6778. DOI: 10.1109/TCOMM.2012.061212.110440.

[GH08] R. Ganti and M. Haenggi. "Interference in ad hoc networks with general motion-invariant node distributions". In: *IEEE International Symposium on Information Theory*. July 2008, pp. 1–5. DOI: 10.1109/ISIT.2008.4594936.

[GLA+07a] J. J. Garcia-Luna-Aceves, H. R. Sadjadpour, and Z. Wang. "Challenges: Towards Truly Scalable Ad Hoc Networks". In: *Proceedings of the 13th Annual ACM International Conference on Mobile Computing and Networking*. MobiCom '07. Montreal,Canada: ACM, 2007, pp. 207–214. ISBN: 978-1-59593-681-3. DOI: 10.1145/1287853.1287878.

[GLA+07b] J. J. Garcia-Luna-Aceves, H. R. Sadjadpour, and Z. Wang. "Extending the Capacity of Ad Hoc Networks Beyond Network Coding". In: *Proceedings of the 2007 International Conference on Wireless Communications and Mobile Computing*. IWCMC '07. Honolulu, Hawaii, USA: ACM, 2007, pp. 91–96. ISBN: 978-1-59593-695-0. DOI: 10.1145/1280940.1280960.

[GPP] 3rd Generation Partnership Project. *Technical Specification Group Radio Access Network; Evolved Universal Terrestrial Radio Access (E-UTRA); Physical Channels and Modulation (Release 9)*. Tech. rep.

[GS07] A. Ghasemi and E. Sousa. "Optimization of Spectrum Sensing for Opportunistic Spectrum Access in Cognitive Radio Networks". In: *Consumer Communications and Networking Conference, 2007. CCNC 2007. 4th IEEE*. Jan. 2007, pp. 1022–1026. DOI: 10.1109/CCNC.2007.206.

[Ghe+88] S. Ghez, S. Verdú, and S. Schwartz. "Stability properties of slotted Aloha with multipacket reception capability". In: *IEEE Transactions on Automatic Control* 33.7 (July 1988), pp. 640–649. ISSN: 0018-9286. DOI: 10.1109/9.1272.

[Ghe+89] S. Ghez, S. Verdú, and S. Schwartz. "Optimal decentralized control in the random access multipacket channel". In: *IEEE Transactions on Automatic Control* 34.11 (Nov. 1989), pp. 1153–1163. ISSN: 0018-9286. DOI: 10.1109/9.40760.

[Gol05] A. Goldsmith. *Wireless communications*. Cambridge university press, 2005.

[GH14] Z. Gong and M. Haenggi. "Interference and Outage in Mobile Random Networks: Expectation, Distribution, and Correlation". In: *IEEE Transactions on Mobile Computing* 13.2 (Feb. 2014), pp. 337–349. ISSN: 1536-1233. DOI: 10.1109/TMC.2012.253.

[Gub06] J. A. Gubner. *Probability and Random Processes for Electrical and Computer Engineers*. New York, NY, USA: Cambridge University Press, 2006. ISBN: 0521864704.

[Gul+12] K. Gulati, R. Ganti, J. Andrews, B. Evans, and S. Srikanteswara. "Characterizing Decentralized Wireless Networks with Temporal Correlation in the Low Outage Regime". In: *IEEE Transactions on Wireless Communications* 11.9 (Sept. 2012), pp. 3112–3125. ISSN: 1536-1276. DOI: 10.1109/TWC.2012.072512.111003.

[Guo+09] M.-F. Guo, X. Wang, and M.-Y. Wu. "On the capacity of $\kappa$-MPR wireless networks". In: *IEEE Transactions on Wireless Communications* 8.7 (July 2009), pp. 3878–3886. ISSN: 1536-1276. DOI: 10.1109/TWC.2009.090265.

[GK00] P. Gupta and P. Kumar. "The capacity of wireless networks". In: *IEEE Transactions on Information Theory* 46.2 (Mar. 2000), pp. 388–404. ISSN: 0018-9448. DOI: 10.1109/18.825799.

[GK03] P. Gupta and P. Kumar. "Towards an information theory of large networks: an achievable rate region". In: *IEEE Transactions on Information Theory* 49.8 (Aug. 2003), pp. 1877–1894. ISSN: 0018-9448. DOI: 10.1109/TIT.2003.814480.

[HG08] M. Haenggi and R. K. Ganti. "Interference in Large Wireless Networks". In: *Foundations and Trends®in Networking* 3.2 (2008), pp. 127–248. ISSN: 1554-057X. DOI: 10.1561/1300000015.

[Haj+97] B. Hajek, A. Krishna, and R. O. LaMaire. "On the capture probability for a large number of stations". In: *IEEE Transactions on Communications* 45.2 (Feb. 1997), pp. 254–260. ISSN: 0090-6778. DOI: 10.1109/26.554374.

[Han+11] W. Han, J. Li, Q. Liu, and L. Zhao. "Spatial False Alarms in Cognitive Radio". In: *Communications Letters, IEEE* 15.5 (2011), pp. 518–520. ISSN: 1089-7798. DOI: 10.1109/LCOMM.2011.031411.102473.

[Han+13] W. Han, J. Li, Z. Li, J. Si, and Y. Zhang. "Spatial False Alarm in Cognitive Radio Network". In: *IEEE Transactions on Signal Processing* 61.6 (2013), pp. 1375–1388. ISSN: 1053-587X. DOI: 10.1109/TSP.2012.2236833.

[HA07] A. Hasan and J. Andrews. "The Guard Zone in Wireless Ad hoc Networks". In: *IEEE Transactions on Wireless Communications* 6.3 (Mar. 2007), pp. 897–906. ISSN: 1536-1276. DOI: 10.1109/TWC.2007.04793.

[Hay05] S. Haykin. "Cognitive radio: brain-empowered wireless communications". In: *IEEE Journal on Selected Areas in Communications* 23.2 (Feb. 2005), pp. 201–220. ISSN: 0733-8716. DOI: 10.1109/JSAC.2004.839380.

[Hea+13] R. W. Heath, M. Kountouris, and T. Bai. "Modeling Heterogeneous Network Interference Using Poisson Point Processes". In: *IEEE Transactions on Signal Processing* 61.16 (Aug. 2013), pp. 4114–4126. ISSN: 1053-587X. DOI: 10.1109/TSP.2013.2262679.

[Her+11] S. Herath, N. Rajatheva, and C. Tellambura. "Energy Detection of Unknown Signals in Fading and Diversity Reception". In: *IEEE Transactions on Communications* 59.9 (Sept. 2011), pp. 2443–2453. ISSN: 0090-6778. DOI: 10.1109/TCOMM.2011.071111.090349.

[HB03] B. Hu and N. Beaulieu. "Exact bit error rate analysis of TH-PPM UWB systems in the presence of multiple-access interference". In: *Communications Letters, IEEE* 7.12 (Dec. 2003), pp. 572–574. ISSN: 1089-7798. DOI: 10.1109/LCOMM.2003.821332.

[HB04] B. Hu and N. Beaulieu. "Accurate evaluation of multiple-access performance in TH-PPM and TH-BPSK UWB systems". In: *IEEE Transactions on Communications* 52.10 (Oct. 2004), pp. 1758–1766. ISSN: 0090-6778. DOI: 10.1109/TCOMM.2004.836424.

[Hua+08] W. L. Huang, K. Letaief, and Y. J. Zhang. "Cross-Layer Multi-Packet Reception Based Medium Access Control and Resource Allocation for Space-Time Coded MIMO/OFDM". In: *IEEE Transactions on Wireless Communications* 7.9 (Sept. 2008), pp. 3372–3384. ISSN: 1536-1276. DOI: 10.1109/TWC.2008.060327.

[Bibb] "IEEE Draft Amendment Standard for Local and Metropolitan Area Networks - Part 16: Air Interface for Broadband Wireless Access Systems - Advanced Air Interface". In: *IEEE P802.16m/D11, January 2011* (Jan. 2011), pp. 1–1120.

[Bibc] "IEEE Draft Standard for Information Technology-Telecommunications and information exchange between systems-Local and metropolitan area networks-Specific requirements-Part 11: Wireless LAN MAC and PHY specifications- Amendment 10: Mesh Networking". In: *IEEE P802.11s/D7.0, July 2010* (Oct. 2010), pp. 1–339.

[Bibd] "IEEE Standard for Information technology– Telecommunications and information exchange between systems Local and metropolitan area networks– Specific requirements–Part 11: Wireless LAN Medium Access Control (MAC) and Physical Layer (PHY) Specifications–Amendment 4: Enhancements for Very High Throughput for Operation in Bands below 6 GHz." In: *IEEE Std 802.11ac-2013* (Dec. 2013), pp. 1–425. DOI: 10.1109/IEEESTD.2013.6687187.

[Ina+12] H. Inaltekin, M. Chiang, H. Poor, and S. Wicker. "Selfish Random Access over Wireless Channels with Multipacket Reception". In: *IEEE Journal on Selected Areas in Communications* 30.1 (Jan. 2012), pp. 138–152. ISSN: 0733-8716. DOI: 10.1109/JSAC.2012.120113.

[Iri+15] L. Irio, A. Furtado, R. Oliveira, L. Bernardo, and R. Dinis. "Path Loss Interference in Mobile Random Waypoint Networks". In: *Proceedings of European Wireless 2015; 21th European Wireless Conference*. May 2015, pp. 1–5.

[Jef+07] A. Jeffrey, D. Zwillinger, I. S. Gradshteyn, and I. M. Ryzhik, eds. *Table of Integrals, Series, and Products (Seventh Edition)*. Seventh Edition. Boston: Academic Press, 2007. ISBN: 978-0-12-373637-6. DOI: 10.1016/B978-0-08-047111-2.50001-7.

[Jia+10] T. Jiang, H.-H. Chen, H.-C. Wu, and Y. Yi. "Channel Modeling and Inter-Carrier Interference Analysis for V2V Communication Systems in Frequency-Dispersive Channels". In: *Mob. Netw. Appl.* 15.1 (Feb. 2010), pp. 4–12. ISSN: 1383-469X. DOI: 10.1007/s11036-009-0177-2.

[JH02] D. Jibetean and B. Hanzon. "Linear Matrix Inequalities for Global Optimization of Rational Functions and H_2 Optimal Model Reduction". In: *Proceedings of the 15th International Symposium on MTNS*. 2002.

[Joh+94] N. L. Johnson, S. Kotz, and N. Balakrishnan. *Continuous Univariate Distributions*. 2nd. Vol. 1. Wiley, 1994.

[JL11] D. Jung and H. Lim. "Opportunistic MAC Protocol for Coordinating Simultaneous Transmissions in Multi-User MIMO Based WLANs". In: *Communications Letters, IEEE* 15.8 (Aug. 2011), pp. 902–904. ISSN: 1089-7798. DOI: 10.1109/LCOMM.2011.061311.110880.

[Jun+12] D. Jung, R. Kim, and H. Lim. "Asynchronous Medium Access Protocol for Multi-User MIMO Based Uplink WLANs". In: *IEEE Transactions on Communications* 60.12 (Dec. 2012), pp. 3745–3754. ISSN: 0090-6778. DOI: 10.1109/TCOMM.2012.090512.110300.

[Kar+08] S. Karande, Z. Wang, H. Sadjadpour, and J. Garcia-Luna-Aceves. "Capacity of wireless ad-hoc networks under multipacket transmission and reception". In: *42nd Asilomar Conference on Signals, Systems and Computers*. Oct. 2008, pp. 2115–2119. DOI: 10.1109/ACSSC.2008.5074807.

[KL75] L. Kleinrock and S. Lam. "Packet Switching in a Multiaccess Broadcast Channel: Performance Evaluation". In: *IEEE Transactions on Communications* 23.4 (Apr. 1975), pp. 410–423. ISSN: 0090-6778. DOI: 10.1109/TCOM.1975.1092814.

[KT75] L. Kleinrock and F. Tobagi. "Packet Switching in Radio Channels: Part I - Carrier Sense Multiple-Access Modes and Their Throughput-Delay Characteristics". In: *IEEE Transactions on Communications* 23.12 (Dec. 1975), pp. 1400–1416. ISSN: 0090-6778. DOI: 10.1109/TCOM.1975.1092768.

[Kos02] V. Kostylev. "Energy detection of a signal with random amplitude". In: *IEEE International Conference on Communications (ICC)*. Vol. 3. May 2002, 1606–1610 vol.3. DOI: 10.1109/ICC.2002.997120.

[KR02] J. F. Kurose and K. Ross. *Computer Networking: A Top-Down Approach Featuring the Internet*. 2nd. Boston, MA, USA: Addison-Wesley Longman Publishing Co., Inc., 2002. ISBN: 0201976994.

[LK75] S. Lam and L. Kleinrock. "Packet Switching in a Multiaccess Broadcast Channel: Dynamic Control Procedures". In: *IEEE Transactions on Communications* 23.9 (Sept. 1975), pp. 891–904. ISSN: 0090-6778. DOI: 10.1109/TCOM.1975.1092917.

[Lau04] A. J. Laub. *Matrix Analysis For Scientists And Engineers*. Philadelphia, PA, USA: Society for Industrial and Applied Mathematics, 2004. ISBN: 0898715768.

[LA08] W.-Y. Lee and I. Akyildiz. "Optimal spectrum sensing framework for cognitive radio networks". In: *IEEE Transactions on Wireless Communications* 7.10 (Oct. 2008), pp. 3845–3857. ISSN: 1536-1276. DOI: 10.1109/T-WC.2008.070391.

[Lew83] D. Lewinski. "Nonstationary probabilistic target and clutter scattering models". In: *IEEE Transactions on Antennas and Propagation* 31.3 (May 1983), pp. 490–498. ISSN: 0018-926X. DOI: 10.1109/TAP.1983.1143067.

[Li+07] A. Li, M. Wang, X. Li, and H. Kayama. "A Cross-Layer Design on the Basis of Multiple Packet Reception in Asynchronous Wireless Network". In: *IEEE International Conference on Communications (ICC)*. June 2007, pp. 3477–3484. DOI: 10.1109/ICC.2007.575.

[Lin+90] J.-P. Linnartz, H. Goossen, R. Hekmat, K. Pahlavan, and K. Zhang. "Comment on slotted ALOHA radio networks with PSK modulation in Rayleigh fading channels (and reply)". In: *Electronics Letters* 26.9 (Apr. 1990), pp. 593–595. ISSN: 0013-5194. DOI: 10.1049/el:19900389.

[Lu+12] J. L. Lu, W. Shu, and M. Y. Wu. "A survey on multipacket reception for wireless random access networks". In: *Journal of Computer Networks and Communications*. 2012. DOI: 10.1155/2012/246359.

[Lui+12] M. Luis, A. Furtado, R. Oliveira, R. Dinis, and L. Bernardo. "Energy sensing parameterization criteria for cognitive radios". In: *International Symposium on Wireless Communication Systems (ISWCS)*. Aug. 2012, pp. 61–65. DOI: 10.1109/ISWCS.2012.6328330.

[Lui+13] M. Luis, A. Furtado, R. Oliveira, R. Dinis, and L. Bernardo. "Towards a Realistic Primary Users' Behavior in Single Transceiver Cognitive Networks". In: *IEEE Communications Letters* 17.2 (Feb. 2013), pp. 309–312. ISSN: 1089-7798. DOI: 10.1109/LCOMM.2012.121912.122175.

[LV90] R. Lupas and S. Verdú. "Near-far resistance of multiuser detectors in asynchronous channels". In: *IEEE Transactions on Communications* 38.4 (Apr. 1990), pp. 496–508. ISSN: 0090-6778. DOI: 10.1109/26.52661.

[Ma+08] J. Ma, Y. J. Zhang, X. Su, and Y. Yao. "On capacity of wireless ad hoc networks with MIMO MMSE receivers". In: *IEEE Transactions on Wireless Communications* 7.12 (Dec. 2008), pp. 5493–5503. ISSN: 1536-1276. DOI: 10.1109/T-WC.2008.071452.

[Mar+09] N. Marchetti, M. Rahman, S. Kumar, and R. Prasad. "OFDM: Principles and Challenges". English. In: *New Directions in Wireless Communications Research*. Ed. by V. Tarokh. Springer US, 2009, pp. 29–62. ISBN: 978-1-4419-0672-4. DOI: 10.1007/978-1-4419-0673-1_2.

[Mas+13] M. Masonta, M. Mzyece, and N. Ntlatlapa. "Spectrum Decision in Cognitive Radio Networks: A Survey". In: *Communications Surveys Tutorials, IEEE* 15.3 (2013), pp. 1088–1107. ISSN: 1553-877X. DOI: 10.1109/SURV.2012.111412.00160.

[McF65] J. A. McFadden. "The Entropy of a Point Process". In: *Journal of the Society for Industrial and Applied Mathematics* 13.4 (1965), pp. 988–994. ISSN: 03684245.

[Mor+07] R. de Moraes, H. Sadjadpour, and J. Garcia-Luna-Aceves. "Many-to-Many Communication: A New Approach for Collaboration in MANETs". In: *INFOCOM 2007. 26th IEEE International Conference on Computer Communications*. May 2007, pp. 1829–1837. DOI: 10.1109/INFCOM.2007.213.

[Mos96] S. Moshavi. "Multi-user detection for DS-CDMA communications". In: *Communications Magazine, IEEE* 34.10 (Oct. 1996), pp. 124–136. ISSN: 0163-6804. DOI: 10.1109/35.544334.

[MK03] A. Muqattash and M. Krunz. "CDMA-based MAC Protocol for Wireless Ad Hoc Networks". In: *Proceedings of the 4th ACM International Symposium on Mobile Ad Hoc Networking &Amp; Computing*. MobiHoc '03. Annapolis, Maryland, USA: ACM, 2003, pp. 153–164. ISBN: 1-58113-684-6. DOI: 10.1145/778415.778434.

[Naw+05] V. Naware, G. Mergen, and L. Tong. "Stability and delay of finite-user slotted ALOHA with multipacket reception". In: *IEEE Transactions on Information Theory* 51.7 (July 2005), pp. 2636–2656. ISSN: 0018-9448. DOI: 10.1109/TIT.2005.850060.

[Ngo+08] M. H. Ngo, V. Krishnamurthy, and L. Tong. "Optimal Channel-Aware ALOHA Protocol for Random Access in WLANs With Multipacket Reception and Decentralized Channel State Information". In: *IEEE Transactions on Signal Processing* 56.6 (June 2008), pp. 2575–2588. ISSN: 1053-587X. DOI: 10.1109/TSP.2007.911284.

[Ngu+06] G. D. Nguyen, A. Ephremides, and J. Wieselthier. "On Capture in Random-Access Systems". In: *2006 IEEE International Symposium on Information Theory*. July 2006, pp. 2072–2076. DOI: 10.1109/ISIT.2006.261915.

[Oli+13] R. Oliveira, M. Luís, A. Furtado, L. Bernardo, R. Dinis, and P. Pinto. "Improving path duration in high mobility vehicular ad hoc networks". In: *Ad Hoc Networks* 11.1 (2013), pp. 89 –103. ISSN: 1570-8705. DOI: 10.1016/j.adhoc.2012.04.009.

[Olv+10] F. W. Olver, D. W. Lozier, R. F. Boisvert, and C. W. Clark. *NIST Handbook of Mathematical Functions*. 1st. New York, NY, USA: Cambridge University Press, 2010. ISBN: 0521140633, 9780521140638.

[OL+03] A. Orozco-Lugo, M. Lara, D. McLernon, and H. Muro-Lemus. "Multiple packet reception in wireless ad hoc networks using polynomial phase-modulating sequences". In: *IEEE Transactions on Signal Processing* 51.8 (Aug. 2003), pp. 2093–2110. ISSN: 1053-587X. DOI: 10.1109/TSP.2003.814472.

[PP02] A. Papoulis and S. Pillai. *Probability, Random Variables, and Stochastic Processes*. McGraw-Hill series in electrical and computer engineering. McGraw-Hill, 2002. ISBN: 9780071226615.

[Per+12] M. Pereira, L. Bernardo, R. Oliveira, P. Carvalho, and P. Pinto. "Performance of Diversity Combining ARQ Error Control in a TDMA SC-FDE System". In: *IEEE Transactions on Communications* 60.3 (Mar. 2012), pp. 735–746. ISSN: 0090-6778. DOI: 10.1109/TCOMM.2012.013112.110096.

[PW10a] P. Pinto and M. Win. "Communication in a Poisson Field of Interferers–Part I: Interference Distribution and Error Probability". In: *IEEE Transactions on Wireless Communications* 9.7 (July 2010), pp. 2176–2186. ISSN: 1536-1276. DOI: 10.1109/TWC.2010.07.060438.

[PW10b] P. Pinto and M. Win. "Communication in a Poisson Field of Interferers-Part II: Channel Capacity and Interference Spectrum". In: *IEEE Transactions on Wireless Communications* 9.7 (July 2010), pp. 2187–2195. ISSN: 1536-1276. DOI: 10.1109/TWC.2010.07.071283.

[Rob73] L. G. Roberts. "Dynamic Allocation of Satellite Capacity Through Packet Reservation". In: *Proceedings of the June 4-8, 1973, National Computer Conference and Exposition*. AFIPS '73. New York, New York, 1973, pp. 711–716. DOI: 10.1145/1499586.1499753.

[Sad+10] H. Sadjadpour, Z. Wang, and J. Garcia-Luna-Aceves. "The capacity of wireless ad hoc networks with multi-packet reception". In: *IEEE Transactions on Communications* 58.2 (Feb. 2010), pp. 600–610. ISSN: 0090-6778. DOI: 10.1109/TCOMM.2010.02.080175.

[SM11] J. Sarker and H. Mouftah. "A Random Access Protocol with Multi-Packet Reception for Infrastructure-Less Wireless Autonomic Networks". English. In: *Wireless Personal Communications* 56.3 (2011), pp. 447–456. ISSN: 0929-6212. DOI: 10.1007/s11277-010-9982-y.

[SU17] M. Sarker and M. F. Uddin. "Saturation throughput analysis of a carrier sensing based MU-MIMO MAC protocol in a WLAN under fading and shadowing". In: *Wireless Networks* (Nov. 2017). ISSN: 1572-8196. DOI: 10.1007/s11276-017-1614-y.

[SC97] T. Schmidl and D. Cox. "Robust frequency and timing synchronization for OFDM". In: *IEEE Transactions on Communications* 45.12 (Dec. 1997), pp. 1613–1621. ISSN: 0090-6778. DOI: 10.1109/26.650240.

[SA00] M. K. Simon and M. S. Alouini. *Digital Communication over Fading Channels: A Unified Approach to Performance Analysis*. first. New York: Wiley, 2000.

[Sof+13] P. Sofotasios, E. Rebeiz, L. Zhang, T. Tsiftsis, D. Cabric, and S. Freear. "Energy Detection Based Spectrum Sensing Over $\kappa-\mu$ and $\kappa-\mu$ Extreme Fading Channels". In: *IEEE Transactions on Vehicular Technology* 62.3 (Mar. 2013), pp. 1031–1040. ISSN: 0018-9545. DOI: 10.1109/TVT.2012.2228680.

[Spe+99] M. Speth, S. Fechtel, G. Fock, and H. Meyr. "Optimum receiver design for wireless broad-band systems using OFDM. I". In: *IEEE Transactions on Communications* 47.11 (Nov. 1999), pp. 1668–1677. ISSN: 0090-6778. DOI: 10.1109/26.803501.

[Sun+10] H. Sun, D. Laurenson, and C.-X. Wang. "Computationally Tractable Model of Energy Detection Performance over Slow Fading Channels". In: *Communications Letters, IEEE* 14.10 (Oct. 2010), pp. 924–926. ISSN: 1089-7798. DOI: 10.1109/LCOMM.2010.090710.100934.

[Sun+13] H. Sun, A. Nallanathan, C.-X. Wang, and Y. Chen. "Wideband spectrum sensing for cognitive radio networks: a survey". In: *Wireless Communications, IEEE* 20.2 (2013), pp. 74–81. ISSN: 1536-1284. DOI: 10.1109/MWC.2013.6507397.

[SY14] S. Szyszkowicz and H. Yanikomeroglu. "A Simple Approximation of the Aggregate Interference From a Cluster of Many Interferers With Correlated Shadowing". In: *IEEE Transactions on Wireless Communications* 13.8 (Aug. 2014), pp. 4415–4423. ISSN: 1536-1276. DOI: 10.1109/TWC.2014.2317709.

[Szy+11] S. Szyszkowicz, F. Alaca, H. Yanikomeroglu, and J. Thompson. "Aggregate Interference Distribution From Large Wireless Networks With Correlated Shadowing: An Analytical–Numerical–Simulation Approach". In: *IEEE Transactions on Vehicular Technology* 60.6 (July 2011), pp. 2752–2764. ISSN: 0018-9545. DOI: 10.1109/TVT.2011.2158012.

[Tan02] A. Tanenbaum. *Computer Networks*. 4th. Prentice Hall Professional Technical Reference, 2002. ISBN: 0130661023.

[Tan05] H. Tang. "Some physical layer issues of wide-band cognitive radio systems". In: *Proceedings IEEE DySPAN 2005*. Nov. 2005, pp. 151–159.

[Ton+01] L. Tong, Q. Zhao, and G. Mergen. "Multipacket reception in random access wireless networks: from signal processing to optimal medium access control". In: *Communications Magazine, IEEE* 39.11 (Nov. 2001), pp. 108–112. ISSN: 0163-6804. DOI: 10.1109/35.965367.

[Tsa+00] M. Tsatsanis, R. Zhang, and S. Banerjee. "Network-assisted diversity for random access wireless networks". In: *IEEE Transactions on Signal Processing* 48.3 (Mar. 2000), pp. 702–711. ISSN: 1053-587X. DOI: 10.1109/78.824666.

[TV05] D. Tse and P. Viswanath. *Fundamentals of Wireless Communication*. New York, NY, USA: Cambridge University Press, 2005. ISBN: 0-5218-4527-0.

[URK+08] K. Ur Rahman Khan, R. Zaman, and A. Venu Gopal Reddy. "Integrating Mobile Ad Hoc Networks and the Internet: challenges and a review of strategies". In: *3rd International Conference on Communication Systems Software and Middleware and Workshops (COMSWARE), 2008*. Jan. 2008, pp. 536–543. DOI: 10.1109/COMSWA.2008.4554470.

[Urk67] H. Urkowitz. "Energy Detection of Unknown Deterministic Signals". In: *Proceedings of the IEEE* 55.4 (Apr. 1967), pp. 523–531.

[Urk69] H. Urkowitz. "Energy Detection of a Random Process in Colored Gaussian Noise". In: *IEEE Transactions on Aerospace and Electronic Systems* AES-5.2 (Mar. 1969), pp. 156–162. ISSN: 0018-9251. DOI: 10.1109/TAES.1969.309901.

[VT02] A.-J. van der Veen and L. Tong. "Packet separation in wireless ad-hoc networks by known modulus algorithms". In: *IEEE International Conference on Acoustics, Speech, and Signal Processing (ICASSP)*. Vol. 3. May 2002, pp. III–2149–III–2152. DOI: 10.1109/ICASSP.2002.5745067.

[Wal96] C. Walck. *Hand-book on STATISTICAL DISTRIBUTIONS for experimentalists*. Dec. 1996.

[WGLA08] X. Wang and J. Garcia-Luna-Aceves. "Embracing Interference in Ad Hoc Networks Using Joint Routing and Scheduling with Multiple Packet Reception". In: *INFOCOM 2008. The IEEE 27th Conference on Computer Communications*. Apr. 2008, pp. –. DOI: 10.1109/INFOCOM.2008.136.

[WT03] X. Wang and J. Tugnait. "A bit-map-assisted dynamic queue protocol for multi-access wireless networks with multiple packet reception". In: *IEEE Transactions on Signal Processing* 51.8 (Aug. 2003), pp. 2068–2081. ISSN: 1053-587X. DOI: 10.1109/TSP.2003.814463.

[Wan+08] Z. Wang, H. Sadjadpour, and J. J. Garcia-Luna-Aceves. "The Capacity and Energy Efficiency of Wireless Ad Hoc Networks with Multi-packet Reception". In: *Proceedings of the 9th ACM International Symposium on Mobile Ad Hoc Networking and Computing*. MobiHoc '08. Hong Kong, Hong Kong, China: ACM, 2008, pp. 179–188. ISBN: 978-1-60558-073-9. DOI: 10.1145/1374618.1374644.

[Win+09] M. Win, P. Pinto, and L. Shepp. "A Mathematical Theory of Network Interference and Its Applications". In: *Proceedings of the IEEE* 97.2 (Feb. 2009), pp. 205–230. ISSN: 0018-9219. DOI: 10.1109/JPROC.2008.2008764.

[Wu+08] J.-Y. Wu, W.-F. Yang, L.-C. Wang, and T.-S. Lee. "Signal modulus design for blind source separation via algebraic known modulus algorithm: A perturbation perspective". In: *IEEE International Symposium on Circuits and Systems (ISCAS)*. May 2008, pp. 3013–3016. DOI: 10.1109/ISCAS.2008.4542092.

[Yar+08] S. Yarkan, A. Maaref, K. H. Teo, and H. Arslan. "Impact of Mobility on the Behavior of Interference in Cellular Wireless Networks". In: *Global Telecommunications Conference, 2008. IEEE GLOBECOM 2008. IEEE*. Nov. 2008, pp. 1–5. DOI: 10.1109/GLOCOM.2008.ECP.457.

[Ye+02] W. Ye, J. Heidemann, and D. Estrin. "An energy-efficient MAC protocol for wireless sensor networks". In: *Proceedings.Twenty-First Annual Joint Conference of the IEEE Computer and Communications Societies*. Vol. 3. June 2002, 1567–1576 vol.3. DOI: 10.1109/INFCOM.2002.1019408.

[Yim+09] R. Yim, N. Mehta, A. Molisch, and J. Zhang. "Dual power multiple access with multipacket reception using local CSI". In: *IEEE Transactions on Wireless Communications* 8.8 (Aug. 2009), pp. 4078–4088. ISSN: 1536-1276. DOI: 10.1109/TWC.2009.080425.

[YA09] T. Yucek and H. Arslan. "A survey of spectrum sensing algorithms for cognitive radio applications". In: *Communications Surveys Tutorials, IEEE* 11.1 (Mar. 2009), pp. 116–130.

[ZG+12] A. Zahedi-Ghasabeh, A. Tarighat, and B. Daneshrad. "Spectrum Sensing of OFDM Waveforms Using Embedded Pilots in the Presence of Impairments". In: *IEEE Transactions on Vehicular Technology* 61.3 (Mar. 2012), pp. 1208–1221.

[ZZ12] A. Zanella and M. Zorzi. "Theoretical Analysis of the Capture Probability in Wireless Systems with Multiple Packet Reception Capabilities". In: *IEEE Transactions on Communications* 60.4 (Apr. 2012), pp. 1058–1071. ISSN: 0090-6778. DOI: 10.1109/TCOMM.2012.021712.100782.

[Zha+14] T. Zhang, L. An, Y. Chen, and K. K. Chai. "Aggregate interference statistical modeling and user outage analysis of heterogeneous cellular networks". In: *IEEE International Conference on Communications (ICC)*. June 2014, pp. 1260–1265. DOI: 10.1109/ICC.2014.6883494.

[Zha+13] X. Zhang, L. Wu, Y. Zhang, and D. K. Sung. "Interference dynamics in MANETs with a random direction node mobility model". In: *Wireless Communications and Networking Conference (WCNC), 2013 IEEE*. Apr. 2013, pp. 3788–3793. DOI: 10.1109/WCNC.2013.6555178.

[Zha+09] Y. J. Zhang, P. X. Zheng, and S. C. Liew. "How Does Multiple-Packet Reception Capability Scale the Performance of Wireless Local Area Networks?" In: *IEEE Transactions on Mobile Computing* 8.7 (July 2009), pp. 923–935. ISSN: 1536-1233. DOI: 10.1109/TMC.2008.169.

[Zha10] Y. Zhang. "Multi-round contention in wireless LANs with multipacket reception". In: *IEEE Transactions on Wireless Communications* 9.4 (Apr. 2010), pp. 1503–1513. ISSN: 1536-1276. DOI: 10.1109/TWC.2010.04.090841.

[ZT03] Q. Zhao and L. Tong. "A multiqueue service room MAC protocol for wireless networks with multipacket reception". In: *IEEE/ACM Transactions on Networking* 11.1 (Feb. 2003), pp. 125–137. ISSN: 1063-6692. DOI: 10.1109/TNET.2002.808403.

[ZT04] Q. Zhao and L. Tong. "A dynamic queue protocol for multiaccess wireless networks with multipacket reception". In: *IEEE Transactions on Wireless Communications* 3.6 (Nov. 2004), pp. 2221–2231. ISSN: 1536-1276. DOI: 10.1109/TWC.2004.837654.

[Zwi03] D. Zwillinger. *CRC Standard Mathematical Tables and Formulae*. 31st. Boca Raton: Chemical Rubber Company, 2003. ISBN: 1-58488-291-3.

APPENDIX A

# PROOF OF LEMMA 3.1

*Proof.* Considering the following integral

$$\int e^{a(r+1)^{-\alpha}}(r+1)^c dr, \tag{A.1}$$

and assuming that $u = (r+1)$, (A.1) is rewritten as follows

$$\int e^{au^{-\alpha}} u^c du. \tag{A.2}$$

The integral in (A.2) is a special integral (Incomplete Gamma function).

From [Jef+07, eq. 2.325.6] we know that

$$\int e^{au^n} u^m du = \frac{(-1)^{z+1} a^z \Gamma[-z, -au^n]}{n}, \tag{A.3}$$

where $z = -\frac{m+1}{n}$, $n \neq 0$ and $z \notin \mathbb{Z}$.

By using (A.3) with $z = \frac{c+1}{\alpha}$, (A.2) can be rewritten as follows

$$\frac{(-1)^{\frac{c+1}{\alpha}+1} a^{\frac{c+1}{\alpha}} \Gamma[-\frac{c+1}{\alpha}, -au^{-\alpha}]}{-\alpha}. \tag{A.4}$$

Knowing that $\Gamma(s,x) = x^s \mathrm{Ei}(1-s,x)$ [Olv+10, pp. 177, eq. 8.4.13], (A.4) can be rewritten as

$$\frac{u^{(c+1)} \mathrm{Ei}[1+\frac{c+1}{\alpha}, -au^{-\alpha}]}{\alpha}, \tag{A.5}$$

where Ei represents the Exponential Integral function ($\mathrm{Ei}(p,x) = \int_1^\infty e^{-xt} t^{-p} \mathrm{d}t$ [Zwi03, eq. 6.15.2]).

Replacing $u$ by $(r+1)$ in (A.5), we finally get,

$$\int e^{a(r+1)^{-\alpha}}(r+1)^c dx = \frac{(r+1)^{(c+1)} \mathrm{Ei}[1+\frac{c+1}{\alpha}, -a(r+1)^{-\alpha}]}{\alpha}, \tag{A.6}$$

for $\alpha \neq 0$ and $\frac{c+1}{\alpha} \notin \mathbb{Z}$. □

APPENDIX B

# EXPECTATION AND VARIANCE OF A TRUNCATED POISSON DISTRIBUTION

**Lemma B.1.** *Let $X$ be a Random Variable (RV) distributed according to a truncated Poisson distribution represented as follows,*

$$P[X = x] = \frac{\frac{(\lambda)^x}{x!}e^{-\lambda}}{1 - \overline{F}(n)}, x = 0, 1, ..., n. \tag{B.1}$$

*where $\overline{F}(n)$ is the complementary CDF of a Poison distribution given by*

$$\overline{F}(n) = \sum_{k=n}^{\infty} \frac{(\lambda)^k}{k!}e^{-\lambda}. \tag{B.2}$$

*Then the expected value and variance are respectively given as follows,*

$$E_X[X] = \frac{\lambda}{1 - \overline{F}(n)}, \tag{B.3}$$

$$Var_X[X] = \frac{\lambda}{1 - \overline{F}(n_I)}\left((1 + \lambda) - \frac{\lambda}{1 - \overline{F}(n_I)}\right). \tag{B.4}$$

*Proof.* Considering the MGF of $X$, which is represented by,

$$M_X(s) = \frac{e^{\lambda(e^s - 1)}}{1 - \overline{F}(n)}. \tag{B.5}$$

By using the MGF (B.5), the first moment of $X$ is given by

$$\begin{aligned} \mathrm{E}_X[X] &= \frac{\partial M_X(0)}{\partial s} \\ &= \frac{\lambda}{1 - \overline{F}(n)}, \end{aligned} \tag{B.6}$$

which correspond to the expected value of $X$.

The second moment of $X$ is given as follows,

$$\begin{aligned} \mathrm{E}_X[X^2] &= \frac{\partial^2 M_X(0)}{\partial s^2} \\ &= \frac{\lambda(1+\lambda)}{1-\overline{F}(n)}, \end{aligned} \tag{B.7}$$

Using (B.6) and (B.7), the variance of $X$ is derive by

$$\begin{aligned} \mathrm{Var}_X[X] &= \mathrm{E}_X[X^2] - \mathrm{E}_X[X]^2 \\ &= \frac{\lambda(1+\lambda)}{1-\overline{F}(n)} - \left(\frac{\lambda}{1-\overline{F}(n)}\right)^2 \\ &= \frac{\lambda}{1-\overline{F}(n_I)}\left((1+\lambda) - \frac{\lambda}{1-\overline{F}(n_I)}\right). \end{aligned} \tag{B.8}$$

□